

AFRL-ML-WP-TR-2000-4083

**ORTHORHOMBIC TITANIUM ALUMINIDE
METAL MATRIX COMPOSITES (O TMCs) –
A REVIEW**



**P.R. SMITH
A.H. ROSENBERGER**

**MATERIALS AND MANUFACTURING DIRECTORATE
METALS, CERAMICS & NDE DIVISION
AIR FORCE RESEARCH LABORATORY
WRIGHT-PATTERSON AFB, OH 45433-7817**

C.G. RHODES

**ROCKWELL SCIENCE CENTER
THOUSAND OAKS, CA 91358**

OCTOBER 1999

FINAL REPORT FOR OCTOBER 1999

APPROVED FOR PUBLIC RELEASE; DISTRIBUTION UNLIMITED

**MATERIALS AND MANUFACTURING DIRECTORATE
AIR FORCE RESEARCH LABORATORY
AIR FORCE MATERIEL COMMAND
WRIGHT-PATTERSON AIR FORCE BASE OH 45433-7750**

REPORT DOCUMENTATION PAGE

1. REPORT DATE (DD-MM-YYYY) 01-10-1999	2. REPORT TYPE	3. DATES COVERED (FROM - TO) xx-10-1999 to xx-10-1999
4. TITLE AND SUBTITLE Orthorhombic titanium aluminide Metal Matrix Composites (O TMS's) - A Review Unclassified		5a. CONTRACT NUMBER
		5b. GRANT NUMBER
		5c. PROGRAM ELEMENT NUMBER
6. AUTHOR(S)		5d. PROJECT NUMBER
		5e. TASK NUMBER
		5f. WORK UNIT NUMBER
7. PERFORMING ORGANIZATION NAME AND ADDRESS Materials and Manufacturing Directorate Metals, Ceramics & NDE Division AFRL Wright Patterson AFB , OH 45433-7817		8. PERFORMING ORGANIZATION REPORT NUMBER
9. SPONSORING/MONITORING AGENCY NAME AND ADDRESS ,		10. SPONSOR/MONITOR'S ACRONYM(S)
		11. SPONSOR/MONITOR'S REPORT NUMBER(S)
12. DISTRIBUTION/AVAILABILITY STATEMENT A PUBLIC RELEASE ,		

13. SUPPLEMENTARY NOTES
14. ABSTRACT See Report
15. SUBJECT TERMS

16. SECURITY CLASSIFICATION OF:			17. LIMITATION OF ABSTRACT Public Release	18. NUMBER OF PAGES 114	19a. NAME OF RESPONSIBLE PERSON Rike, Jack jrike@dtic.mil
a. REPORT Unclassified	b. ABSTRACT Unclassified	c. THIS PAGE Unclassified			19b. TELEPHONE NUMBER International Area Code Area Code Telephone Number DSN

NOTICE

WHEN GOVERNMENT DRAWINGS, SPECIFICATIONS, OR OTHER DATA ARE USED FOR ANY PURPOSE OTHER THAN IN CONNECTION WITH A DEFINITELY GOVERNMENT-RELATED PROCUREMENT, THE UNITED STATES GOVERNMENT INCURS NO RESPONSIBILITY OR ANY OBLIGATION WHATSOEVER. THE FACT THAT THE GOVERNMENT MAY HAVE FORMULATED OR IN ANY WAY SUPPLIED THE SAID DRAWINGS, SPECIFICATIONS, OR OTHER DATA, IS NOT TO BE REGARDED BY IMPLICATION OR OTHERWISE IN ANY MANNER CONSTRUED, AS LICENSING THE HOLDER OR ANY OTHER PERSON OR CORPORATION, OR AS CONVEYING ANY RIGHTS OR PERMISSION TO MANUFACTURE, USE, OR SELL ANY PATENTED INVENTION THAT MAY IN ANY WAY BE RELATED THERETO.

THIS REPORT IS RELEASABLE TO THE NATIONAL TECHNICAL INFORMATION SERVICE (NTIS). AT NTIS, IT WILL BE AVAILABLE TO THE GENERAL PUBLIC, INCLUDING FOREIGN NATIONS.

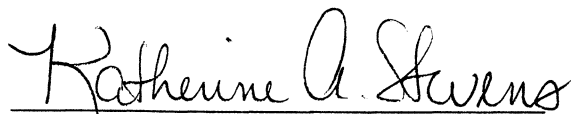
THIS TECHNICAL REPORT HAS BEEN REVIEWED AND IS APPROVED FOR PUBLICATION.



A.H. ROSENBERGER, Project Engineer
Metals Development & Materials
Processing Branch
Metals, Ceramics & NDE Division



P.R. SMITH, Project Engineer
Metals Development & Materials
Processing Branch
Metals, Ceramics & NDE Division



KATHERINE A. STEVENS, Chief
Metals Development & Materials
Processing Branch
Metals, Ceramics & NDE Division



GERALD J. PETRAK, Asst Chief
Metals, Ceramics & NDE Division
Materials & Manufacturing Directorate

IF YOUR ADDRESS HAS CHANGED, IF YOU WISH TO BE REMOVED FROM OUR MAILING LIST, OR IF THE ADDRESSEE IS NO LONGER EMPLOYED BY YOUR ORGANIZATION, PLEASE NOTIFY, AFRL/MLLM, WRIGHT-PATTERSON AFB OH 45433-7817 TO HELP US MAINTAIN A CURRENT MAILING LIST.

COPIES OF THIS REPORT SHOULD NOT BE RETURNED UNLESS RETURN IS REQUIRED BY SECURITY CONSIDERATIONS, CONTRACTUAL OBLIGATIONS, OR NOTICE ON A SPECIFIC DOCUMENT.

REPORT DOCUMENTATION PAGE			Form Approved OMB No. 0704-0188	
Public reporting burden for this collection of information is estimated to average 1 hour per response, including the time for reviewing instructions, searching existing data sources, gathering and maintaining the data needed, and completing and reviewing the collection of information. Send comments regarding this burden estimate or any other aspect of this collection of information, including suggestions for reducing this burden, to Washington Headquarters Services, Directorate for Information Operations and Reports, 1215 Jefferson Davis Highway, Suite 1204, Arlington, VA 22202-4302, and to the Office of Management and Budget, Paperwork Reduction Project (0704-0188), Washington, DC 20503.				
1. AGENCY USE ONLY (Leave blank)		2. REPORT DATE OCTOBER 1999		3. REPORT TYPE AND DATES COVERED FINAL REPORT FOR OCTOBER 1999
4. TITLE AND SUBTITLE ORTHORHOMBIC TITANIUM ALUMINIDE METAL MATRIX COMPOSITES (O TMCs) -- A REVIEW			5. FUNDING NUMBERS C IN-HOUSE PE 62102 PR 4347 TA OI WU HR	
6. AUTHOR(S) P.R. SMITH, A.H. ROSENBERGER -- Materials and Manufacturing Directorate C.G. RHODES -- Rockwell Science Center				
7. PERFORMING ORGANIZATION NAME(S) AND ADDRESS(ES) Materials and Manufacturing Directorate Metals, Ceramics & NDE Division Air Force Research Laboratory Wright-Patterson AFB, OH 45433-7817			8. PERFORMING ORGANIZATION REPORT NUMBER	
9. SPONSORING/MONITORING AGENCY NAME(S) AND ADDRESS(ES) MATERIALS AND MANUFACTURING DIRECTORATE AIR FORCE RESEARCH LABORATORY AIR FORCE MATERIEL COMMAND WRIGHT-PATTERSON AFB, OH 45433-7750 POC: P.R. Smith, AFRL/MLLM, & A.H. Rosenberger AFRL/MLLN			10. SPONSORING/MONITORING AGENCY REPORT NUMBER AFRL-ML-WP-TR-2000-4083	
11. SUPPLEMENTARY NOTES				
12a. DISTRIBUTION AVAILABILITY STATEMENT APPROVED FOR PUBLIC RELEASE, DISTRIBUTION UNLIMITED.			12b. DISTRIBUTION CODE	
13. ABSTRACT (Maximum 200 words) Continuous silicon carbide (SiC) reinforced titanium matrix composites (TMCs) utilizing matrices based upon the intermetallic orthorhombic (O) phase, Ti ₂ AlNb, have been the subject of a significant development activity over the past several years. These O TMCs are considered enabling materials for rotating engine components in order to meet the requisite increased thrust/weight ratios and decreased specific fuel consumption targets for the next generation of advanced propulsion systems being developed under the Air Force IHPTET (Integrated High Performance Turbine Engine Technology) initiative. The O-based class of titanium aluminides has demonstrated significant advantages as a matrix for continuous reinforcement for use at temperatures up to 700°C compared to their alpha-2 (α ₂) Ti ₃ Al and conventional titanium matrix predecessors. Amongst these advantages and increased elevated temperature strength and creep resistance, improved ambient temperature fracture resistance, and decreased reactivity with SiC reinforcing fibers. Additionally, O TMCs have met or exceeded most generic performance requirements for hoop wound engine hardware such as bladed rings (blings) or bladed disks (blisks). The subject review summarizes significant findings for the numerous research activities undertaken in the development and evaluation of this important class of TMCs.				
14. SUBJECT TERMS Orthorhombic Titanium Aluminide Metal Matrix Composites (O TMCs)			15. NUMBER OF PAGES 110	
			16. PRICE CODE	
17. SECURITY CLASSIFICATION OF REPORT UNCLASSIFIED	18. SECURITY CLASSIFICATION OF THIS PAGE UNCLASSIFIED	19. SECURITY CLASSIFICATION OF ABSTRACT UNCLASSIFIED	20. LIMITATION OF ABSTRACT SAR	

Table of Contents

	Page
Section I Abstract	1
Section II Introduction	2
Section III SiC Fiber Reinforcements	6
Section IV Matrix Development	18
Section V Interface Studies	44
Section VI Composite Processing	50
Section VII Mechanical Behavior of Composites	62
Section VIII Damage Mechanisms	72
Section IX Constituent Effects on Composite Properties.....	80
Section X Summary	87
Section XI References	91

List of Figures

Figure		Page
1	Schematic Showing the Architecture of the SCS-6 Fiber	7
2	Columnar Growth of Course β SiC Portion of SCS-6 Fiber	7
3	POS versus UTS Data for SCS-6 Fiber	8
4	Schematic Showing Architecture of Ultra SCS™ Fiber	9
5	Fine-Grained Microstructure of SiC Portion of Ultra SCS™ Fiber	9
6	POS versus UTS Data for Ultra SCS™ Fiber	10
7	Schematic Showing Architecture of Large Diameter Ultra SCS Fiber	11
8	Microstructure of Large Diameter Ultra SCS Fiber	11
9	POS versus UTS Data for Large Diameter Ultra SCS	12
10	Schematic Showing Architecture of Trimarc® 1 Fiber	13
11	Columnar Growth of β SiC Portion of Trimarc® 1 Fiber	13
12	Kirkendall Porosity in W/SiC Reaction Zone of Trimarc® 1 Fiber	14
13	POS versus UTS Data for Trimarc®1 Fiber.....	15
14	Reaction Zone Growth versus Time at 982°C for Ti-24Al-11Nb and Ti-22Al-23Nb.....	16
15	As-Consolidated Fiber/Matrix Reaction Zones for Trimarc®1, SCS-6™ and Ultra SCS™ Fibers in Ti-22Al-23Nb	17
16	Density corrected tensile yield strengths (m^2/sec^2) as a function of test temperature for selected titanium aluminide alloys (from R. G. Rowe, Ref 44).....	18
17	Proposed Ti-Al-Nb phase diagram at 900°C (from Kester-Weykamp et al., Reference 48)	19
18	Ti-27.5Al vertical section. (From Banerjee et al., Ref. 49)	20
19	Ti-22Al-Nb isopleth (From Miracle et al., Ref. 50)	20
20	Density corrected tensile strengths for Ti-21Al-22Nb and Ti-24Al-11Nb (from Smith et al., Ref. 13).....	21
21	Portion of the Ti-Al-Nb ternary system at 1038°C (1900°F). (From Ref. 8)	23
22	Portion of the Ti-Al-Nb ternary system at 815°C (1500°F). The three-phase field is speculation. (From Ref. 8).....	23
23	Portion of the Ti-Al-Nb ternary system at 760°C (1400°F). The three-phase field is speculation. (From Ref. 8).....	24

24	Portion of the Ti-Al-Nb ternary system at 650°C (1200°F). The three-phase field is speculation. (From Ref. 8).....	24
25	Ti-22Al-23Nb processed at 1025°C and rapidly cooled. Microstructure consists of retained B2 phase.	25
26	Ti-22Al-23Nb showing large O-phase platelets at grain boundaries.....	26
27	Ti-22Al-23Nb processed at 1025°C cooled at 50°C/hr to 815°C, held 4 hrs and a.c. Microstructure consists of transformed B2 matrix	26
28	Ti-20Al-25Nb illustrating B2→O+B2 transformation. (a) quenched from 1038°C, 100% B2; (b) as in (a) plus aged for 1000 hours at 815°C, O + B2 phases.....	27
29	Ti-22Al-23Nb after hot working in B2 + α_2 phase field. (a) as hot worked showing primary α_2 particles in transformed matrix, (b) after 2000 hours at 704°C showing apparent retention of primary α_2 particles.	28
30	Primary α_2 particles in Ti-22Al-23Nb (A) hot worked plus slow cool, showing untransformed structure; (b) after 2000 hours at 704°C, showing in-situ transformation from α_2 to α_2 + O	28
31	Electron diffraction from primary α_2 particle in Ti-22Al-23Nb. Pattern is analyzed as overlapping [0001] α_2 and [001] O.....	29
32	The effect of transformation product size on discontinuous coarsening in Ti-22Al-23Nb aged at 650°C. (a) Quenched from solution temperature and aged 100 hrs. (b) Slowly cooled from solution temperature and aged 100 hrs.....	30
33	Influence of oxygen on the B2 ↔ B2 + α_2 transus temperatures in Ti-22Al-23Nb and Ti-22Al-27Nb [Ref. 58].....	31
34	Ti-22Al-23Nb, beta solutionized and aged 500 hours at 900°C. (a) O+B2 in alloy containing 220 wppm oxygen; (b), B2 + α_2 + O alloy containing 980 wppm oxygen [Ref. 58]	32
35	Ti-22Al-27Nb, beta solutionized and aged 500 hours at 900°C. O +B2 in alloy containing 1120 wppm oxygen. [Ref. 58].....	32
36	Comparison of yield strength and elongation of three heat treatments of Ti-22Al-27Nb. (From Rowe et al., Ref. 61)	35
37	Full life creep behavior at 650°C/172 MPa for several titanium alloys. (After Smith et al., Ref. 65)	36
38	Weight Change vs. Time at Temperature for Ti-22Al-23Nb in an Air Environment (Ref 68) .	39
39	Time to breakaway oxidation and time to 5 μ m depth of embrittlement as a function of temperature for air exposed Ti-19Al-23Nb. (After Brindley et al., Ref. 69).....	40
40	Tensile strengths of Ti-22Al-24Nb-1.4Mo-0.5Si in two microstructural conditions as a function of temperature. Condition A, with 7 v/o primary α_2 and fully transformed, O + β , matrix, exceeds the most stringent impeller goal strength. (After Porter et al., Ref. 8).....	41

41	Larson-Miller plot for 0.24% ϵ of Ti-22Al-24Nb-1.4Mo-0.5Si in two microstructural conditions. (After Porter et al., Ref. 8)	42
42	Larson-Miller plot for 0.5% ϵ of Ti-22-Al-24Nb-1.4Mo-0.5Si in two microstructural conditions. (After Porter et al., Ref. 8)	42
43	TEM cross sections showing fiber/matrix interface reaction products: 1 = mixed carbides and silicides, 2 = (Ti, Nb) C, 3 = Al(Ti,Nb) ₃ C, 4 = (Ti, Nb) ₅ (Si,Al) ₃ in (a) Ti-24Al-11Nb/SCS-6 SiC, and (b) Ti-22Al-23Nb/SCS-6 SiC	44
44	Cruciform tensile specimen for measurement of transverse loading response of single-fiber composites. (After Gundel et al., Ref 82).....	46
45	SiC/TaC/W/Ti-22Al-23Nb diffusion couple after bonding at 1000°C/4 hours. (after Porter et al., Ref. 8).....	47
46	SiC fiber with NbC/W coating in Ti-22Al-23Nb matrix. (After Porter et al., Ref. 8).....	48
47	Spartially varied interface design concepts. (After Maruyama et al., Ref. 19).....	49
48	Schematic of Allison's "Helical" Foil-Fiber-Foil Fabrication Process	51
49	Schematic of Textron's "Grooved Disc" Foil-Fiber-Foil Fabrication Process.....	51
50	Ti-22Al-26Nb Foil Produced by Wah Chang.....	52
51	Hot rolled 0.2 cm. Sheet of Ti-22Al-24Nb-1.5Mo-0.5Si (Ref 23)	53
52	YS vs Orientation to Rolling Direction for Ti-22Al-23Nb Foil (Ref 96).....	54
53	Schematic of ARS's Tape Casting Process	55
54	Ultra SCS/Ti-22Al-26Nb Composite Fabrication via Tape Casting	56
55	Schematic of the Crucible Research Inert Gas Atomization Unit	56
56	a) Cellular Dendritic Structure Present in As-atomized Ti-22Al-26Nb; and b) Contiguous Alpha-2 Network due to Microsegregation in Neat Ti-22Al-26Nb.	57
57	Fracture Along Contiguous Alpha-2 in Tape Cast P/M Ti-22Al-26Nb.....	58
58	Schematic of ARC's Wire Winding Process	59
59	Ti-22Al-26Nb Wire Produced by Dynamet.....	61
60	Comparison of ultimate tensile strength of longitudinal composites.....	65
61	Comparison of ultimate tensile strength of transverse composites.....	65
62	Residual RT tensile strength as a function of thermal cycling temperature range for 500 cycles at 815°C maximum temperature (after [13])	66
63	Creep-rupture comparison on longitudinal composites using the Larson-Miller Parameter	67
64	Comparison of creep behavior of transverse composites using the Larson-Miller Parameter to 0.5% creep strain	67

65	Comparison of the isothermal fatigue behavior of longitudinal composites at 650°C	68
66	Comparison of the out-of-phase (a) and in-phase (b) thermomechanical fatigue behavior of longitudinal composites.....	69
67	Comparison of the fatigue crack propagation behavior of the three composite systems at; (a) room temperature and (b) 650°C (after Ref. 114).....	70
68	Comparison of the fatigue life at 430°C and 650°C for specimens tested at 900Mpa, 0.1 Hz, R=0.1. Arrow indicates runout at 10 ⁵ cycles [116].....	73
69	Comparison of creep behavior of transverse composites in air (from Fig. 64) and vacuum [117-118] using the Larson-Miller Parameter to 0.5% creep strain.....	74
70	Influence of temperature, maximum stress and environment on fatigue life for SCS-6 TM /Ti-22Al-23Nb [0] ₄ composites, arrows indicate runout (after [116]).....	75
71	Ultrasonic surface-wave C-scans of 900 MPa tests at (a) 20°C, (b) 320°C, (c) 430°C, (d) 540°C, and (e) 650°C. C, tc, and N indicate cracks, thermocouple weld marks, and no damage optically identified, respectively [116].....	76
72	Simplified compressor mission incorporating thermomechanical loading, lags in temperature, hold times at max load and a mix of major and minor cycles [121].....	77
73	Comparison of baseline mission spectrum fatigue to isothermal, IP-TMF, OP-TMF, and OP non-isothermal fatigue date [121].....	78
74	Effect of spectrum maximum stress and maximum temperature on the mission life [121].....	78
74	Comparison of the baseline mission cycle fatigue life with isothermal fatigue and a generic mission cycle incorporating various hold periods at maximum load [122]	79
76	Comparison of the ultimate tensile strength of the three composite systems [29].....	81
77	Comparison of the longitudinal creep behavior of the three composite systems [29]	81
78	Fatigue behavior of SCS-6 TM , Trimarc 1®, and Ultra SCS TM composites at 650°C, R=0.1, frequency = 1.0 Hz (*indicates 0.1 Hz) [29]	82
79	Temperature effects on the fatigue behavior of O TMCs with SCS-6 TM and Ultra SCS TM fiber reinforcements (σ_{max} =900 MPa, R=0.1; frequency = 1.0Hz for Ultra SCS TM /Ti-22Al-23Nb, 0.1 Hz for SCS-6 TM /Ti-22Al-23Nb) [29]	83
80	Thermomechanical fatigue comparison of the three orthorhombic composites (150-650°C, R=0.1, Frequency = 0.006 Hz) [29].....	83
81	Comparison of the tensile strength of Ultra SCS TM reinforced O TMCs having Ti-2Al-23Nb [29] and Ti-22Al-26Nb [123] matrices (v_f =0.3).....	84
82	Comparison of the isothermal fatigue of Ultra SCS TM reinforced O TMCs having Ti-22Al-23Nb [29] and Ti-22Al-26Nb [123] matrices (v_f =0.3).....	85
83	Comparison of the transverse creep resistance of As-HIP'd and heat treated SCS-6 TM /Ti-22Al-23Nb composites (from [124]).....	86

List of Tables

Table	Page
1 Fiber/Matrix Reaction Zone Size for SiC Fibers in Ti-22Al-23Nb	17
2 Matrix Property Requirements for Blisk/Bling and Impeller Applications (from Ref. 8)	22
3 Effect of Solution Treatment on Tensile Properties in Ti-22Al-23Nb (from Smith et al., Ref. 42)....	34
4 Effect of Solution Temperature on Creep Behavior of Ti-22Al-23Nb at 650°C/172 MPa. (Beta Transus = 1100°C) (After Smith et al. Ref 42)	37
5 Effect of Forging Temperature on Creep Behavior of Ti-22Al-26Nb at 650°C/172 MPa (Beta Transus ≈ 1066°C) (After Woodfield et al., Ref 6)	38
6 Effect of Elevated Temperature Air Exposure on Ductility of Ti-22Al-26Nb.....	39
7 Fiber/Matrix Interface Goal Properties (After Porter et al., Ref. 8)	45
8 Effect of Preliminary Heat Treatment on Room Temperature Tensile Properties of Tape Cast Ti-22Al-26Nb	57
9 Room Temperature Tensile Properties for As-Consolidated Tape Cast Orthorhombic Compositions	58
10 Room Temperature Tensile Properties of Ti-22Al-26Nb in Wire, Tape Cast Neat and Consolidated Neat Foil Forms (from Smith ref 100).	61
11 Composite Property Requirements for Blisk/Bling and Impeller Applications (after Ref. 8)	63
12 Heat treatment of SCS-6™/Ti-22Al-23Nb Composite [124]	86

I. Summary

Continuous silicon carbide (SiC) reinforced titanium matrix composites (TMCs) utilizing matrices based upon the intermetallic orthorhombic (O) phase, Ti_2AlNb , have been the subject of a significant development activity over the past several years. These O TMCs are considered enabling materials for rotating engine components in order to meet the requisite increased thrust/weight ratios and decreased specific fuel consumption targets for the next generation of advanced propulsion systems being developed under the Air Force IHPTET (Integrated High Performance Turbine Engine Technology) initiative. The O-based class of titanium aluminides has demonstrated significant advantages as a matrix for continuous reinforcement for use at temperatures up to 700°C compared to their α_2 (α_2) Ti_3Al and conventional titanium matrix predecessors. Amongst these advantages are increased elevated temperature strength and creep resistance, improved ambient temperature fracture resistance, and decreased reactivity with SiC reinforcing fibers. Additionally, O TMCs have met or exceeded most generic performance requirements for hoop wound engine hardware such as bladed rings (blings) or bladed disks (blisks). The subject review summarizes significant findings for the numerous research activities undertaken in the development and evaluation of this important class of TMCs.

II. Introduction

The Materials and Manufacturing Directorate of the Air Force Research Laboratory has been spearheading the development of a new class of continuously reinforced high temperature metal matrix composites based upon the orthorhombic (O) titanium aluminide phase, Ti_2AlNb . The approach used for this material system development was multi-disciplinary in nature and was conducted through the use of external contract studies, in-house research and cooperative programs with industry, academia and other government laboratories.

The O phase was initially discovered by Banerjee et al. [1] who found that it formed for high levels of Nb (16-30at%) in the $\text{Ti}_3\text{Al}+\text{Nb}$ system. The crystal structures of the Ti_2AlNb and Ti_3Al (α_2) systems are similar, in that the Ti_2AlNb structure has a common Cmc symmetry and is only a slight distortion of the DO_{19} structure found in Ti_3Al . The primary difference between the two structures is that one of the titanium subsites in the DO_{19} structure is preferentially occupied by Nb in Ti_2AlNb and randomly occupied by Nb in Ti_3Al [2,3]. Despite its ternary ordered structure and lower symmetry than α_2 , the O phase deforms by at least as many slip systems and exhibits a more extensive "c" component of slip [4]. This latter characteristic results in increased levels of ambient temperature fracture resistance, while maintaining higher levels of elevated temperature strength and creep resistance. Studies by Rowe [5] on monolithic O alloys yielded a ternary composition, Ti-22Al-26Nb (at%), which exhibited the best balance of mechanical performance for all ternaries evaluated. This latter alloy has been the subject of detailed research studies examining microstructure/processing/property relationships sponsored primarily under external contract by the Navy [6]. Additional studies conducted under Air Force in-house [7] and contractual [8] sponsorship have since identified higher order O alloy systems incorporating Mo and Si additions that afford improved levels of elevated temperature strength and creep resistance compared to the baseline ternary.

A number of commercially available continuous SiC fibers have been evaluated as candidate reinforcements for orthorhombic titanium aluminide composites (O TMCs) [9]. Amongst these is the Trimarc 1[®] fiber produced by Amercom/Atlantic Research Corporation (ARC). This fiber is manufactured by chemical vapor deposition (CVD) on a tungsten (W) core. Unfortunately, due to deleterious chemical reactions between the W and the SiC, this fiber was found not suitable for reinforcement of O TMCs, which undergo high temperature exposures for consolidation and secondary component processing [10]. CVD processed fibers manufactured by Textron including the SCS-6[™] and Ultra SCS[™], are deposited on a carbon monofilament (CMF), which is stable with respect to SiC at elevated temperatures. Therefore, these fibers have demonstrated the best chemical stability and strength retention within an O matrix, with the Ultra SCS[™] exhibiting much higher strength [9,11]. More recently, ARC in a joint venture with 3M have developed a SiC fiber, Trimarc 2[®] [12] deposited on a CMF substrate which should exhibit good high temperature stability and possesses tensile properties similar to the SCS-6[™] fiber. All of the aforementioned fibers have a multiple-layer carbon-rich coating applied to their

surface to increase their handleability and to increase their resistance to degradation by chemical reaction within titanium matrices.

Like all TMCs utilizing continuous SiC reinforcement, O TMCs exhibit a chemical reaction between the SiC and the O matrix during high temperature excursions for composite consolidation and secondary processing. This chemical reaction produces a continuous series of complex intermetallic compounds (i.e. a reaction zone) at the interface between the SiC fiber surface and the O matrix. The size and composition of this reaction zone depends not only upon the thermal excursion time and temperature, but the fiber and matrix chemistries as well. Indeed, Smith et al. [13] found that the SCS-6TM/Ti-22Al-23Nb composite exhibited a significantly reduced reaction rate constant compared to the SCS-6TM/Ti-24Al-11Nb system. Rhodes [14] has examined in detail via transmission electron microscopy the reaction zone which forms for the SCS-6TM/Ti-22Al-23Nb composite system. He found the as-consolidated zone width to be on the order of 0.3 μ m thick and to consist of three distinct layers of complex titanium carbides and silicides. The effect of this reaction zone (in combination with the fiber carbon-rich coatings) on off-axis properties such as tensile strength and creep resistance is significant, as the interface can support only very modest transverse loads [15,16]. Conversely, the same weak interface allows for good crack growth resistance [17,18] due to interface debonding and crack deflection around the fibers (i.e. crack bridging). Studies have been conducted to examine means of increasing this off-axis load-carrying capability by modification of the interface via fiber coatings. Most recently, Maruyama and Gundel [19] demonstrated for conventional TMCs that increased interfacial strengths can be obtained through the application of spatially varied interfacial coatings to SiC fibers without the loss of crack deflection capability. In addition to intermetallic compound formation, outward diffusion of carbon from the fiber surface into the O matrix has been found to stabilize titanium carbides at substantial distances from the fiber/matrix interface [20]. The effects of these carbides on composite mechanical performance is not totally understood at this time.

Processing techniques for the fabrication of O TMC composites have included matrices produced by both rolled foil and powder metallurgy (P/M)-based methods. O foil production incorporates multiple thermomechanical processing steps including: ingot melting, forging, hot rolling, and cold rolling, with the latter two steps requiring numerous intermediate stress relief anneals [21]. Not surprisingly, foil processing can be very time consuming and costly, with Ti-22Al-26Nb foil costs approaching \$700/lb [22]. However, a recent Air Force sponsored program produced Ti-22Al-24.5Nb-1.5Mo-0.5Si sheet (0.22 mm) consistent with a cost model that predicted foil costs on the order of ~\$300/lb by incorporating several process improvement practices [23]. In addition to the raw material costs (both matrix and fiber), costs associated with the component fabrication (i.e. bling) can be significant. P/M processing has the potential to be significantly more cost effective with demonstrated Ti-22Al-26Nb powder costs on the order of \$70/lb [24]. However, studies are currently in progress to assess the effects of direct consolidation of powders to green tapes

(i.e. without significant mechanical working) on the mechanical properties of O alloys and thus, their viability to function as matrices for O TMCs [25]. More recently, fine wires (0.13 mm dia.) of Ti-22Al-26Nb have been produced from consolidated powders by hot extrusion and cold drawing. These wires have exhibited very attractive combinations of tensile strength and ductility [26]. Although raw material costs for wire are expected to be on the order of those for foil, component processing costs are expected to be reduced due to lower material losses and ease of fabrication.

In parallel with the aforementioned research studies involving monolithic alloy development, fiber studies, and process development, the Propulsion Directorate of the Air Force Research Laboratory has been conducting an initiative to double the thrust/weight ratio of future gas turbine engines within the first few years of the new millennium [27]. One essential element of this Integrated High Performance Turbine Engine Technology (IHPTET) initiative is the development of high strength, light-weight materials. Rotating components including the compressor rotor have targeted titanium metal matrix composites as an enabling material system to meet the associated thrust/weight and specific fuel consumption goals established for the IHPTET program. Early phases of IHPTET have successfully utilized SCS-6TM reinforced conventional titanium matrices such as Ti-6Al-4V and Ti-1100 to meet intermediate thrust/weight targets. However, full realization of the 2x thrust-to-weight increase will require TMCs with higher temperature matrix capability and higher strength reinforcements. As such, titanium aluminide MMCs based upon an O phase matrix with Ultra SCSTM fibers are being evaluated for their ability to meet these demanding performance requirements at temperatures up to 700°C. Early work by Smith et al. [28] examined the SCS-6TM/Ti-22Al-23Nb system produced using a foil-based matrix. This first generation O TMC system was found to have a number of significant performance advantages compared to earlier results for the SCS-6TM/Ti-24Al-11Nb (i.e. SiC/Ti₃Al) system. These advantages included: increased transverse tensile strength, improved transverse creep resistance, and decreased reactivity with the SCS-6TM reinforcement. Subsequent studies by Russ et al. [15] found that this early O TMC system met or exceeded most generic performance requirements for a bling/blisk structure, and many of the requirements for the more demanding impeller component. With the advent of a higher strength Ultra SCSTM fiber, Ultra SCSTM/Ti-22Al-23Nb composites were examined by Rosenberger et al. [29] who demonstrated improved mechanical performance for those composite properties that were fiber-dominated. More recently, an Air Force program [30] is conducting an extensive mechanical property assessment of the Ultra SCSTM/Ti-22Al-26Nb system including tensile, fatigue, fatigue crack growth and creep behavior. Finally, although all of the aforementioned studies were conducted on composites using foil as the input material for the "O" matrix, current studies are examining powder-based processes (and wire) for fabricating ternary and higher order matrix systems [31].

In order for this new class of TMCs to function in a high temperature environment (up to 700°C) for extended periods of time (1000's of hours), matrix oxidation and interstitial embrittlement of the O matrix needs to be addressed.

Studies by Cerchiara et al. [32] and Brindley et al. [33] suggest that this material system will have to be protected by an environmental coating or functionally graded layer to be considered for full life applications at temperatures $\geq 600^{\circ}\text{C}$. Preliminary efforts have been undertaken in an attempt to mitigate the oxidation and embrittlement issue via matrix coating [34].

The following review will discuss in detail the development of this important class of TMCs including: matrix development, fiber studies, fiber/matrix interface research, processing studies and mechanical behavior. It will conclude with a summary of the status of their development.

III. SiC Fiber Reinforcements

Microstructure and Properties

O TMCs studied to date have exclusively utilized continuous SiC fibers as the reinforcement medium. The fibers which have been primarily investigated include: 1) Textron's SCS-6™; 2) Textron's Ultra SCS™; 3) Atlantic Research Corp.'s (ARC) Trimarc 1® and more recently, 4) ARC's Trimarc 2® fiber. Details regarding each fiber will be presented in turn.

The SCS-6™ fiber is ~142 μm in diameter and is produced via chemical vapor deposition (CVD) in a single-stage reactor. A schematic of the fiber is shown in Figure 1. The salient features of the fiber architecture include a 33 μm diameter carbon monofilament (CMF) core (originally spun from a coal-pitch based material) which is then sealed by a ~1.5 μm thick overcoat of pyrolytic carbon. The pyrolytic coating is added to smooth the substrate surface and enhance the electrical conductivity of the fiber. The CMF and pyrolytic coating are in chemical equilibrium with the SiC such that there is no observable reaction between the two. Das [35] has determined by TEM selected area diffraction (SAD) that the SiC deposit has the β structure. This β SiC grows radially outward in a columnar fashion during the CVD processing and forms two distinct zones. The first zone which extends approximately 15 μm is relatively fine-grained (10-60 nm) and from a compositional standpoint is slightly carbon-rich [36]. Although not depicted in the schematic, Ning [37] has determined that the inner zone actually consists of three subzones with thicknesses starting at the pyrolytic coating of 6 μm , 4.5 μm and 4.5 μm , respectively. The second zone is approximately 35 μm wide and exhibits a coarser grain structure (70-140 nm) and is essentially stoichiometric in composition (Figure 2). The change in grain size is due to the change in chemistry of the SiC deposit. Casey et al. [36] had used Auger spectroscopy to determine that the inner layer of SiC is non-stoichiometric and is carbon-rich (55-60% C and 40-45% Si), while the outer region is essentially stoichiometric SiC. The interface where the grain size and chemistry changes occur, forms what is referred to as the fiber mid-radius. The β SiC in both zones is close-packed (face centered cubic) with {111} planes oriented radially. These subgrains have a large aspect ratio, with their length oriented in the radial direction. The external surface of the SCS-6™ fiber is coated with three carbonaceous layers which total ~3 μm in thickness. This triplex coating system serves two primary purposes: 1) to blunt intrinsic surface flaws resulting from the CVD of the SiC; and 2) to reduce susceptibility to strength degradation due to chemical reaction with titanium matrices. The first layer of the coating system (adjacent to the SiC) is amorphous carbon, ~0.5 μm thick, and acts to "seal" the end of the columnar β SiC grains. The next two layers (i.e. double pass) are carbon-rich and are doped with β SiC crystallites. The approximate thicknesses of these inner and outer carbon layers are 1.0 μm and 1.5 μm , respectively. Casey et al. [36] determined that the inner layer was somewhat more C-rich (90 at% C, 10 at% Si) than the outer coating (80 at% C, 20 at% Si).

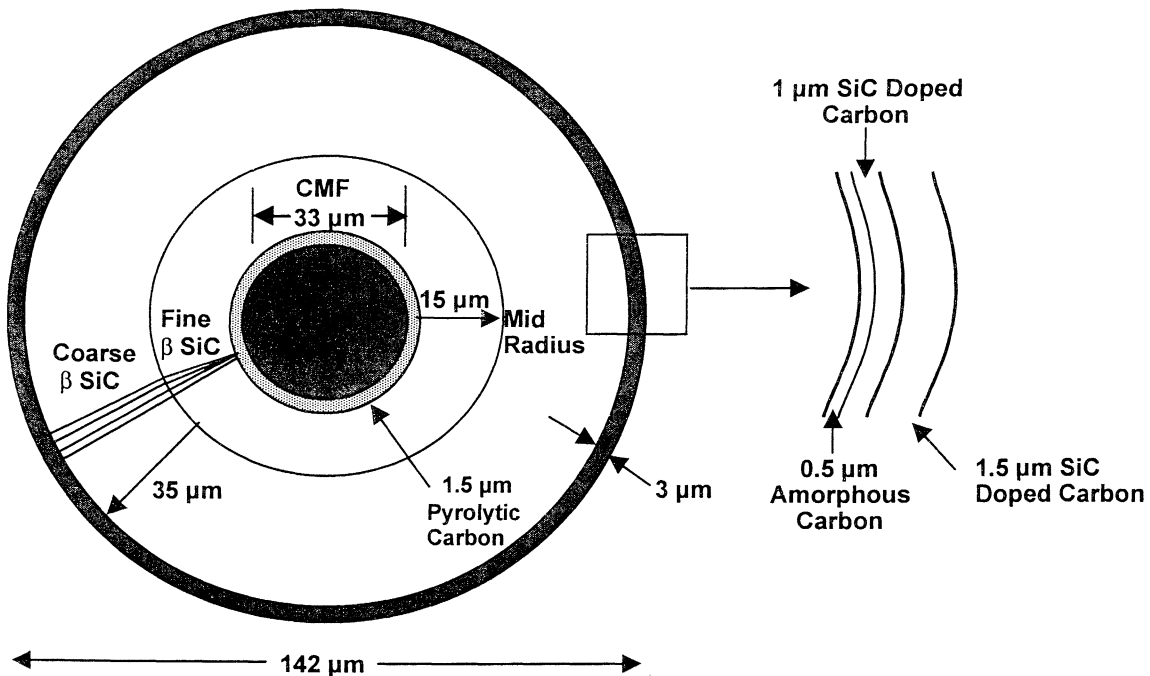


Figure 1. Schematic Showing the Architecture of the SCS-6 Fiber

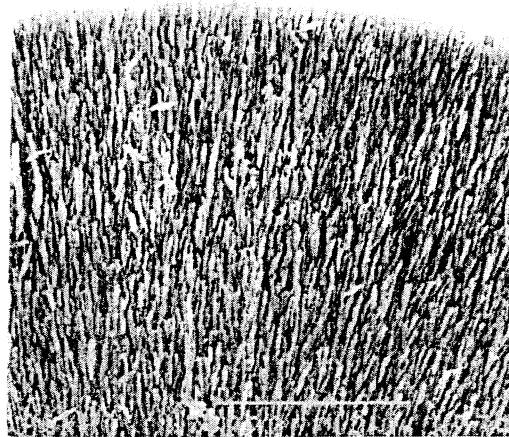


Figure 2. Columnar Growth of Course β SiC Portion of SCS-6 Fiber

The SCS-6TM fiber had essentially been established as the industry standard over the past 15+ years due to its relatively high strength and strength retention at elevated temperatures within TMCs. Figure 3 contains data from Smith et al. [9] showing tensile strength (UTS) versus probability of survival (POS) for SCS-6TM, in both the as-received condition, and after heat treatment (virgin fiber and extracted from a Ti-22Al-23Nb matrix). The heat treatment conditions used in the study were:

1085°C/2hr cool @ 2.8°C/m to 815°C/8hr/FC (sub-matrix β transus)
 1160°C/2hr cool @ 2.8°C/m to 815°C/8hr/FC (super-matrix β transus)

It can be noticed that the UTS at a 0.5 POS is on the order of 4400 MPa, with 93% of the fibers failing at strengths of ≥ 3000 MPa. Furthermore, sub-solvus and super-solvus thermal exposures had little effect of fiber UTS retention. These results are consistent with those reported by Gambone [11] wherein SCS-6TM fibers extracted from a Ti-22Al-23Nb matrix after 225 hours at 1000°C exhibited no strength reduction. Textron is currently selling the SCS-6TM fiber at \$2500/lb, and expects the price to drop to around \$1000/lb by the end of CY 2000 [38].

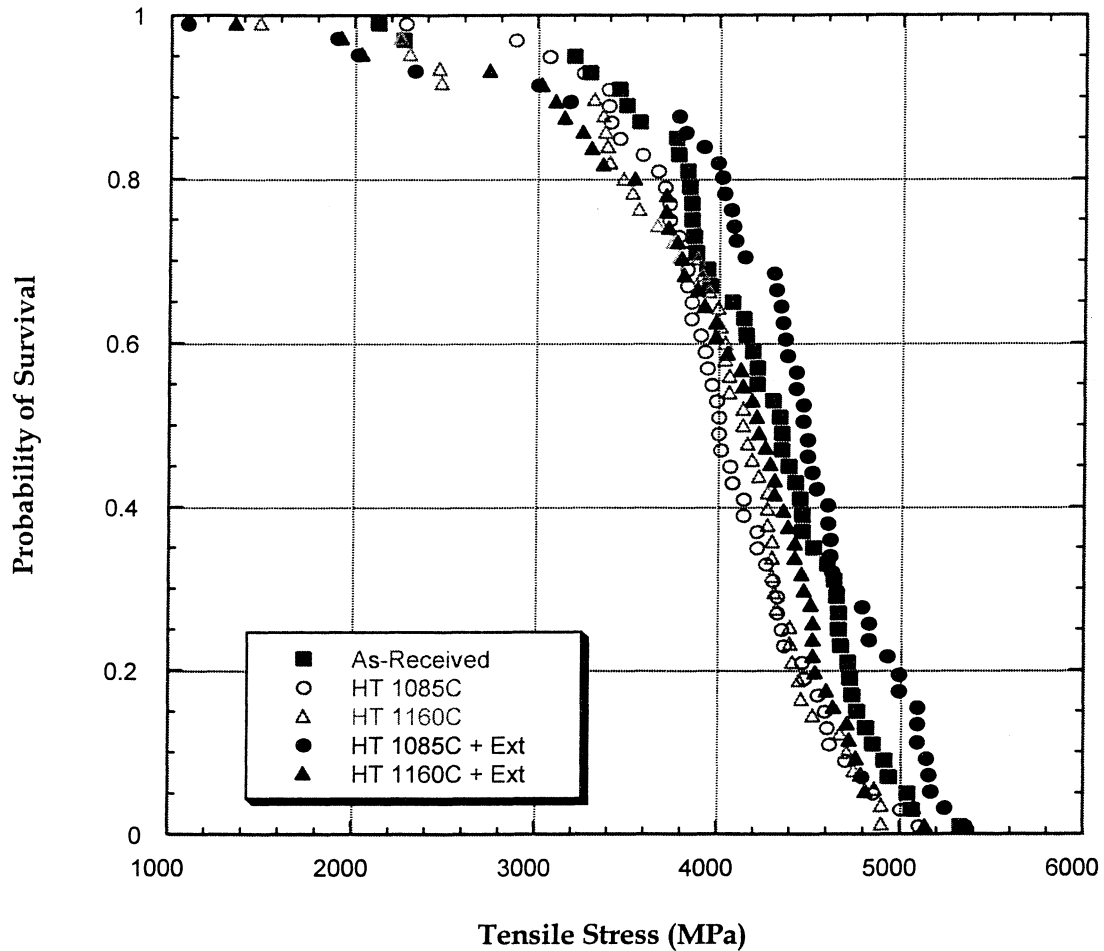


Figure 3. POS versus UTS Data for SCS-6 Fiber

The Ultra SCSTM fiber is ~140 μ m in diameter and was produced by Textron as an alternative to the SCS-6TM fiber for those applications requiring higher strengths. The fiber is produced via CVD in a single stage reactor. The architecture of Ultra SCSTM is in many ways similar to SCS-6TM. In Figure 4 it can be seen that, like the SCS-6TM fiber, Ultra SCSTM is deposited on a 33 μ m CMF, which is overcoated with a 1.5 μ m thick pyrolytic carbon layer. The microstructure of the SiC is equiaxed and much finer in scale than SCS-6TM

(Figure 5). Furthermore, since the fiber is produced in a single stage reactor, the growth process is continuous with the fine grain size transcending the entire fiber radius (i.e. from the pyrolytic coating on the CMF to the external surface coating). As such, there is no mid-radius observable for this fiber. Like the SCS-6™ fiber, the Ultra SCS™ utilizes a multi-layer coating system designed for improved handling characteristics and strength retention in titanium matrices. The coating system applied to the Ultra SCS™ is not only slightly thicker than the SCS-6™ fiber (~3.3 μm versus 3.0 μm), but there may be some chemistry and structural differences as well. However, these details have not yet been made available.

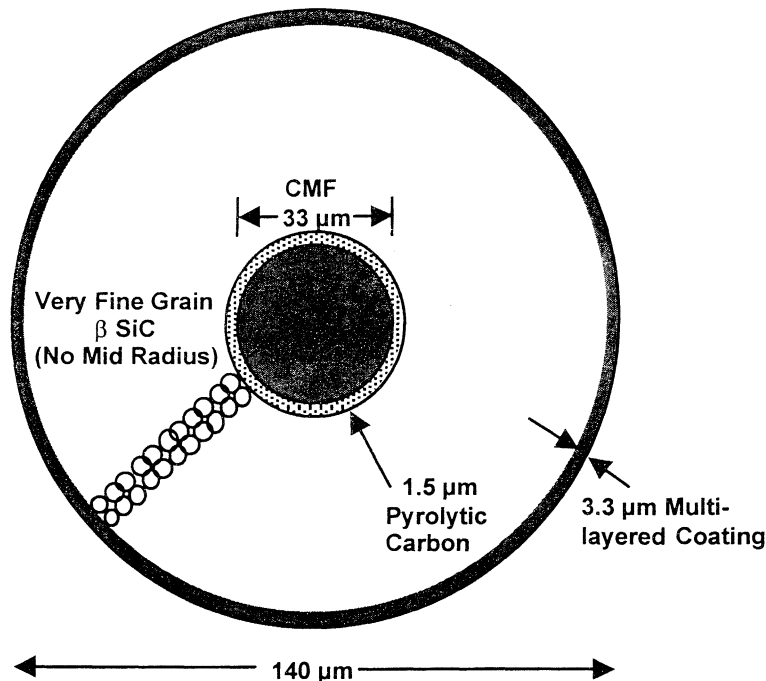


Figure 4. Schematic Showing Architecture of Ultra SCS™ Fiber

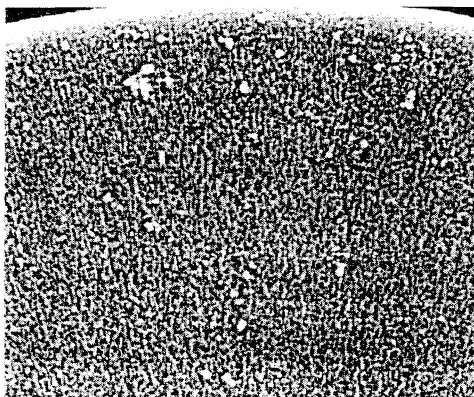


Figure 5. Fine-Grained Microstructure of SiC Portion of Ultra SCS™ Fiber

As was previously mentioned, the primary benefit of the Ultra SCS™ fiber compared to the SCS-6™ fiber is that of increased as-produced strength. Figure

6 shows the UTS versus POS data for the Ultra SCS™ fiber in the as-received and thermally exposed (virgin fiber and extracted from a Ti-22Al-23Nb matrix) conditions [9]. It can be noticed that the 0.5 POS as-produced strength is on the order of 5700 MPa. (Gambone found even higher as-produced 0.5 POS values (~6200 MPa) for a different batch of Ultra SCS™ fiber [39]). This strength is considerably higher than was previously measured for the SCS-6™ fiber (i.e. 4400 MPa). There appears to be a very modest effect of heat treatment on strength retention, with $\geq 80\%$ of the failures occurring at 4800 MPa, and $\geq 96\%$ at 4000 MPa. The increase in fiber strength is thought to be due to the very fine grain size present in the Ultra SCS™ system. In addition, it is possible that modifications to the external fiber coating system could also have contributed to this strength increase.

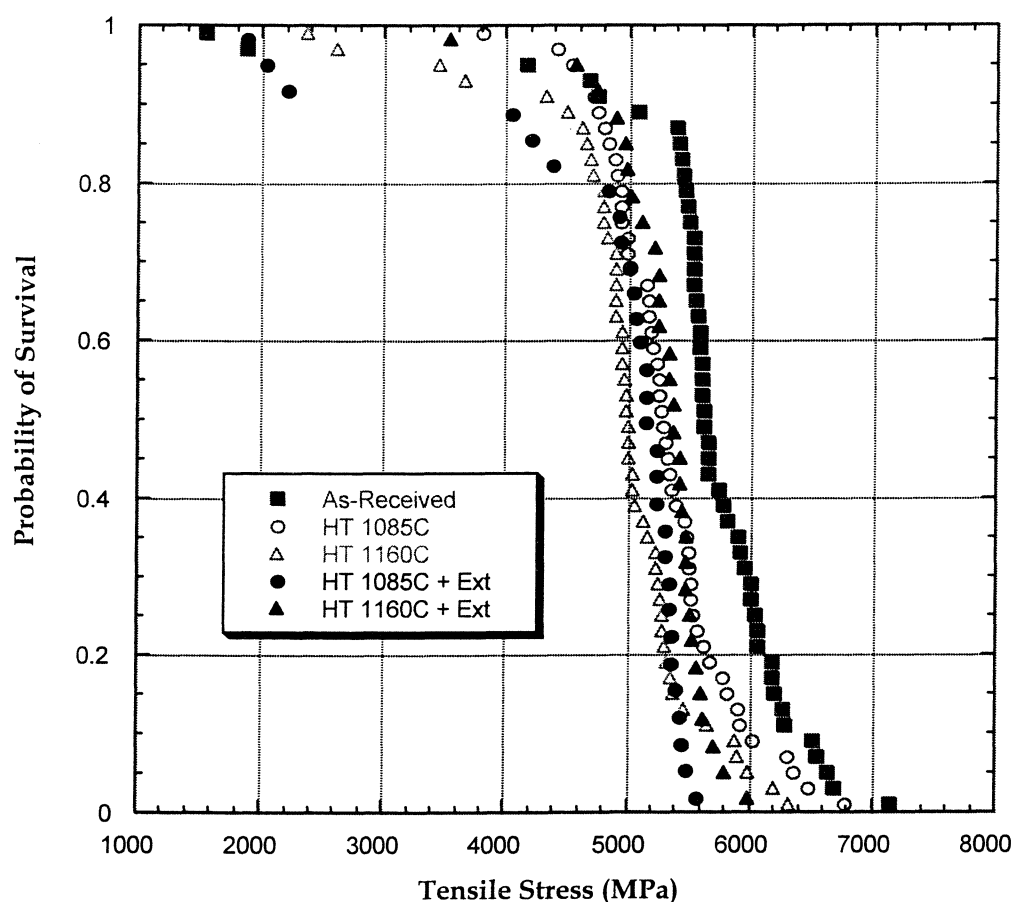


Figure 6. POS versus UTS Data for Ultra SCS™ Fiber

Textron has also made a very modest quantity (< 500 g) of an experimental large diameter (184 μm) Ultra SCS fiber. A schematic of the LD Ultra SCS fiber is shown in Figure 7, where it can be seen that the SiC is CVD deposited in a single stage reactor on a 42 μm CMF. In addition, the β SiC microstructure has a very fine grain structure (Figure 8) similar to that previously discussed for the Ultra SCS™ fiber which provided for the high strengths

observed for that monofilament. The external coating is multi-layered and is $\sim 2.4 \mu\text{m}$ in total thickness. Among the potential benefits of this larger diameter fiber are: 1) increased foil thicknesses can be used for the same fiber volume loading with the potential to decrease foil processing costs, and hence, composite costs; 2) increased inter-fiber spacings can be obtained for the same fiber volume loading, which may enable higher off-axis properties (strength and creep) to be realized; and 3) since the CMF does not carry any substantial load, higher volume fractions of the SiC portion of the fiber may lead to improved tensile strengths.

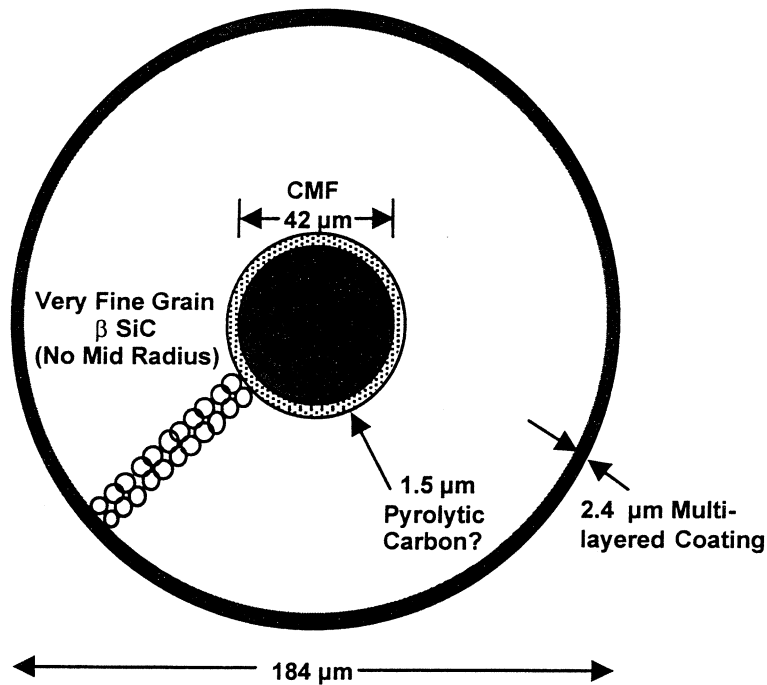


Figure 7. Schematic Showing Architecture of Large Diameter Ultra SCS Fiber

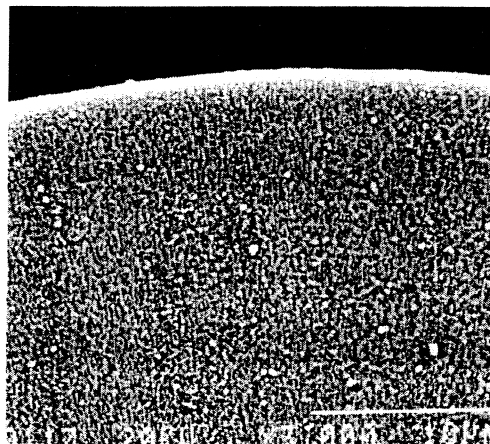


Figure 8. Microstructure of Large Diameter Ultra SCS Fiber

UTS versus POS data for the large diameter Ultra SCS fiber in the as-received condition and after thermal exposure (virgin fiber and extracted from Ti-22Al-23Nb matrix) is shown in Figure 9. The as-received fiber strengths (0.5 POS = 6300 MPa) are the highest of any of the SiC fibers discussed. This strength increase is thought to be the result of the fine SiC microstructure and the relatively higher volume fractions of the SiC portion of the fiber. Thermally exposed virgin fiber seems to show a modest, but finite decrease in strength, 13% after 1085°C exposure and 20% after 1160°C exposure. The β SiC grain structure appeared stable and no reaction between the CMF and SiC was observed or would be expected. Therefore, the cause of this strength reduction was not conclusively identified. Further strength debits to very low UTS values, 80% < 2000 MPa, were found for the thermally exposed and extracted fibers. This debit appeared to be associated with the non-optimized external coating thickness. Due to insufficient markets, the large diameter fiber is not being commercially produced at the present time, but should needs arise; Textron is willing to continue the development and production of this promising fiber [38].

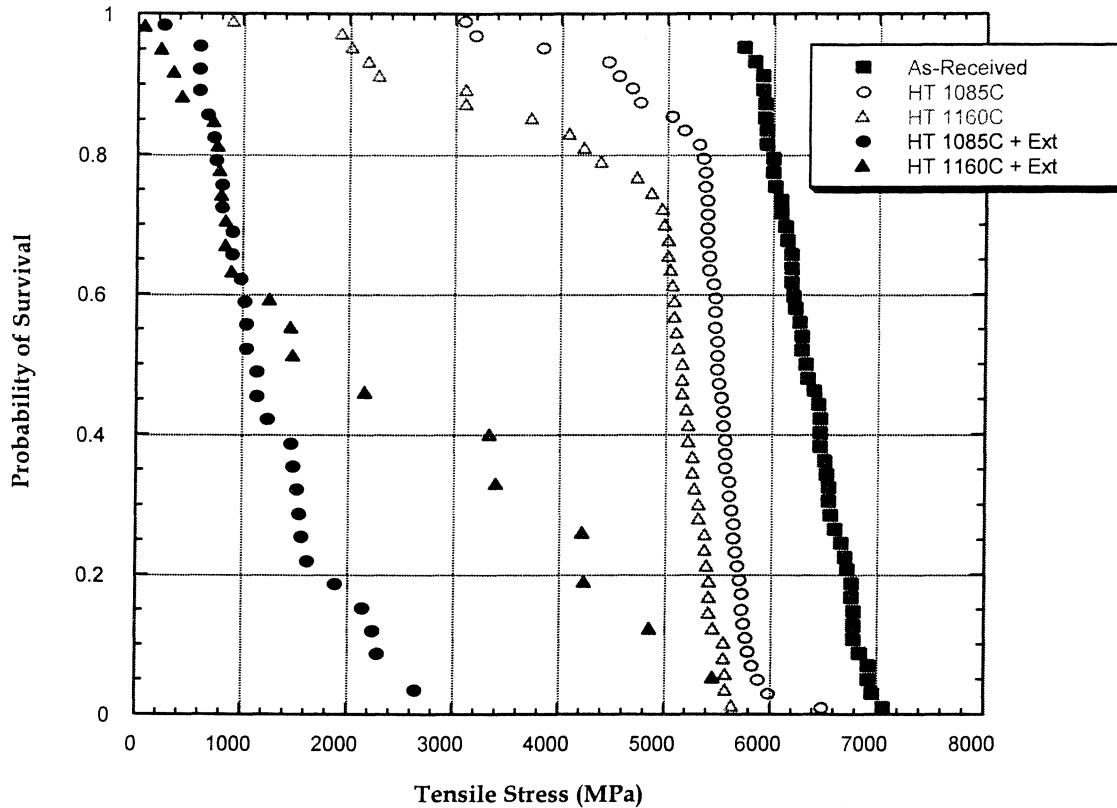


Figure 9. POS versus UTS Data for Large Diameter Ultra SCS

The Trimarc[®] 1 fiber is a first generation continuous SiC filament developed by Amercom, Inc., (formerly a subsidiary of Atlantic Research Corp) in a multi-stage “flexible” reactor via CVD. The fiber structure is shown schematically in Figure 10. The salient features of the ~127 μ m diameter

Trimarc® 1 fiber include its deposition upon a 12.5 μm tungsten core. The β SiC deposit grows radially outward in a columnar fashion (Figure 11), and is protected at the surface by a triplex coating system. The cubic β SiC {111} close-packed planes orient normal to the radial direction. The external fiber coating is applied in-line and consists of three alternating layers of “hard” and “soft” carbon, with individual layers ranging in thickness between 0.5 μm and 2.0 μm . The degree of hardness associated with the individual layers is dictated by the level and size of the dopant SiC particles. Details regarding the development and production of the Trimarc® 1 fiber can be found elsewhere [40].

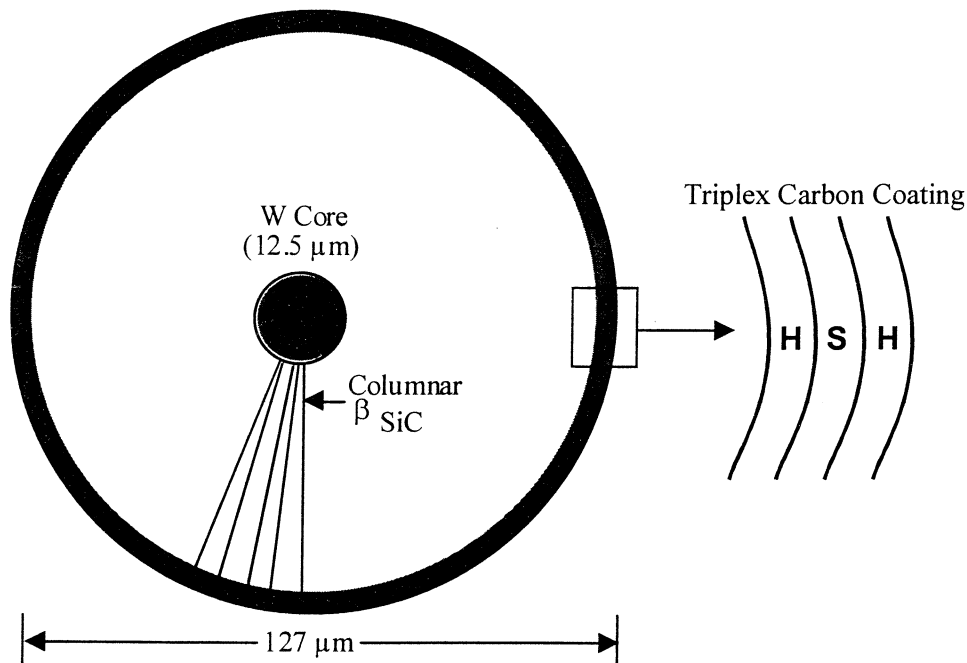


Figure 10. Schematic Showing Architecture of Trimarc® 1 Fiber

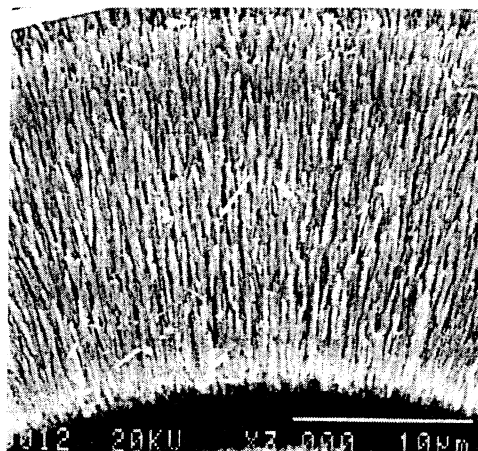


Figure 11. Columnar Growth of β SiC Portion of Trimarc® 1 Fiber

Unlike the SCS-6™ and Ultra SCS™ fibers which use a CMF that is chemically compatible with the SiC deposit, the Trimarc® 1 fiber tungsten substrate reacts with the SiC to form a layer of tungsten carbide, on the order of 0.38 μm thick in the as-deposited condition [9]. The outer portion of this chemical reaction layer contains Kirkendall porosity formed as the result of higher diffusivity rates of carbon relative to tungsten (Figure 12). Gambone and Gundel [10] previously demonstrated that this porosity could act as a stress concentration site and result in degradation of the fiber tensile strength.

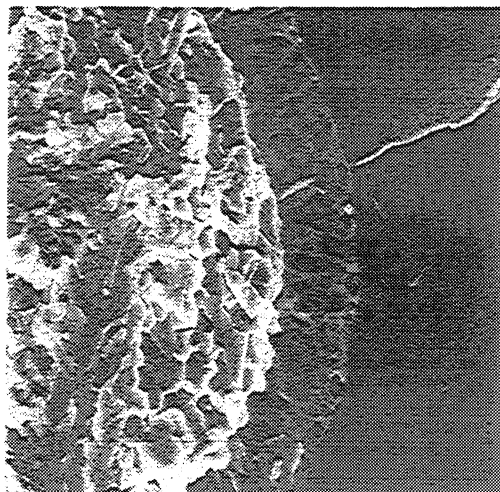


Figure 12. Kirkendall Porosity in W/SiC Reaction Zone of Trimarc®1 Fiber

Ambient temperature UTS versus POS data for the Trimarc® 1 fiber in the as-received and thermally exposed (virgin fiber and extracted from a Ti-22Al-23Nb matrix) conditions is shown in Figure 13. The 0.5 POS as-received strength is on the order of 3050 MPa, which is significantly lower than previously noted values for the SCS-6™ (4400 MPa) and Ultra SCS™ (5700 MPa) fibers. In addition, thermal exposure of the fiber at 1085°C and 1160°C (i.e. sub- β solvus and super- β solvus heat treatment temperatures for the Ti-22Al-23Nb matrix) resulted in 0.5 POS strength losses to 2700 MPa and 2150 MPa, respectively. Furthermore, similar thermal exposures within a Ti-22Al-23Nb matrix resulted in extracted 0.5 POS strength levels of 2200 MPa and 1650 MPa, for the 1085°C and 1160°C solutionizing temperatures, respectively. These reductions in UTS were due to continued reaction between the SiC and W-core and the associated porosity, with most of the failures occurring at, or near, the core region of the fiber [9]. Gambone and Gundel [10] concluded the W/SiC reaction was parabolic with time, which is consistent with a diffusion-controlled reaction. Furthermore, they concluded there was a range of exposure times and temperatures below which the Trimarc®1 fiber would not experience strength degradation. These values were 1100°C/2hr for composite consolidation, and 750°C for composite use temperature. They also noted that the modulus of W-core/SiC fibers (410-430 GPa) is generally greater than for C-core/SiC fibers (370-400 GPa), which may provide an advantage in stiffness critical applications.

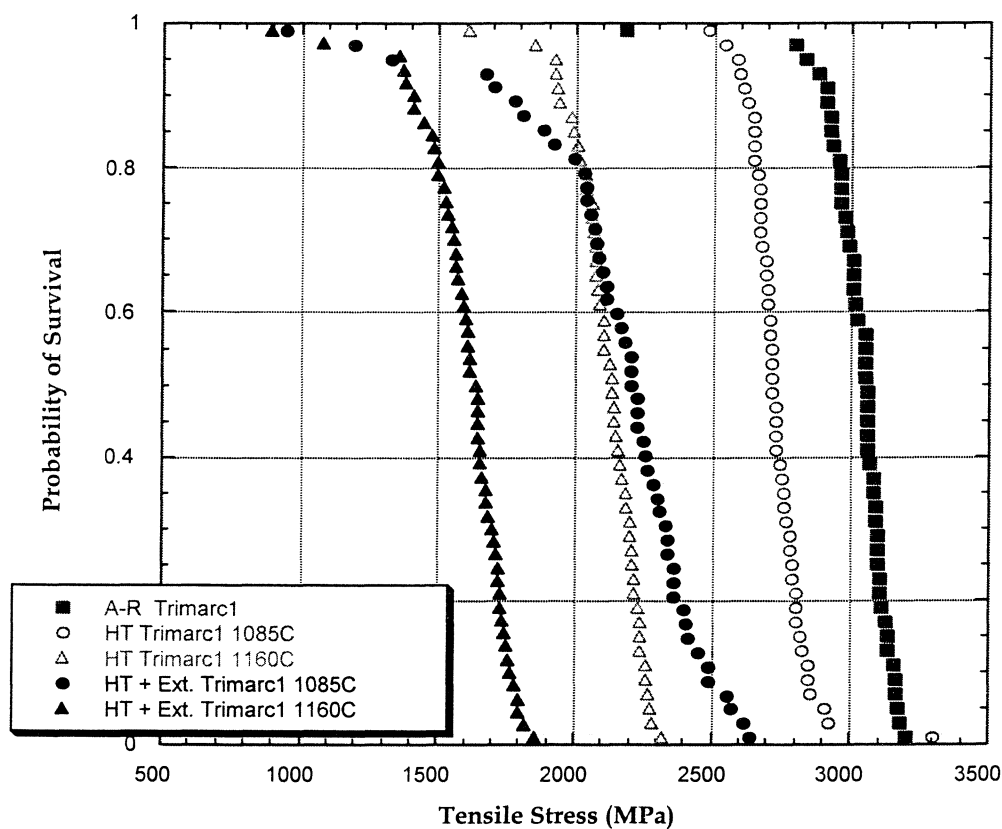


Figure 13. POS versus UTS Data for Trimarc[®]1 Fiber

More recently ARC in a joint venture with the 3M Corporation has developed a second generation continuous SiC fiber referred to as Trimarc[®] 2. Although little information was available at the time of this writing regarding the microstructure of the SiC portion of the fiber, as well as the external coating system, the primary difference between it and the first generation Trimarc[®] 1 fiber is that the second generation fiber is CVD deposited upon a 33 μm diameter carbon monofilament (CMF) which is coated with a 1-2 μm amorphous carbon layer. This ~140 μm diameter fiber is currently being manufactured by ARC at their newly acquired facility in Middleway, W. Va. UTS mean values for this fiber have been reported of between 4020-4450 MPa [42]. In addition, with the deposition on a carbon monofilament core, strength reductions observed in the W-core Trimarc[®] 1 fiber due to core/SiC reactions, should not occur in this second generation fiber. ARC indicated the price of both the Trimarc[®] 1 and Trimarc[®] 2 fibers [41] are similar to that of the Textron SCS-6[™] fiber.

Fiber/Matrix Reactions

The aforementioned fibers react with all titanium matrices, including orthorhombic-based titanium aluminides. However, due to the higher levels of refractory additions (i.e. Nb) present in O-based matrices, chemical reaction rates are considerably slower in O TMCs than for their predecessors based upon

the Ti_3Al phase [13], as can be seen in Figure 14. Rhodes [14] has performed the most extensive study of the fiber/matrix interface reaction in a SiC/orthorhombic composite. The system he studied via transmission electron microscopy incorporating electron diffraction and x-ray energy dispersive analysis was SCS-6TM/Ti-22Al-23Nb. The as-consolidated reaction zone consisted of at least three distinct layers with a total thickness of 0.3 μm (shown later in Figure 43). The zone adjacent to the fiber consisted of very fine equiaxed grains ($\sim 20\text{-}50\text{ nm}$) containing titanium carbides (TiC_{1-x}) and titanium silicides (Ti_5Si_3). The intermediate layer also was made up of equiaxed grains larger in size ($\sim 150\text{ nm}$) which were identified as a complex titanium carbide containing Al and Nb $(\text{Ti,Nb,Si})\text{C}_{1-x}$. The outer layer consisted of slightly elongated grains about 100nm wide, which were identified as complex titanium silicides containing Nb and Al: $(\text{Ti,Nb,Al})_5(\text{Si,Al})_3$. More details regarding the formation of these reaction compounds and the controlling mechanisms for the rate of their growth is discussed by Rhodes [14].

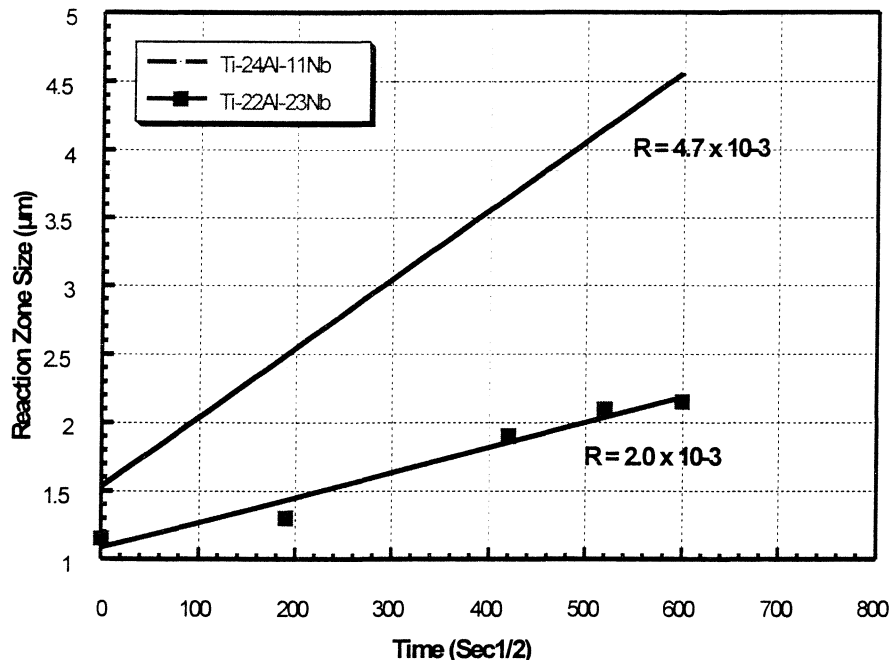


Figure 14. Reaction Zone Growth versus Time at 982°C for Ti-24Al-11Nb and Ti-22Al-23Nb

Since the outer coatings of all the SiC fibers discussed are similar in chemistry, one might expect similar types of reaction products to form for each in an "O"-based matrix. Smith et al. [9] has examined the formation of fiber/matrix interface reaction products for Trimarc[®] 1, SCS-6TM, Ultra SCSTM and large diameter Ultra SCS in a Ti-22Al-23Nb matrix. The Trimarc[®] 1 reinforced composite had seen a 1025°C/3hr exposure cycle during its consolidation, while the remaining fiber composites had been consolidated at 1100°C/3hr. The as-consolidated composites were subjected to post-consolidation solutionizing treatments of 1085°C/2hr (sub- β solvus) and 1160°C (super- β solvus), each of

which was followed by a direct aging treatment of 815°C/8hr. These heat treatments had been examined for potentially improving matrix-dominated mechanical performance in a parallel study [42]. Table I contains the fiber/matrix reaction zone and remaining external fiber coating thickness data for each fiber type in the as-consolidated and heat treated conditions. As would be expected, the lower consolidation temperature used for the Trimarc® 1 fiber composite resulted in the narrowest as-consolidated fiber/matrix reaction zone. Furthermore, it remained the thinnest with thermal exposure. One important observation is that the initial coating thickness for the LD Ultra SCS fiber (2.41 μm) was significantly smaller than any of the other fibers studied ($\geq 2.88 \mu\text{m}$). As was previously noted the LD Ultra SCS fiber experienced a significant debit in tensile strength with heat treatment and extraction from the Ti-22Al-23Nb matrix. This debit is most likely the result of the non-optimized thickness (and perhaps, chemistry) of the external carbon coating for this fiber. An example of the as-consolidated fiber/matrix reaction zones for each fiber reinforcement in Ti-22Al-23Nb is shown in Figure 15.

Table 1: Fiber/Matrix Reaction Zone Size for SiC Fibers in Ti-22Al-23Nb

Condition	Trimarc® 1 (μm)	SCS-6™ (μm)	Ultra SCS™ (μm)	LD Ultra SCS (μm)
As-Consol'd Rxn Zone	0.51	0.93	0.65	0.72
Coating	2.88	2.90	3.30	2.41
1085°C Rxn Zone	1.15	2.02	2.30	2.17
Coating	2.98	2.68	2.93	2.31
1160°C Rxn Zone	1.98	2.48	2.78	2.69
Coating	2.35	2.02	2.75	1.93

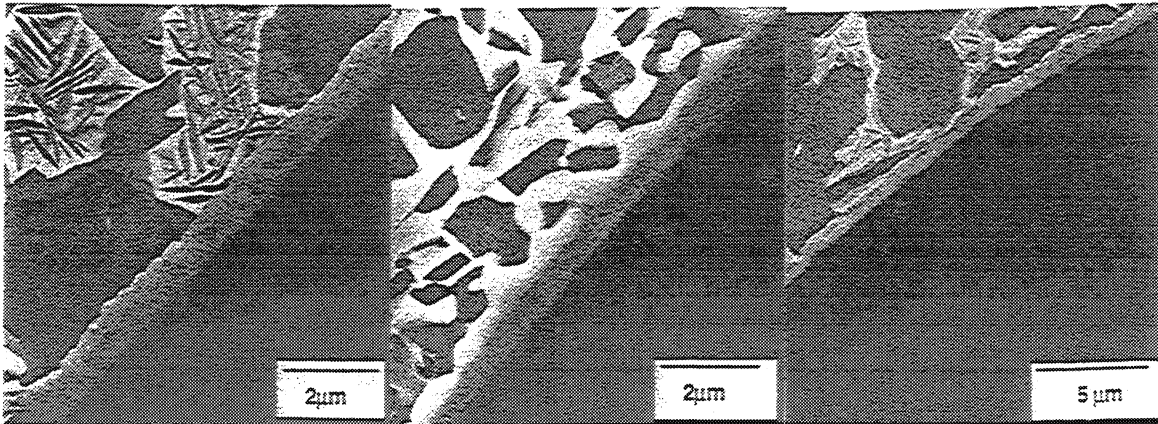


Figure 15. As-Consolidated Fiber/Matrix Reaction Zones for Trimarc®1, SCS-6™ and Ultra SCS™ Fibers in Ti-22Al-23Nb

IV. Matrix Development

Early Work

The development of orthorhombic titanium aluminide alloys for use as a matrix in a continuous fiber reinforced composite has followed from composite requirements. That is, alloys have been developed specifically for composite use, which is unique from earlier composite research in which alloys developed for monolithic applications were used in composites. The orthorhombic alloys now designed for use as composite matrices evolved from considerable research on basic ternary, Ti-Al-Nb, alloys.

As previously noted, the orthorhombic phase, Ti_2AlNb , was first detected in an 'alpha-two' alloy ($Ti_3Al + Nb$) by Banerjee and co-workers in 1988 [1]. It was then Rowe and co-workers who followed up Banerjee's work with studies of alloys based on the orthorhombic phase [43,44]. Mechanical property testing quickly showed that a single-phase orthorhombic alloy lacked room-temperature ductility and toughness, but that two-phase structures, $B2 + O$, were much more promising [44]. For instance, Ti-22Al-27Nb (all compositions by at. pct.) had room temperature fracture toughness values around $24 \text{ MPa}\sqrt{\text{m}}$ while those with higher Nb or higher Al showed values that were considerably lower [44]. Even more encouraging were the tensile yield strengths for which Ti-22Al-27Nb was far superior to existing α_2 alloys, Ti-24Al-11Nb, Ti-25Al-10Nb-3V-1Mo, and Ti-24Al-17Nb-1Mo, even on a density corrected basis, Figure 16.

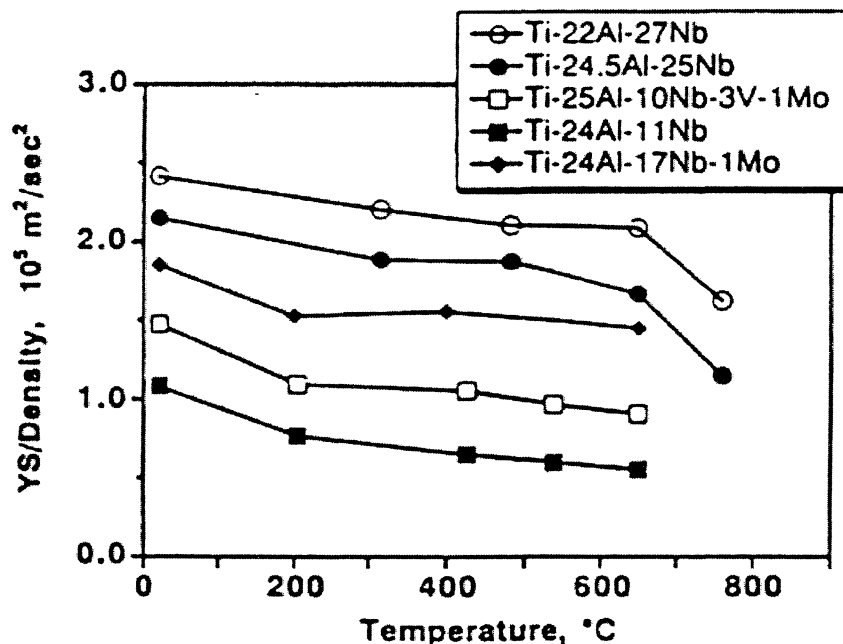


Figure 16. Density corrected tensile yield strengths (m^2/sec^2) as a function of test temperature for selected titanium aluminide alloys (from R.G. Rowe, Ref. 44).

Phase Equilibria

Phase diagram studies were carried out by several workers [45,46,47] in parallel with alloy development efforts. Kester-Weykamp et al. [48] summarized the results for a 900°C isotherm, Figure 17. The salient features in the area of interest are the existence of $\alpha_2 + B2$, $\alpha_2 + O + B2$, and O-phase fields. Das et al. showed that only the bcc phase exists at 1200°C over the composition range of interest [45]. However, there are scant additional isotherm data. Banerjee and co-workers [49] constructed a pseudo-binary phase diagram (isopleth) for Ti-27.5Al-Nb, Figure 18, and Miracle et al. [50] published an isopleth for Ti-22Al, Figure 19. Although the phase boundaries will shift to the left for lower aluminum or oxygen levels and to the right for higher aluminum or oxygen, the diagrams in Figures 18 and 19 show that the $\alpha_2 + B2$ and $\alpha_2 + B2 + O$ phase fields are much broader for an alloy such as Ti-22Al-23Nb than for an alloy such as Ti-22Al-27Nb. Consequently, the volume fraction of α_2 is typically higher in Ti-22Al-23Nb than in Ti-22Al-27Nb.

The ordered bcc phase, designated B2, extends over a broad temperature and composition range and varies by alloy composition range. For instance, Kester-Weykamp et al. [48] demonstrated that Ti-24Al with 11 or 20 Nb is disordered at 1200°C (single-phase bcc field), but that Ti-24Al-30Nb is ordered at that temperature. Consistent with this observation, Muraleedham et al. [46] reported the order/disorder temperature for the bcc phase in Ti-24Al-15 Nb to be 1130°C. Rhodes has recently shown that the order/disorder temperature in Ti-21Al-26Nb is ~1070°C and that the order/disorder temperature tends to be ~20°C above the $\beta/(\beta + \alpha_2)$ transus temperature [51].

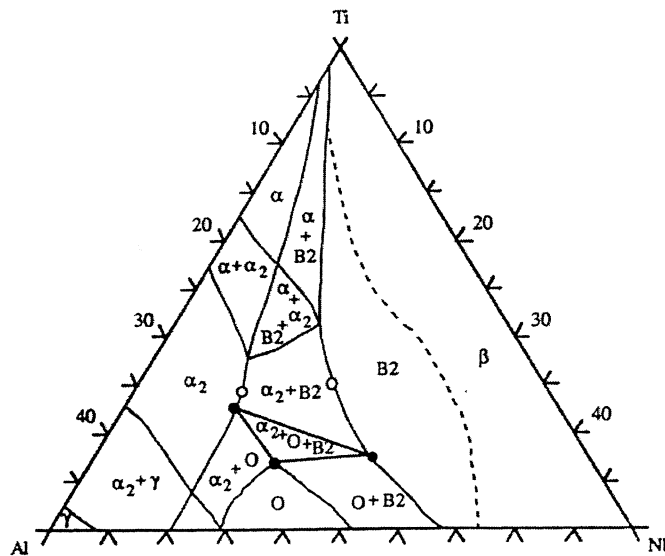


Figure 17. Proposed Ti-Al-Nb phase diagram at 900°C (from Kester-Weykamp et al., Reference 48)

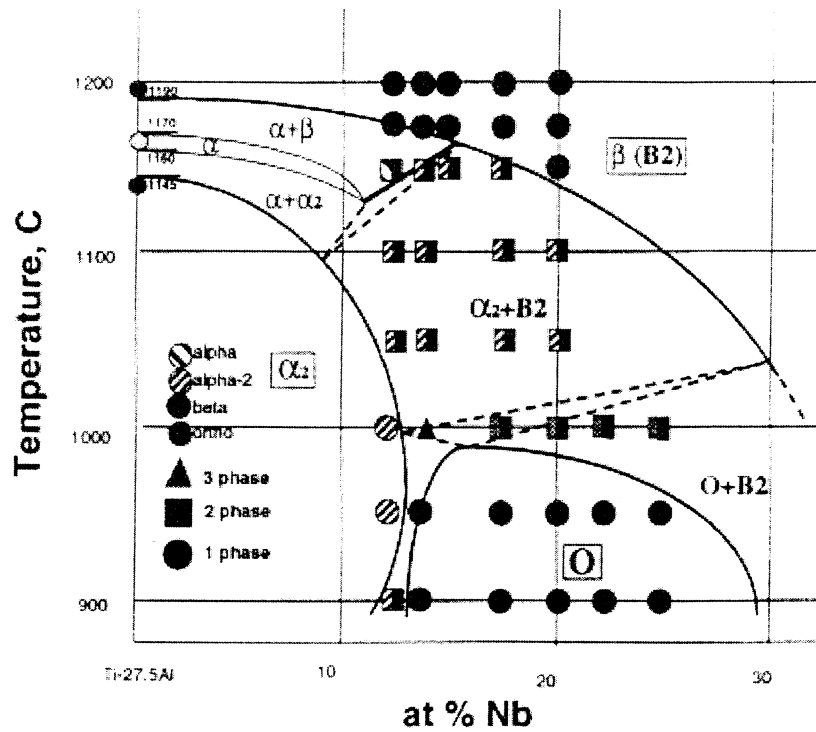


Figure 18. Ti-27.5Al vertical section. (From Banerjee et al., Ref. 49)

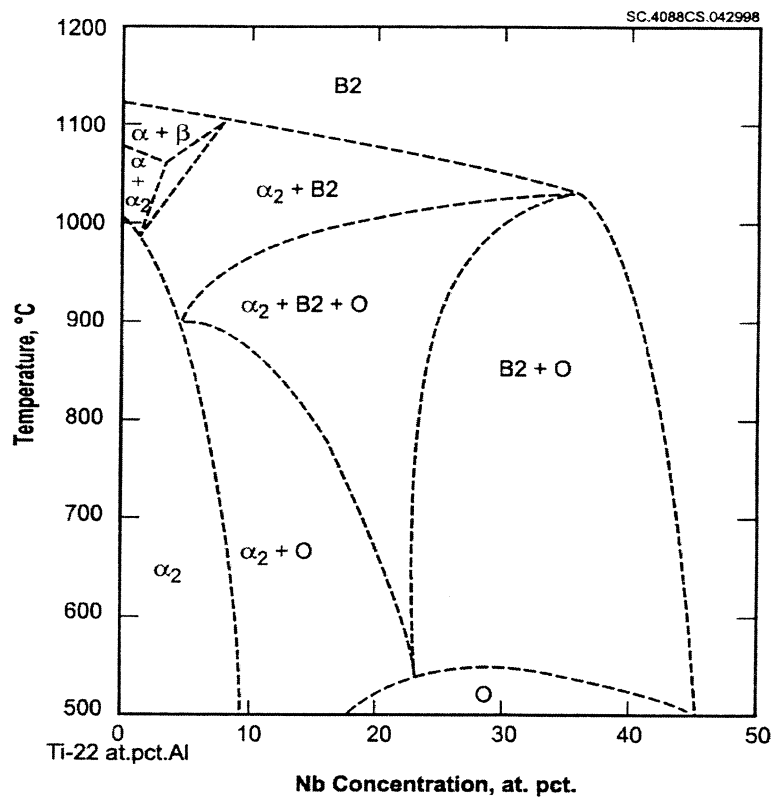


Figure 19. Ti-22Al - Nb isopleth (From Miracle et al., Ref. 50)

Additional Studies

The encouraging results published by Rowe led others to explore the B2 + O alloys by examining alternate compositions [5]. From these studies, Ti-22Al-23Nb, with its lower density, emerged as equally promising as Ti-22Al-27Nb. For instance, a nominal Ti-22Al-23Nb (actually Ti-21Al-22Nb) alloy exhibited density-corrected tensile strengths superior to Ti-24Al-11Nb for all temperatures tested (up to 760°C), Figure 20. These encouraging early results spawned numerous studies of alloy development, processing, and composite fabrication.

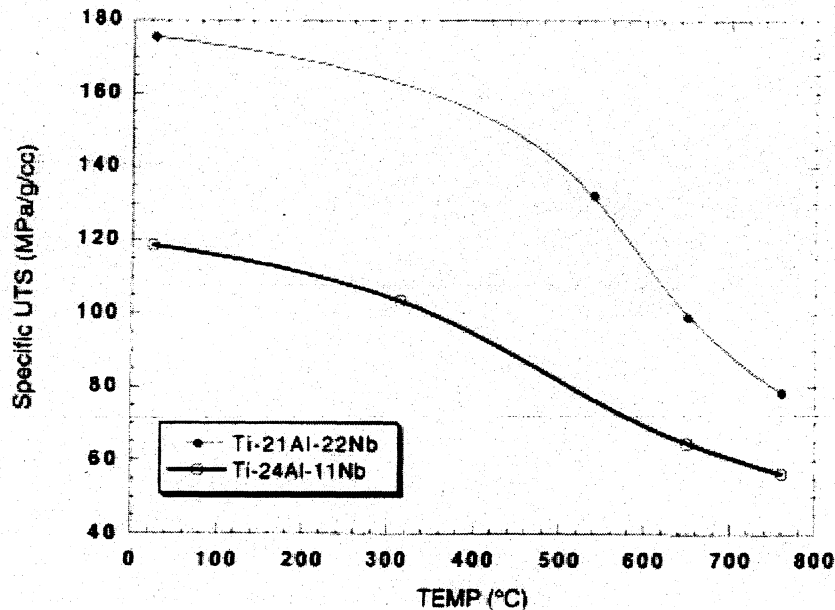


Figure 20. Density corrected tensile strengths for Ti-21Al-22Nb and Ti-24Al-11Nb (from Smith et al., Reference 13)

Applications of Composites and Property Requirements of Matrices

The use of Ti matrix composites (TMCs) is being evaluated for a variety of turbine component applications, including exhaust nozzle actuation links, frame struts, mounting links, fan blades, guide vanes, bladed rings (blings), bladed disks (blisks), impellers, shafts, and ducts. For many of these applications, operating temperatures do not exceed 540°C (1000°F), however, among those that do exceed 540°C are compressor rotors [8], as designed for demonstration within the Integrated High Performance Turbine Engine Technology (IHPTET) program.

Compressor rotating components, such as blisks/blings, impellers and remote rings, will need to operate at temperatures up to 760°C (1400°F) in an oxidizing atmosphere and will undergo high circumferential and moderate radial loading. Generic TMC property requirements for application of blisk/bling and impeller components have been calculated (using finite element analyses), from which matrix and matrix/reinforcement interface property requirements have been derived, Table 2 [8]. The matrix requirements were based on the

assumptions of 450 ksi (3103 MPa) fiber strength, a 35% volume fiber loading in the composite, and rule-of-mixtures properties in the composite.

Amato and Pank [52] have shown that approximately 2.5% room temperature ductility is required for the matrix to effectively load the SiC fiber and to overcome matrix/fiber CTE mismatch, thus obtaining rule-of-mixtures composite tensile strength.

Table 2: Matrix Property Requirements for Blisk/Bling and Impeller Applications (From Ref. 8)

Property	Blisk/Bling		Impeller
Tensile Strength, longitudinal (hoop)	760 MPa / 650°C (110 ksi / 1200°F)		>827 MPa / 705°C (>120 ksi / 1300°F)
Tensile Strength, transverse (radial)	242 MPa / 705°C (33 ksi / 1300°F)		>827 MPa / 705°C (>120 ksi / 1300°F)
Creep, longitudinal	290 MPa / 650°C (42 ksi / 1200°F) 10 hrs to 0.24% ϵ	290 MPa / 510°C (42 ksi / 950°F) 900 hrs to 0.24% ϵ	240 MPa / 620°C (35 ksi / 1150°F) 600 hrs to 0.5% ϵ
Creep, transverse	110 MPa / 705°C (16 ksi / 1300°F) 10 hrs to 0.24% ϵ	110 MPa / 565°C (16 ksi / 1050°F) 900 hrs to 0.24% ϵ	345 MPa / 620°C (50 ksi / 1150°F) 600 hrs to 0.5% ϵ
Low cycle fatigue	705°C (1300°F) 24,000 cycles 415 to 660 MPa (60 to 95 ksi)		485°C (900°F) 15,000 cycles 0.5% strain range
Thermal Cycle	Ambient to 815°C (Ambient to 1500°F)		Ambient to 705° (Ambient to 1300°F) 15,000 cycles

First Generation Alloys

Extensive studies on the ternary alloys that showed the most promise, Ti-22Al-23Nb and Ti-22Al-26Nb, have been reported. There have been phase equilibria, microstructure processing, microstructure/ properties, and environmental studies. This section will review the highlights of those research efforts.

Phase Equilibria Studies

A 900°C isotherm and a Ti-22Al isopleth were presented in Figures 17 and 19. Additional isotherms [8] are presented in Figures 21-24 for 1038°C (1900°F),

815°C (1500°F), 760°C (1400°F), and 650°C (1200°F). These diagrams are consistent with the isopleth shown in Figure 19. They indicate that, in the temperature range of 815°C - 650°C, the equilibrium phases in both Ti-22Al-23Nb and Ti-22Al-27Nb are O + bcc. Furthermore, it is evident that the equilibrium composition of the bcc phase is low in Al (<12%) and high in Nb (>30%). This is significant because Kestner-Weykamp et al. [48], and, more recently, Rhodes [8], have shown that the bcc phase will be disordered at this composition. Thus, whenever these alloys are processed at elevated temperature in the B2 or B2 + α_2 phase fields, the resultant microstructure will contain ordered bcc (B2) but that bcc phase will disorder on exposures at 815°C and below.

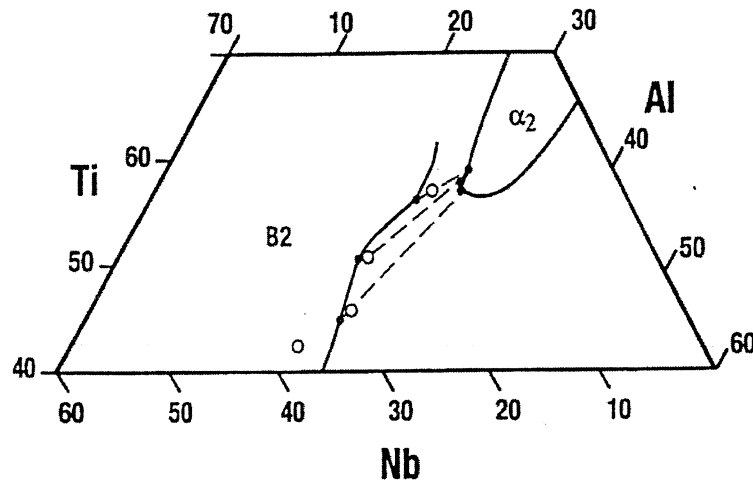


Figure 21. Portion of the Ti-Al-Nb ternary system at 1038°C (1900°F). (From Ref. 8)

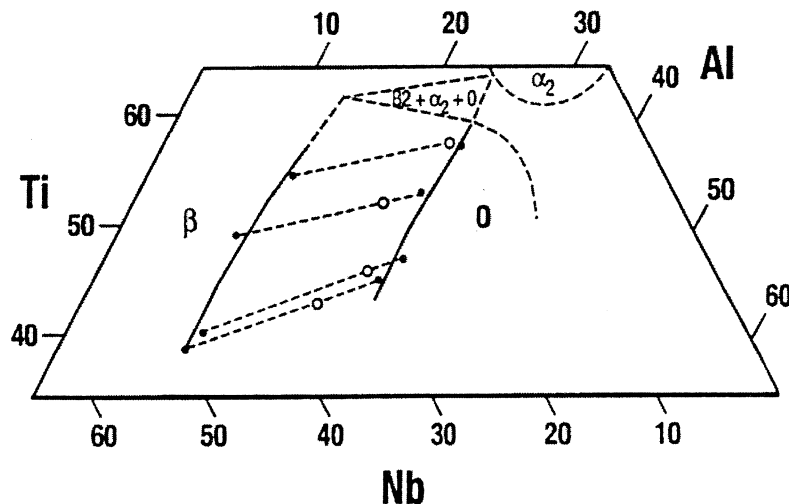


Figure 22. Portion of the Ti-Al-Nb ternary system at 815°C (1500°F). The three-phase field is speculation. (From Ref. 8)

Continuing to follow the isopleth of Figure 19, we see that cooling from the processing temperature puts the alloy through the three-phase field, α_2 +B2+O, and then, for an alloy like Ti-22Al-27Nb, quickly into the B2+O field. However, an alloy like Ti-22Al-23Nb, as it is cooled, will remain in the three-phase field to a much lower temperature, meaning that any primary α_2 formed at the higher temperature will persist to a much lower temperature. Of course, we know from the isotherms that Ti-22Al-23Nb will be in the two-phase field, B2+O, by the time it reaches 815°C, Figure 22.

Although the equilibrium phases are known, it will be kinetics that determines the actual microstructures in an alloy following any treatment. Typically, these orthorhombic alloys are processed (forged or hot rolled) in the two-phase, α_2 +B2, field to promote dynamic recrystallization without significant grain growth. After air cooling, the resultant microstructure consists of primary α_2 particles in a retained B2 matrix if the product is thin enough to cool fairly rapidly, Figure 25.

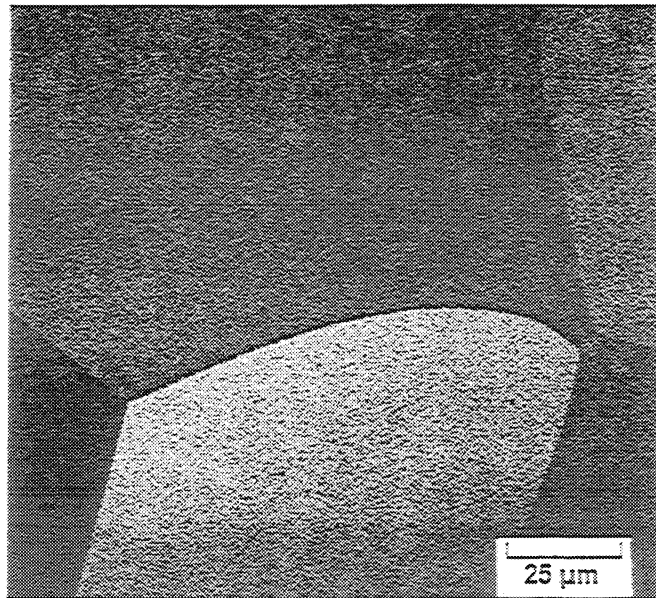


Figure 25. Ti-22Al-23Nb processed at 1025°C and rapidly cooled. Microstructure consists of retained B2 phase.

If the cooling rate is slower, however, such as in a larger forging, the B2 matrix will decompose into O-phase needles or platelets plus an enriched bcc phase. Unfortunately, the easiest nucleation sites are grain boundaries, resulting in large O-phase plates at these boundaries, Figure 26. These plates tend to act as crack nucleation and propagation sites when the material is subsequently stressed and are, therefore, undesirable features in the microstructure. Woodfield et al. [6] developed continuous cooling/transformation curves for Ti-22Al-26Nb, from which was extracted a processing procedure that includes a controlled cool at 50°C/hr from the processing temperature to 815°C (just inside the B2+O phase field) and a hold (for 4 hours) at 815°C to generate a more uniform

nucleation of the O-phase, Figure 27. It is now typically used as the cooling path during composite consolidation.

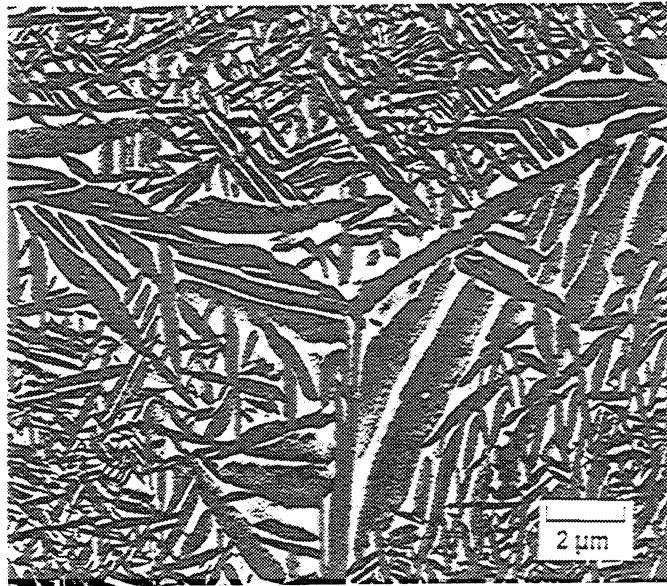


Figure 26. Ti-22Al-23Nb showing large O-phase platelets at grain boundaries.

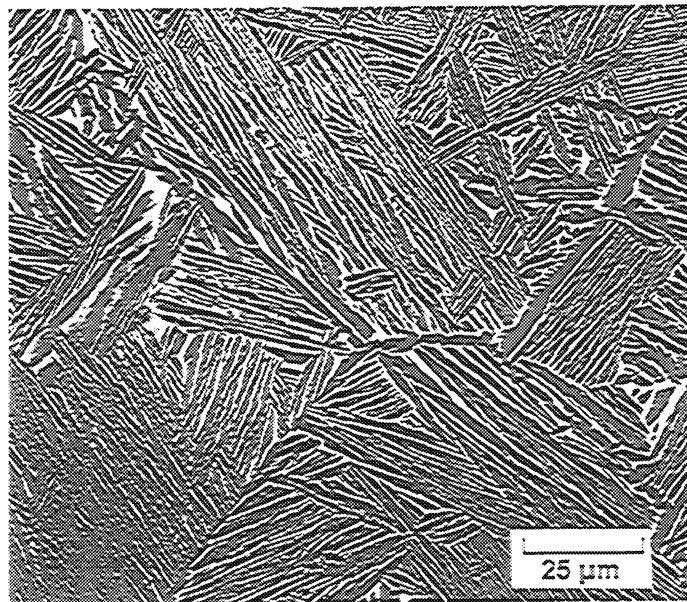


Figure 27. Ti-22Al-23Nb processed at 1025°C cooled at 50°C/hr to 815°C, held 4 hrs and a.c. Microstructure consists of transformed B2 matrix.

Transformation Mechanisms

The transformation mechanisms in these orthorhombic alloys containing ordered phases tend to be complex. For instance, when a metastable B2 phase

(i.e., B2 phase retained from high temperature via rapid cooling) is held for a period of time in the O+B2 phase field, it will decompose to the equilibrium O and bcc phases through a somewhat devious transformation path. The microstructure starts out as single-phase B2 and ends up as B2 (or β) precipitates in a continuous O-phase matrix, Figure 28. The transformation sequence has been described by Bendersky et al. as 1) complete transformation of B2 to faulted O-phase, 2) recrystallization of faulted orthorhombic phase, and 3) precipitation of B2 platelets or discs [3]. The first step, transformation from B2 to O, takes place very quickly; Bendersky et al. [3] observed the completion after only 15 minutes at 700°C. The second step, recrystallization of the O-phase, requires more time, on the order of 100-200 hours at 700°C, after which the precipitation of B2 phase follows rather quickly.

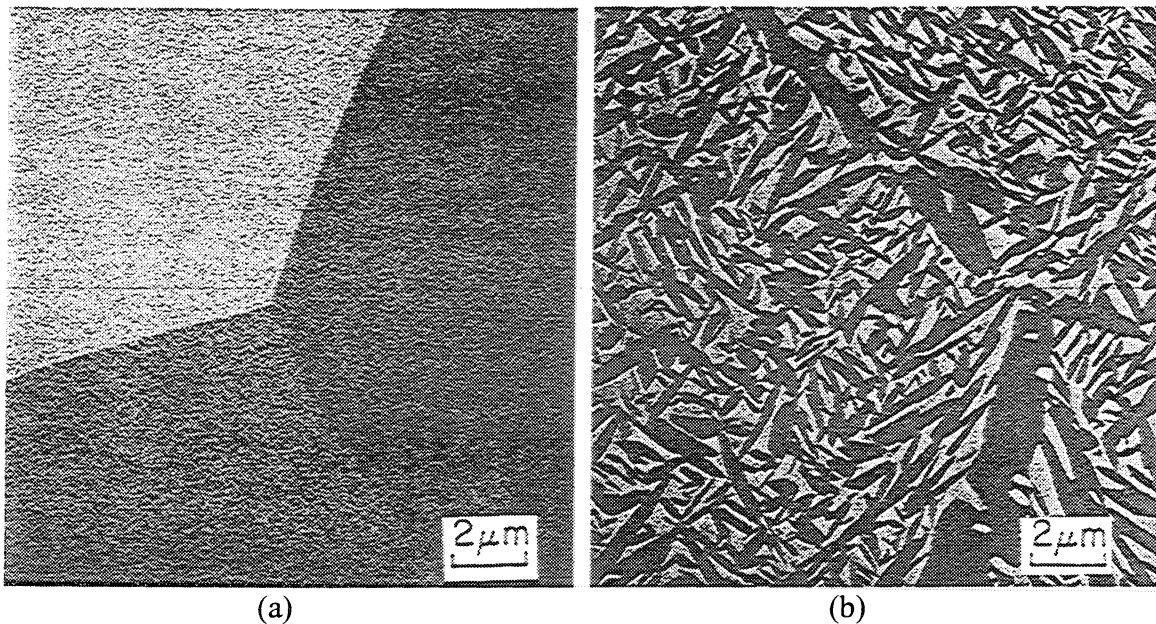


Figure 28. Ti-20Al-25Nb illustrating B2 \rightarrow O+B2 transformation. (a) quenched from 1038°C, 100% B2; (b) as in (a) plus aged for 1000 hours at 815°C, O + B2 phases.

Another of the complex phase transformations is that of primary α_2 -phase \rightarrow O-phase. When these alloys are hot worked in the B2 + α_2 phase field, large equiaxed primary α_2 particles are formed within the B2 matrix. Subsequent thermal exposures at lower temperatures typically do not alter the appearance of these particles, Figure 29. However, Banerjee et al. [1] suggested that the $\alpha_2 \rightarrow$ O or $\alpha_2 \rightarrow$ O+ α_2 transformation may take place *in-situ* as a phase separation reaction in these large particles. Using transmission electron microscopy, Rhodes has recently shown that this is indeed the mechanism for the transformation [53], as illustrated in Figures 30 and 31. A transformation reaction has clearly taken place during the exposure at 704°C, Figure 30, and tilting to a basal zone reveals the structure of the transformation, Figure 31. The overlapping basal zones in the electron diffraction patterns demonstrate that both

α_2 and O phases co-exist within the former α_2 particle, similar to that observed at the surfaces of α_2 particles in Ti-25Al-12.5Nb by Banerjee and co-workers [1]. The retention of some α_2 phase after 2000 hours at 704°C indicates that Ti-22Al-23Nb is in the three-phase field, B2 + O + α_2 , at this temperature, which is consistent with the isopleth shown in Figure 19.

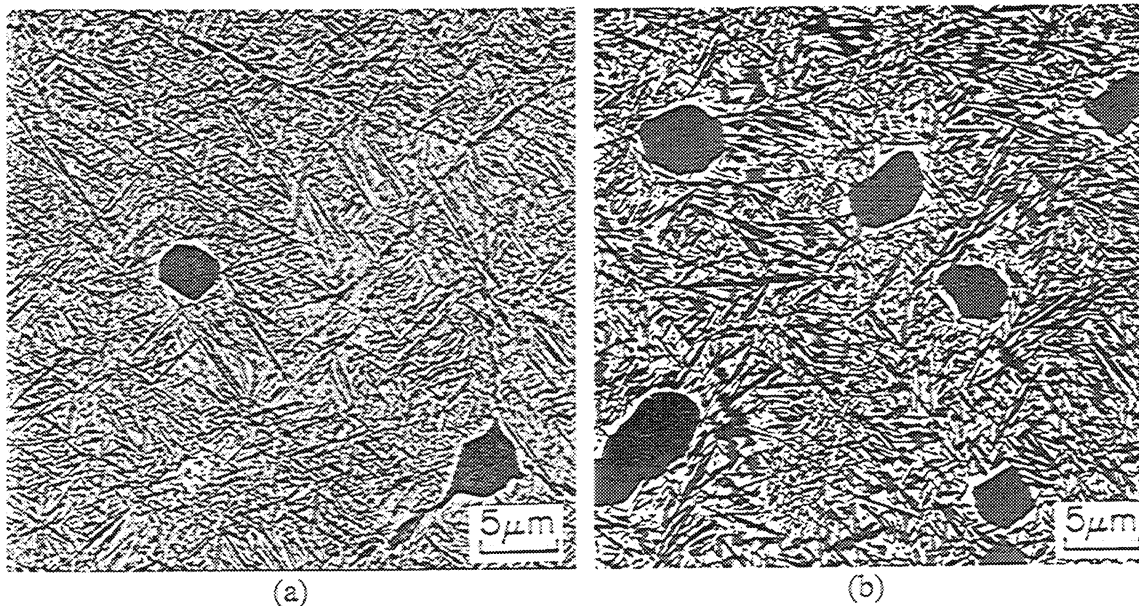


Figure 29. Ti-22Al-23Nb after hot working in B2 + α_2 phase field. (a) as hot worked showing primary α_2 particles in transformed matrix, (b) after 2000 hours at 704°C showing apparent retention of primary α_2 particles.

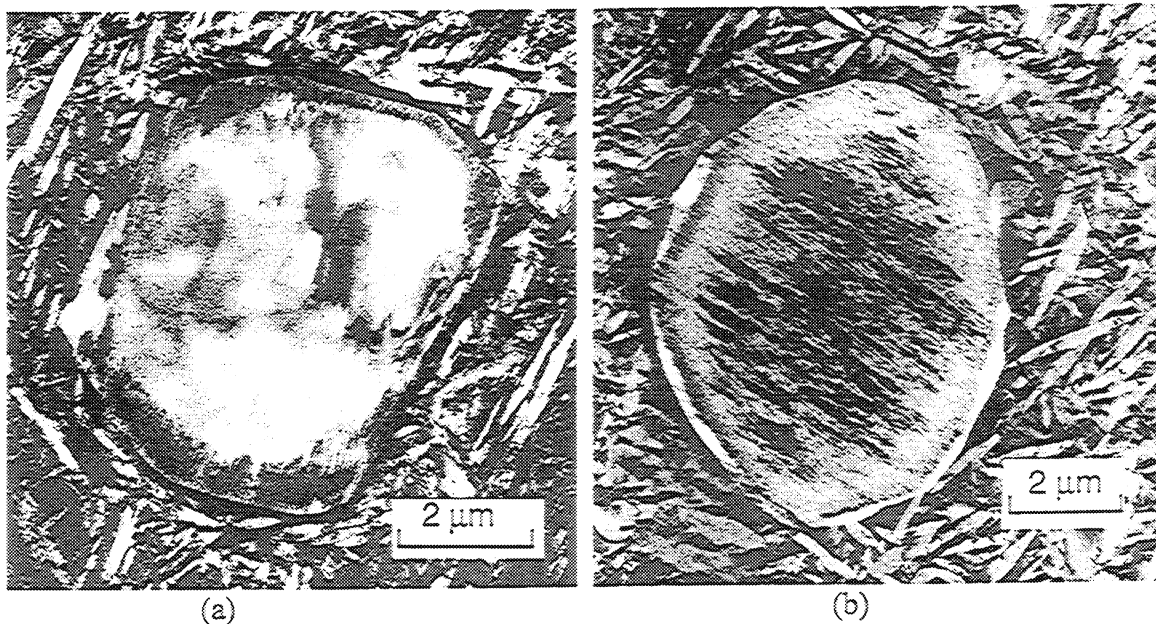


Figure 30. Primary α_2 particles in Ti-22Al-23Nb (a) hot worked plus slow cool, showing untransformed structure; (b) after 2000 hours at 704°C, showing *in-situ* transformation from α_2 to α_2 + O.

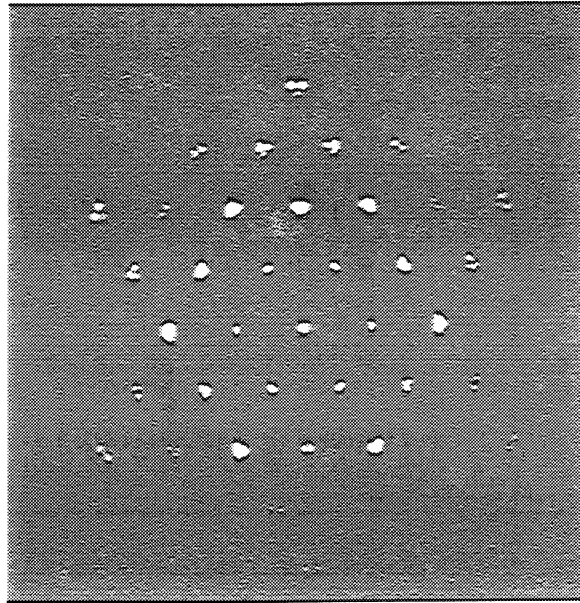


Figure 31. Electron diffraction from primary α_2 particle in Ti-22Al-23Nb. Pattern is analyzed as overlapping [0001] α_2 and [001] O.

Cellular Coarsening

There are many observations of discontinuous coarsening during low-temperature aging of orthorhombic alloys [8, 53, 54 55]. This phenomenon occurs in long-time aged material. However, it appears to be limited to a microstructure consisting of extremely fine O+bcc transformation product. For instance, when an alloy is quenched from the B2 or α_2 + B2 phase field, retaining the B2, and then aged in the temperature range of 815°C to 650°C, the resulting transformation product is extremely fine. Continued aging will eventually result in the formation of cellular coarsening nucleating at grain boundaries or inter-phase boundaries, Figure 32a. However, when the material is slowly cooled from the solution temperature, a much coarser transformation product is formed which resists subsequent cellular coarsening, Figure 32b.

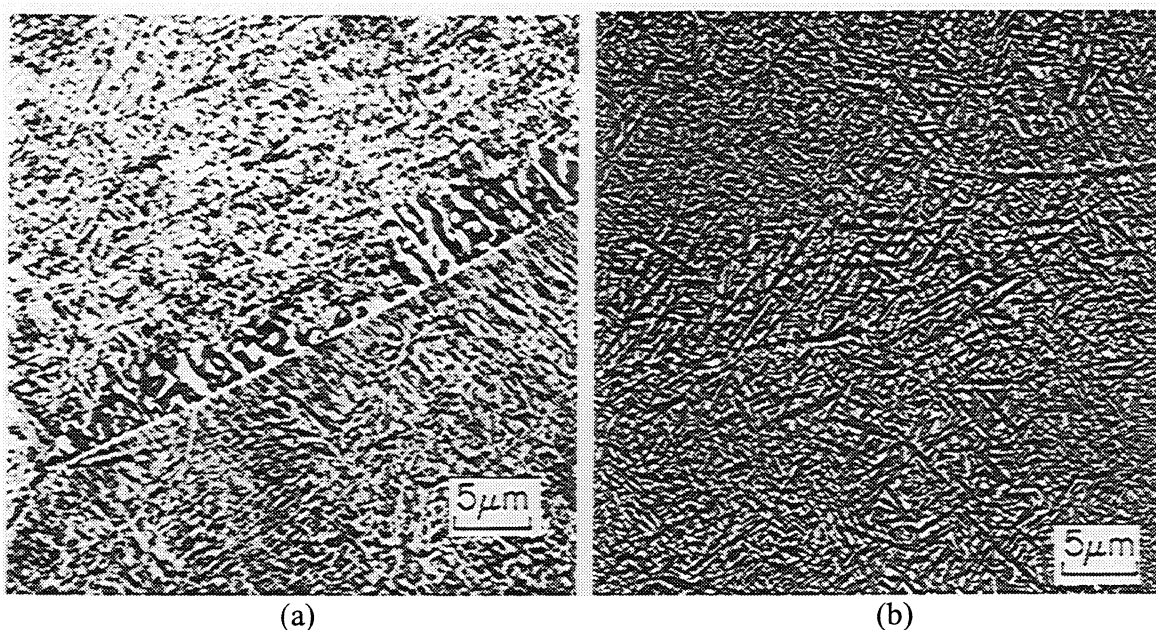


Figure 32. The effect of transformation product size on discontinuous coarsening in Ti-22Al-23Nb aged at 650°C. (a) Quenched from solution temperature and aged 100 hrs. (b) Slowly cooled from solution temperature and aged 100 hrs.

It is generally accepted that the driving force for discontinuous coarsening is a reduction in the chemical free energy of the system [56]. However, Yamabe et al. [56] has shown that the finer the primary precipitate structure, the more extended the discontinuous coarsening, suggesting a strong contribution of the interfacial free energy to the driving force of reaction. The observations made on orthorhombic titanium aluminide alloys also suggest that the O/B2 interface makes a large contribution to the driving force. This mechanism has also been put forth by Yi and Park [57] in their studies of discontinuous precipitation growing into a matrix that already contains continuous precipitate structure.

So, irrespective of the precise driving force, chemical or interfacial free energy, or both – the condition for discontinuous coarsening lies in the size of the O+bcc transformation product. A rule-of-thumb, then, is that in the case of a slow cool from the solution temperature, no discontinuous coarsening would be expected, whereas when there is a more rapid cool, discontinuous coarsening should occur after long-time aging. Thus, discontinuous coarsening should not be an issue in an orthorhombic matrix composite in which cooling is always slow following thermal exposures.

Oxygen Effects on Phase Equilibria

Being an alpha-phase stabilizer in titanium alloys, oxygen will have an effect on the phase boundaries in the orthorhombic alloys. For instance, Rhodes et al. [58] have shown the influence of oxygen on the $B2 \leftrightarrow B2 + \alpha_2$ transus temperatures of Ti-22Al-23Nb and Ti-22Al-27Nb, Figure 33. Clearly there is a strong influence of oxygen on the transus temperature, especially for Ti-22Al-

23Nb, where one might expect $\sim 7^{\circ}\text{C}$ increase in the transus temperature for each increase of ~ 100 wppm (350 appm) oxygen.

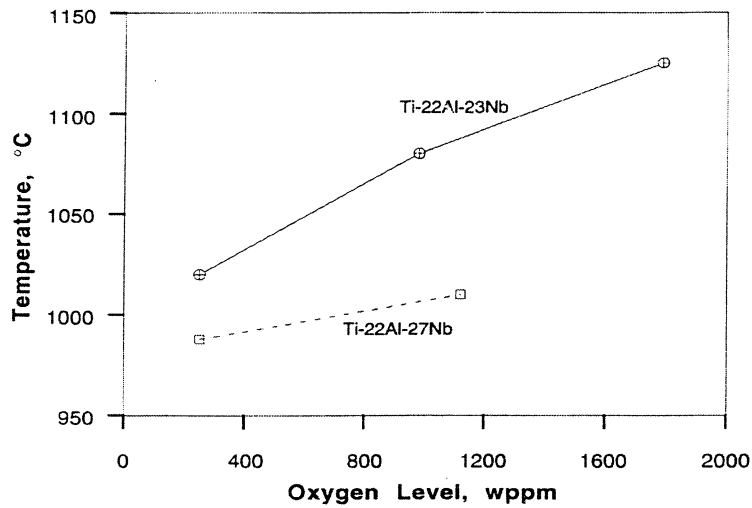


Figure 33. Influence of oxygen on the $\text{B2} \leftrightarrow \text{B2} + \alpha_2$ transus temperatures in Ti-22Al-23Nb and Ti-22Al-27Nb. [Ref. 58]

Heat treatments at 800°C and 900°C for 300-500 hours resulted in three phases, $\text{B2} + \alpha_2 + \text{O}$, in those Ti-22Al-23Nb materials containing ≥ 220 wppm oxygen, whereas no α_2 was detected in this alloy with 220 wppm oxygen [58], Figure 33. However, no α_2 was present in Ti-22Al-27Nb containing up to 1120 wppm oxygen when given the same heat treatments; only B2 and O phases were present [58], Figure 35. The observations for Ti-22Al-27Nb and the higher oxygen containing Ti-22Al-23Nb are consistent with the Ti-22Al-Nb isopleth in Figure 19. That is, at 800°C and 900°C , Ti-22Al-27Nb falls within the two-phase, $\text{B2} + \text{O}$, field; and varying the oxygen between 260 and 1120 wppm has not moved the $(\text{B2} + \text{O}) \leftrightarrow (\text{B2} + \alpha_2 + \text{O})$ phase boundary to the right of 27% Nb at either 800°C or 900°C . On the other hand, reducing the oxygen level of Ti-22Al-23Nb to 220 wppm has shifted the $(\text{B2} + \text{O}) \leftrightarrow (\text{B2} + \alpha_2 + \text{O})$ phase boundary significantly to the left, such that this alloy now lies within the two phase, $\text{B2} + \text{O}$, field at 900°C . Conversely, for oxygen levels > 900 wppm, the Ti-22Al-23Nb alloy falls in the three phase, $\text{B2} + \alpha_2 + \text{O}$, field at 900°C , as described by the isopleth in Figure 19.

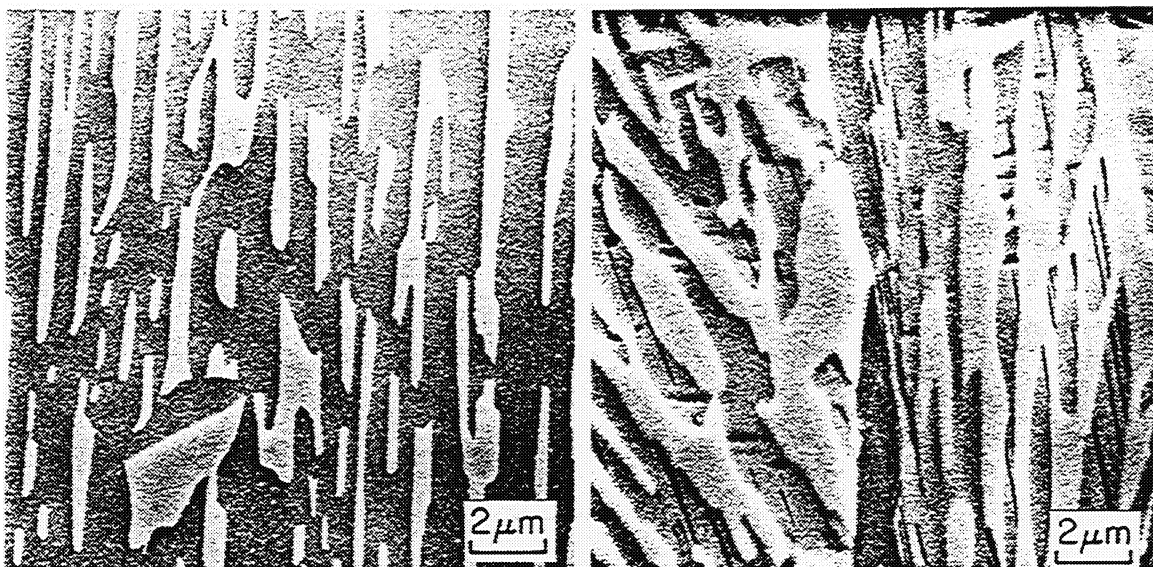


Figure 34. Ti-22Al-23Nb, beta solutionized and aged 500 hours at 900°C. (a) O+B2 in alloy containing 220 wppm oxygen; (b) , B2 + α_2 + O in alloy containing 980 wppm oxygen. [Ref. 58]



Figure 35. Ti-22Al-27Nb, beta solutionized and aged 500 hours at 900°C. O+B2 in alloy containing 1120 wppm oxygen. [Ref. 58]

Processing-related Microstructures

The use of orthorhombic titanium aluminide alloys as matrices in a fiber reinforced composite requires the production of foil ~0.13mm (5 mils) thick. Sheet and foil rolling techniques are thus significant in the processing. Hot rolling to some minimum thickness is followed by cold rolling to thin sheet and finished by

cold rolling to foil. The microstructure is basically determined by the hot-rolling parameters, although intermediate heat treatments in the cold-rolling stage can modify that structure.

Depending on the alloy composition and the finish temperature of the hot rolling procedure, a two-phase or a three-phase microstructure can develop. Typically, hot-rolled sheet is rapidly cooled (the thin gauge is sensitive to roller quenching and air cooling) and so the microstructure tends to be representative of that developed at the rolling temperature. For example, a finish temperature in the $B2 + \alpha_2$ phase field will result in primary α_2 particles in a single-phase B2 matrix, as was shown in Figures 25 and 29. When the sheet is finished at a lower temperature, in the $B2 + \alpha_2 + O$ phase field, the primary second phase may be either α_2 or O phase, depending upon the starting temperature of rolling. In either case, the matrix will be a fine mixture of B2 + O phases, as was shown in Figure 26.

Semiatin and Smith [59] have shown that the B2 phase does not recrystallize during hot working of Ti-22Al-23Nb in the temperature range of 1100°C (reheat temperature) to 950°C (calculated finish temperature). In their pack-rolling studies, they concluded that the rapid precipitation of either α_2 or O phase at B2 grain boundaries inhibited recrystallization [59]. It has been subsequently shown that post-rolling anneals can produce a recrystallized B2 matrix [23,60].

Microstructure/Property Effects

The microstructures developed during hot and cold rolling in the production of foil will not necessarily be the microstructures in the composite. That is, composite consolidation will alter the microstructure of the foil as it is integrated into the fiber-reinforced composite. Thus, mechanical properties of the foil prior to consolidation will be salient only to the extent that they influence consolidation parameters.

Tensile and creep properties have been reported for many ternary, Ti-Al-Nb, alloy compositions [1,5,42,54,61-63], but we will concentrate on Ti-22Al-23Nb and Ti-22Al-26 (or 27) Nb in this section.

Tensile Properties

Like conventional titanium alloys, mechanical properties of the orthorhombic alloys are sensitive to microstructure and to oxygen levels. When processed in the $\alpha_2 + B2$ phase field, equiaxed primary α_2 particles develop within the microstructure, while the cooling rate from the processing temperature controls the degree and size of the bcc decomposition product, O + bcc. Examples of microstructural effects have been reported by Smith et al. [42,62] and by Rowe et al. [61]. By changing the solution treatment temperature within, and above, the $\alpha_2 + B2$ phase field in Ti-22Al-23Nb, Smith et al. [42,62] found the room temperature tensile properties could be improved over those of the initial microstructural condition, Table 3. The best balance of properties was produced by the 1075°C / 2 hr solution treatment (all conditions included a 28°C / min. cool

to 815°C, followed by a hold at 815°C for 8 hrs and furnace cooling). Smith et al. concluded that the improvement in tensile properties is associated with an increase in the volume fraction of lenticular O-phase and a corresponding decrease in primary α_2 . Their work demonstrated that Ti-22Al-23Nb can be heat treated to improve tensile properties following composite consolidation.

Rowe and co-workers studied the effects of solution treatment and subsequent aging on tensile properties in Ti-22Al-27Nb [61]. Their results, shown in Figure 36, indicate that long-term aging leads to improved ductility and reduced strength. They suggested that coarsening of the two-phase O + B2 microstructures may contribute, but composition shifts during low temperature aging are more likely. This latter conclusion is most likely the proper one, as there is little, to no, coarsening of the O+B2 laths at this low temperature (760°C), and disordering of the B2 phase is associated with the composition shift.

Table 3: Effect of Solution Treatment on Tensile Properties in Ti-22Al-23Nb (from Smith et al., Ref. 42)

Condition	UTS (MPa)	YS (MPa)	Elong. (%)	Modulus (GPa)
As-fabricated*	972	805	8.4	105
1025°C/2hr**	1096	848	9.0	119
1050°C/2hr**	1111	836	14.8	121
1075°C/2hr**	1059	810	11.5	120
1100°C/2hr**	1053	926	4.0	135

* as-consolidated panel using non-reinforced 0.13mm (5 mil) foil.

**solution treatment followed by cooling at 28°C/min. to 815°C, held 8 hrs and furnace cooled.

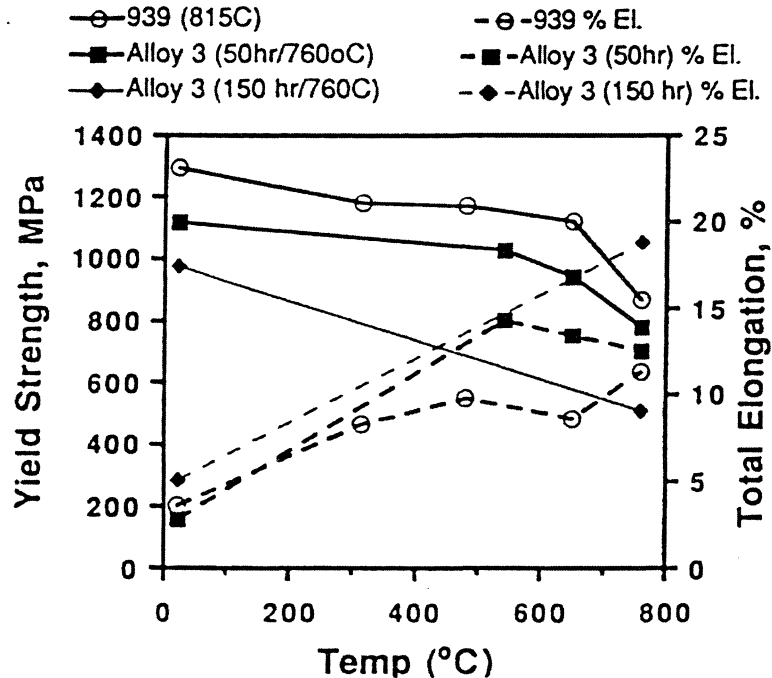


Figure 36. Comparison of yield strength and elongation of three heat treatments of Ti-22Al-27Nb. (From Rowe et al., Ref. 61)

Gogia and co-workers summarized the microstructural factors that influence tensile properties in the orthorhombic alloys [64]. They point out that the various parameters influencing yield strength are (1) volume fractions of α_2 /O and B2 phases, (2) strength of individual phases as affected by changes in composition with cooling rate, (3) grain size of prior B2 phase, (4) colony size, (5) lath size, and (6) dislocation substructure. The relative contributions will be different depending upon whether the solution temperature is above or below the B2/(α_2 +B2) transus [64]. For the former, the strength is controlled by the α_2 / O phase and its geometrical features and ductility is controlled by cleavage facet size [64].

For the sub-transus, i.e., α_2 +B2, treatment, Gogia et al. describe the strength in terms of rule-of-mixtures, in which the strength of the alloy is a function of the strengths of the primary α_2 and the aged B2 phases [64]. The strength of the aged B2 phase is, in turn, dependent upon the sizes and volume fractions of the decomposition products (α_2 , O, β). Generally, maintaining the volume fraction of primary α_2 at approximately 0.4 and reducing the sizes of the B2 decomposition products tend to increase the strength of the alloy. Ductility is also influenced by the sizes of the α_2 and O phases, as well as by the volume fraction of bcc phase [64]. Gogia et al. suggested that B2 phase delays the onset of cleavage and that its presence as a film around α_2 and O particles is significant in improving ductility [64].

Creep Properties

Banerjee et al. [49], Rowe et al. [61], and Smith et al. [13,65] have shown that the orthorhombic alloys exhibit improved creep resistance over the α_2/β alloys such as Ti-24Al-11Nb. An example of these early results is shown in Figure 37. This improvement appears to lie in the fact that the orthorhombic phase is significantly more creep resistant than the α_2 phase [42,49].

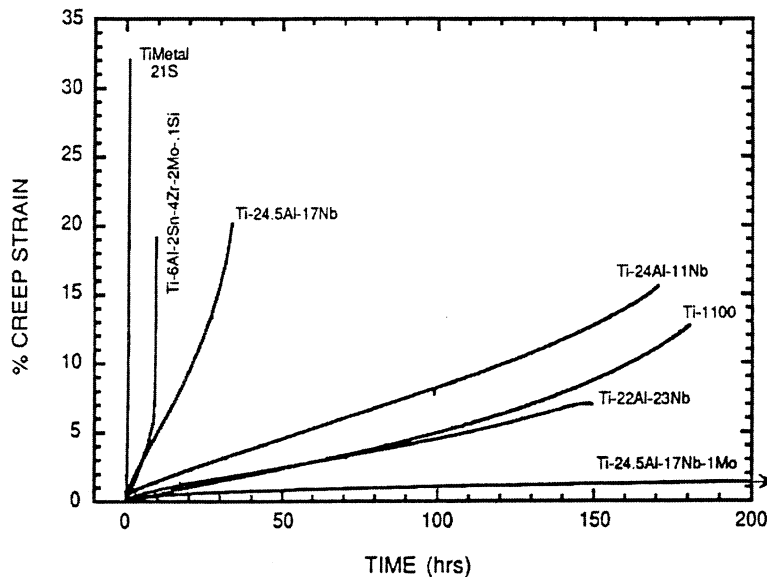


Figure 37. Full life creep behavior at 650°C/172 MPa for several titanium alloys. (After Smith et al., Ref. 65)

The design limits described in Table 2 define a maximum allowable creep strain of 0.24% for the blisk/bling and 0.5% for the impeller. In examining creep curves for the ternary orthorhombic alloys, it becomes clear that a significant portion of the allowable creep strain is consumed by primary creep [65,66]. Thus, comparing alloys by their steady-state creep rates, a generally accepted technique, does not adequately describe the material for these applications. Time to reach 0.24% or 0.5% strain is most meaningful for comparing these composite matrix alloys. Of course, testing at the specified temperatures and stresses is required to determine if goal properties are met. For test results obtained under other conditions, Larson-Miller plots are a convenient method for comparing alloys.

Another issue of concern in the creep testing of orthorhombic (and α_2/β alloys as well) is the development of surface cracks during test. The alloys are susceptible to oxygen intrusion which stabilizes and embrittles the α_2 phase. This embrittled surface layer then cracks under the creep load, initiating failure. Consequently, many creep tests are not a measure of the intrinsic strength of the alloy, but rather a measure of its oxidation resistance.

It is well established for titanium alloys that a lath or Widmanstätten structure offers better creep resistance than an equiaxed structure and the orthorhombic alloys are no exception [42,49]. For instance, Smith et al. [42]

demonstrated that a solution treatment above the beta transus resulted in improved creep behavior in Ti-22Al-23Nb, Table 4. The super-transus treatment produced a fully lath microstructure compared to the finer and lower volume fraction of laths in those treated below the transus. Note that all of the time spent in reaching 0.4% strain is in the primary creep regime.

Table 4: Effect of Solution Temperature on Creep Behavior of Ti-22Al-23Nb at 650°C / 172 MPa. (Beta Transus = 1100°C) (After Smith et al. Ref 42)

Condition*	Time to reach % ϵ , hrs.			Primary Creep, hrs
	0.2%	0.4%	1.0%	
As-fabricated	1.4	5.4	28	57
1025°C	3.0	12.4	63	180
1050°C	8.7	31.1	179	200
1075°C	8.5	41.0	290	220
1125°C	22.5	87.5	>300	225

* solution treated samples were cooled at 28°C/min. to 815°C and held for 8 hrs then furnace cooled

A somewhat strange phenomenon has been observed in the microstructure of $\alpha_2 + \beta$ processed Ti-22Al-23Nb (and other orthorhombic alloys) following long-time creep tests. Small dark features appear on the surfaces of the primary α_2 particles which have the appearance of creep cavities, and have been interpreted as such by several workers. However, a detailed study of these features has shown them to be α_2 -phase particles [67]. The growth of these α_2 particles is associated with the equilibration of the bcc phase during which there is the formation of high-Nb, low-Al β phase grains. As this Nb-rich β phase forms at and near the surfaces of the pre-existing primary α_2 particles (that are also undergoing an in-situ transformation to O-phase), the rejected Al promotes the formation of equilibrium α_2 phase. The creep test temperatures at which this phenomenon occurs (650°-760°C) fall well within the 3-phase, $\beta + \alpha_2 + O$, field, see Figure 19. Thus, while the primary α_2 particles are transforming to O-phase, new α_2 particles are forming at the surfaces of those primary particles.

Creep resistance of the Ti-22Al-27Nb type alloys has also been shown to be equivalent or superior to the $\alpha_2 + \beta$ alloys [6,65]. Woodfield [6] studied the influence of super-transus and sub-transus forging temperatures in Ti-22Al-26Nb in which the major difference was the volume fraction of lath structure. The super-transus forging, containing 100% lath, exhibited better creep resistance than the sub-transus forging, containing equiaxed primary α_2 in a lath matrix, Table 5.

Although the test conditions of 650°C/172MPa do not correspond to the design goals listed in Table 2, it seems clear that, while the properties may be close, neither Ti-22Al-23Nb nor Ti-22Al-26Nb meets the goal properties. As a consequence, if these orthorhombic alloys are to be used as a composite matrix

for blisk/bling or impeller applications, additional alloying will be necessary to achieve the creep goals.

Table 5: Effect of Forging Temperature on Creep Behavior of Ti-22Al-26Nb at 650°C / 172 MPa (Beta Transus \approx 1066°C) (After Woodfield et al., Ref 6)

Condition	Time to % Strain, hrs		
	0.1%	0.2%	0.5%
β forge + age	4.9	26.1	224.0
$\alpha_2+\beta$ forge + age	2.9	10.3	60.4

Environmental Effects

Like all titanium alloys, orthorhombic titanium aluminide alloys are susceptible to environmental degradation when exposed in air at elevated temperatures via oxidation or interstitial embrittlement. The previously mentioned development of surface cracks on creep specimens being tested in air is a manifestation of this latter problem. Several studies [33,68,69] have shown that oxidation can be a serious problem at temperatures above \sim 600°C.

Cerchiara et al., (68) studied the oxidation behavior of neat Ti-22Al-23Nb in the temperature interval from 500-900°C. Their studies included the effects of air, oxygen and water vapor environments under both isothermal and cyclic conditions. They found that the kinetics of oxidation were controlled by the transport of TiO_2 at aluminum concentrations of 20-25 at% and niobium concentrations up to 10 at%. These kinetics were slower than for those alloys with higher levels of aluminum (e.g. TiAl), which form protective Al_2O_3 scales, but slower than for the growth of TiO_2 on titanium. At niobium levels above 10 at%, the parabolic rate constants increase and the kinetics become linear, after initial periods of parabolic oxidation. This increase was attributed to the development of Nb_2O_5 within the oxide scales which allows for enhanced transport and cracking of the scales. Oxidation in dry air at temperatures $> 700^\circ\text{C}$ was found to be excessive (Figure 38), such that use of Ti-22Al-23Nb for extended periods of time would require an environmental protection system (e.g. coating). These kinetics increased if water vapor was present.

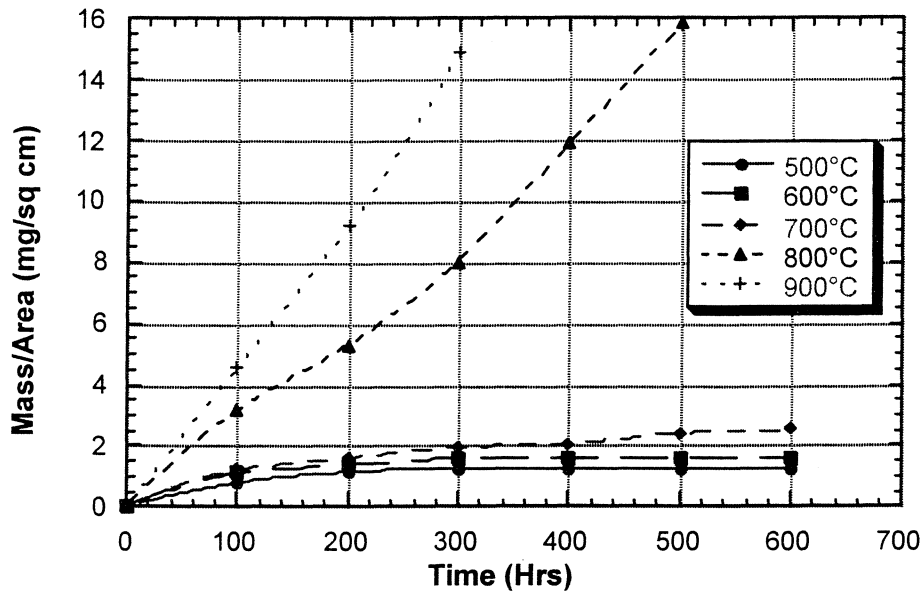


Figure 38. Weight Change vs. Time at Temperature for Ti-22Al-23Nb in an Air Environment (Ref 68)

With respect to embrittlement, Cerchiara et al. (68) have shown for Ti-22Al-26Nb that pre-exposures in air at low temperatures (400°C) resulted in a reduction of ductility of specimens tested in 3-point bending and uniaxial tension (Table 6). This reduction was attributed to a thin (several micron) surface layer embrittled by interstitial ingression, which is easily cracked and acts as premature sites for failure. Once this thin embrittled layer is removed, the material exhibits full unexposed elongation.

Table 6: Effect of Elevated Temperature Air Exposure on Ductility of Ti-22Al-26Nb

Condition	Plastic Elongation (%)
Unexposed	3.3
72 hr @ 300°C	3.1
8 hr @ 400°C	1.0
72 hr @ 400°C	0.0
55 min @ 650°C	0.5

Brindley et al., (69) similarly observed embrittlement in a variety of orthorhombic compositions. He concluded that although alloy modification can mitigate to some degree the oxidation resistance of orthorhombic alloys, the embrittlement issue was the dominating environmental problem (Figure 39), and it was observed to be relatively unaffected by alloying. However, those alloys with higher levels of Al:Nb ratios had reduced depths of surface embrittlement. In addition, the application of environmental protective coatings at best resulted

in LCF resistance similar to uncoated material. This was attributed to chemical and mechanical incompatibilities between the coating and orthorhombic alloy, as well as, to coating brittleness. However, there was evidence that producing a compressive residual stress state on the substrate surface via grit blasting may provide for LCF improvement.

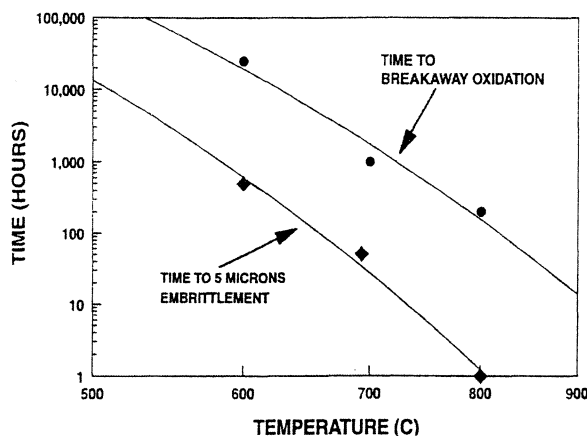


Figure 39. Time to breakaway oxidation and time to 5 μ m depth of embrittlement as a function of temperature for air exposed Ti-19Al-23Nb. (After Brindley et al., Ref. 69)

Rosenberger et al. (34) evaluated a TiAl+two-phase glass coating for protecting Ti-22Al-23Nb during fatigue cycling at elevated temperature in an air environment. While the coating system provided for an improvement in oxidation rate, there was a corresponding reduction in fatigue life. It was noted that the coating system was not optimized for either the Ti-22Al-23Nb composition or the cyclic conditions used.

The role of microstructure on environmental embrittlement was examined by Cerchiara et al., (68) where it was found that the distribution of the O phase had a notable effect on mechanical properties. Specimens with a continuous layer of "O" phase on the prior beta boundaries were softer and more ductile than for microstructures with O phase dispersed within the prior beta grains.

Some improvement in oxidation behavior was found when Ta and Mo were added to Ti-22Al-22Nb [32]. Small additions of tantalum (i.e. 2 at%) resulted in a slight decrease in parabolic rate constant, but the kinetics remained linear. The alloy, Ti-22Al-22Nb-2Ta-1Mo had weight gains a factor of 20 lower than the baseline alloy. These results and those reported earlier by Pettit et al. [70] were a significant factor in the design of the next generation alloys.

Second Generation Matrix Alloy Development

Improved creep strength and oxidation resistance were the primary drivers for the work on the next generation of orthorhombic titanium aluminide alloys [8]. Cyclic oxidation studies of several alloy compositions suggested that weight gain is reduced by increasing Al, adding Mo, and reducing Nb [8]. One of the most

promising alloys in this study was Ti-22Al-24Nb-1.4Mo-0.5Si (at. pct.). (The total Nb and Mo content was designed to be ~27 at. pct. to simulate the Ti-22Al-27Nb ternary alloy that had shown promise. No attempts were made to examine a similarly alloyed version of Ti-22Al-23Nb.)

Tensile Properties

The quinary alloy easily met the tensile strength (from room temperature to 705°C) and ductility goals set forth in Table 2, Figure 40 [8]. The most stringent tensile strength goal, 827MPa at 705°C for the impeller, is met by the Ti-22Al-24Nb-1.4Mo-0.5Si alloy in the rolled plus creep flattened condition.

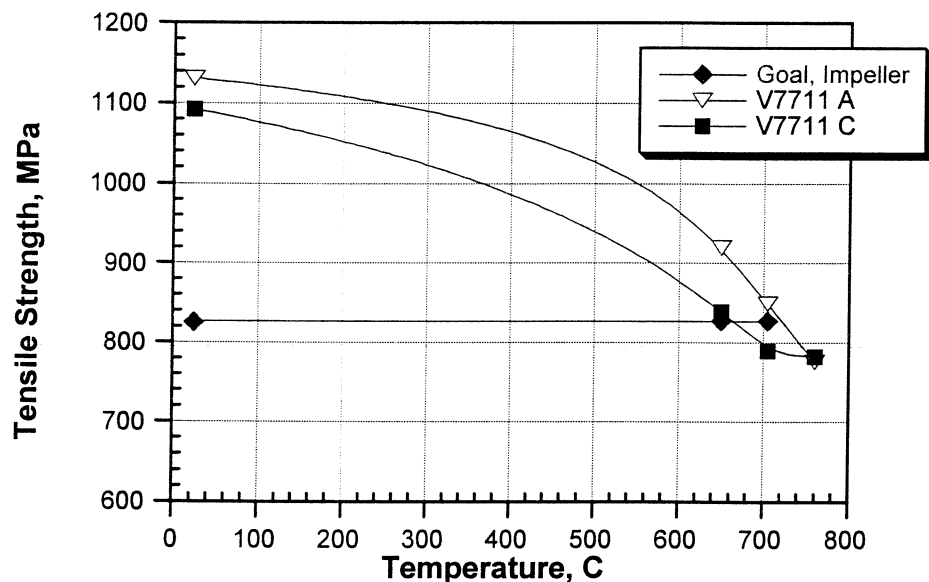


Figure 40. Tensile strengths of Ti-22Al-24Nb-1.4Mo-0.5Si in two microstructural conditions as a function of temperature. Condition A, with 7 v/o primary α_2 and fully transformed, O + β , matrix, exceeds the most stringent impeller goal strength. (After Porter et al., Ref. 8).

Creep Properties

The quinary alloy was creep tested in two microstructural conditions [8]. In Condition A, the material was hot rolled to sheet and then creep flattened in the three phase, α_2 +B2+O, field resulting in about 7 v/o primary α_2 in a fully transformed, O + β , matrix. For Condition C, the above treated material was given an additional long-time heat treatment the O + B2 phase field, resulting in a conversion of many of the primary α_2 particles to O phase leaving 'pseudo-primary' O-phase grains [8].

The creep test results are summarized as Larson-Miller plots in Figures 41 and 42 for 0.24% and 0.5% creep strain, respectively. The goal for the blisk/bling application in the longitudinal orientation, 900 hours at 510°C and 10 hours at 650°C to reach 0.24% strain at a stress of 290 MPa, is plotted along with the test results in Figure 41. The alloy in the C condition has exceeded both longitudinal and transverse creep goals for the blisk/bling component.

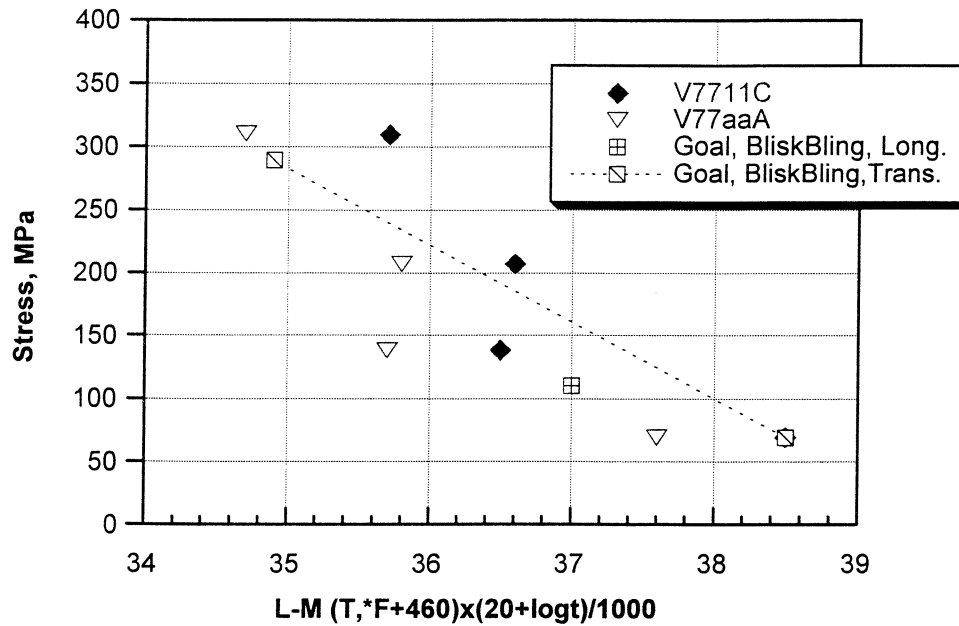


Figure 41. Larson-Miller plot for 0.24% ϵ of Ti-22Al-24Nb-1.4Mo-0.5Si in two microstructural conditions. (After Porter et al., Ref. 8)

The design goals for the impeller are more stringent than those for the blisk/blisk. The Larson-Miller plot for 0.5% strain, Figure 42, demonstrates that the quinary alloy does not meet those goals in either microstructural condition [8].

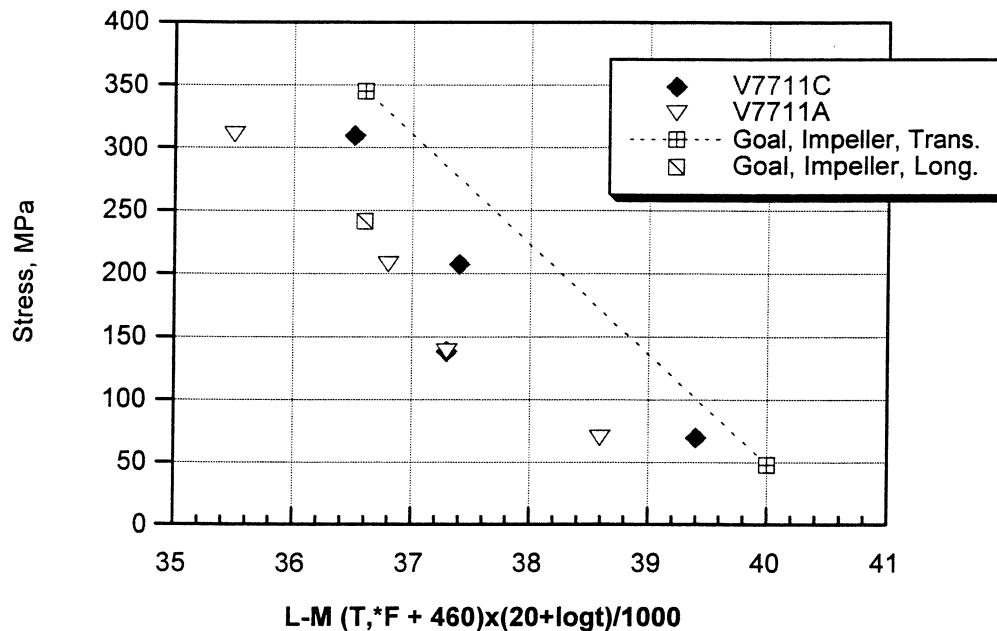


Figure 42. Larson-Miller plot for 0.5% ϵ of Ti-22Al-24Nb-1.4Mo-0.5Si in two microstructural conditions. (After Porter et al., Ref. 8)

Further Studies

In an attempt to improve its mechanical properties and oxidation resistance, the quinary alloy was modified to increase the Mo level to 1.5 at. pct. and to include 1 at. pct. Ta [8]. Unfortunately, the alloy was difficult to process and the program ended prior to any mechanical or oxidation testing [8]. Among the lessons learned in the alloy development study was that initial ingot breakdown should include sufficient work and temperature as to homogenize the inherent segregation in large ingots. This is especially true if heavy elements such as Mo and Ta are added to the alloy [8].

V. Interface Studies

A critical element in the overall properties of a continuous fiber reinforced composite is the fiber/matrix interface. This interface contributes, either positively or negatively, to the composite's residual stress state, its transverse strength and fracture behavior.

As previously mentioned, one of the leading reinforcing fiber candidates for titanium alloys, SCS-6TM fibers developed by Textron Specialty Materials, has a carbon-rich surface that produces a very weak interface when incorporated into a composite. This architecture not only provides for easy handling of the fiber before and during composite fabrication, but also promotes improved longitudinal toughness in the composite by inducing crack deflection around fibers.

It has also been well documented that the SiC fibers react with the titanium matrix during consolidation and secondary processing or subsequent service exposures [14,71-77]. These reaction products, which occur in composites reinforced with uncoated SiC, such as the Sigma fiber produced by British Petroleum, as well as with SCS-6TM fibers, also tend to weaken the fiber/matrix interface. The orthorhombic alloys have an advantage over the $\alpha_2+\beta$ alloys in that the extent of fiber/matrix reaction is reduced for a given thermal exposure, Figure 43 [14].

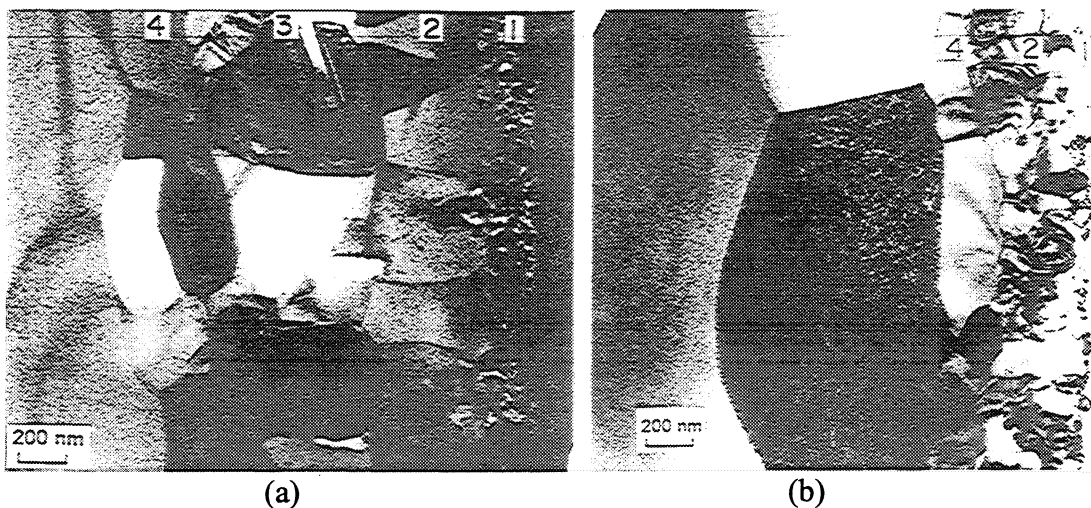


Figure 43. TEM cross sections showing fiber/matrix interface reaction products: 1 = mixed carbides and silicides, 2 = $(\text{Ti,Nb})\text{C}$, 3 = $\text{Al}(\text{Ti,Nb})_3\text{C}$, 4 = $(\text{Ti,Nb})_5(\text{Si,Al})_3$ in (a) Ti-24Al-11Nb/SCS-6 SiC, and (b) Ti-22Al-23Nb/SCS-6 SiC. Fiber is at far right and titanium aluminide matrix at left in both photographs.

Interface Strength Requirements

Unfortunately, the weak fiber/matrix interface that is so crucial to toughness results in poor transverse strength of the composite. Thus, one method for improving transverse creep and tensile strengths of the composite would be to strengthen the fiber/matrix interface. Of course, an upper bound is imposed on the interfacial strength by the bridging mechanism necessary for toughness requirements. Schuyler and co-workers [78] have analyzed the

interface strength problem by calculating crack tip stresses and the ratios of the stresses in the fiber to the interfacial shear stresses and the interfacial normal stresses. Using those results, they calculate that the interface in an SCS-6TM-reinforced Ti₃Al-Nb alloy will be sufficiently weak to promote crack deflection as long as its shear and normal strengths are less than 813 MPa (118 ksi) and 1102 MPa (160 ksi), respectively [78]. The significant result of Schuyler's [78] calculations is that longitudinal toughening via fiber bridging of an advancing crack does not require a zero strength interface. Thus there is room for improving transverse strength by means of interface strengthening without negatively affecting crack bridging.

Just as the matrix property requirements were calculated for a blisk/bling and an impeller application, see Table 2, fiber/matrix interface strength requirements were calculated. Those requirements were defined in terms of an "optimum range," wherein transverse properties are improved while longitudinal toughening due to interface debonding is retained [8], Table 7.

Table 7: Fiber/Matrix Interface Goal Properties (After Porter et al., Ref. 8)

Application	Interface Normal Strength*	Interface Shear Strength*
Blisk/Bling	$103 < \sigma_1 < 965$ MPa	448 MPa
Impeller	$276 < \sigma_1 < 965$ MPa	621 MPa

* assumes a fiber strength of 3101 MPa

Interface Strength Testing Techniques

The testing of interfaces to measure normal and shear strengths is non-trivial. Various approaches have been used including tests such as fiber pull-out [79], fiber push-out [80], dogbone (or straight-sided) single fiber composites [81], and cruciform single fiber composites [82]. The pull-out test was devised to overcome some failings of the push-out test, namely in the difficulty in interpreting debond energy and sliding parameters due to end effects and residual stresses [80]. The pull-out test, although very effective, also can suffer from end effects and requires detailed interpretation. These tests typically measure interface shear stresses.

Another approach for interface measurement is to fabricate composites with few fibers and test in tension with the fibers oriented transversely. Testing of straight-sided or dogbone specimens (i.e., non-reduced or reduced gauge section) has indicated zero interfacial strength in SCS-6TM reinforced titanium aluminides once the compressive residual stress on the fiber is overcome [81, 83]. These types of tests, however, rely on the observation of an exposed fiber end for the measurement of interface separation stresses.

The cruciform tensile specimen was designed to eliminate end effects from the measurement of interface strength [82], Figure 44. Although Gundel et al. did not specify the dimensions of their cruciform, a subsequent paper indicated the arm to be 38 mm (1.5 in) in span with the length being 50.8 mm (2 in) [84]. Initial stress analyses indicated that the remotely applied tensile stress

was uniform across the center of the cross causing interface damage and matrix plasticity in the center section [82].

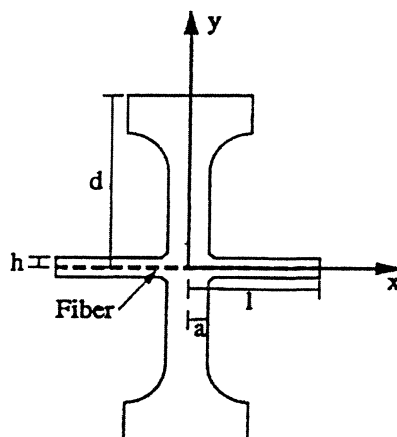


Figure 44. Cruciform tensile specimen for measurement of transverse loading response of single –fiber composite. (After Gundel et al., Ref 82)

Interface Strengths

Initial measurements of fiber/matrix interface strengths were made on specimens with exposed fiber ends [79-81, 83]. Typically, matrix compressive stresses on fibers are relaxed at these exposed ends, and are thus different from the residual compressive stresses on the fibers in the composite interior.

To calculate the interface strength in a tensile test, the compressive stresses, which have been measured or calculated for these materials [84-86], must be subtracted from the total applied stress. When this is done for results measured on exposed fiber ends, the interface strengths are calculated to be zero for SCS-6TM fibers [79, 84]. However, the results from embedded fibers indicate non-zero interface strengths for Ti-6Al-4V matrix composite [82, 87]. The interface strengths calculated for SCS-6TM /Ti-6Al-4V (wt. %) were 115-130 MPa. It is not unreasonable to assume that the fiber/matrix interface strength for an orthorhombic titanium aluminide matrix reinforced with SCS-6TM fibers would be near to that of the Ti-6Al-4V matrix composite, inasmuch as the carbon-rich surface of the fiber produces a very weak interface irrespective of the matrix. Furthermore, Gundel et al. [82] showed that a SiC fiber with a much thinner carbon-rich layer, ACMF, doubles the fiber/matrix interface strength over the SCS-6TM fiber.

Reference to Table 7 shows that there is a considerable increase in interface strength that can be accommodated without sacrificing crack-bridge toughening. The ACMF fiber results confirm that the double carbon layers on the SCS-6 fibers are the source of a very weak interface and that the interface strength can be improved by reducing the layer thickness.

Approaches to Improving Fiber/Matrix Interface Strength

The obvious approach to strengthening the fiber/matrix interface is to eliminate the carbon coating on the SiC fibers. However, there are at least two

factors to be considered: fiber handleability and fiber reaction with the matrix. The primary reasons for the carbon coatings on the SiC fibers are to promote handleability and to maintain fiber strength. Thus, any approach to improving interface strengthening via fiber surface alteration must include considerations of these issues.

Alternatives to carbon coatings on SiC fibers have been considered [8, 86-88]. Porter et al.[8] have defined a potential fiber coating as follows. "The ideal interface material would bond with both the SiC fiber and the titanium matrix, without severe chemical reaction. The interdiffusion between components would be minimal to prevent C, O, N, and Si from reaching the titanium matrix and to prevent Ti from reaching the SiC fiber. The interface material would also be strong enough to withstand residual thermal stresses arising from cooling from consolidation temperature. No single material that will meet all of these requirements can be found" [8].

Dual Coatings Approach

A program to develop a dual layer system for coating fibers arrived at a combination of refractory metal carbide-refractory metal as meeting the aforementioned requirements [8]. Detailed studies of chemical compatibility and diffusion bonding led to the selection of NbC/W and TaC/W as the most promising fiber coating combinations. Diffusion couple studies demonstrated that the W layer interdiffused with the titanium matrix to develop a ductile beta-phase layer in the matrix adjacent to the fibers with slight interdiffusion between the TaC (or NbC) and W, Figure 45 [8].

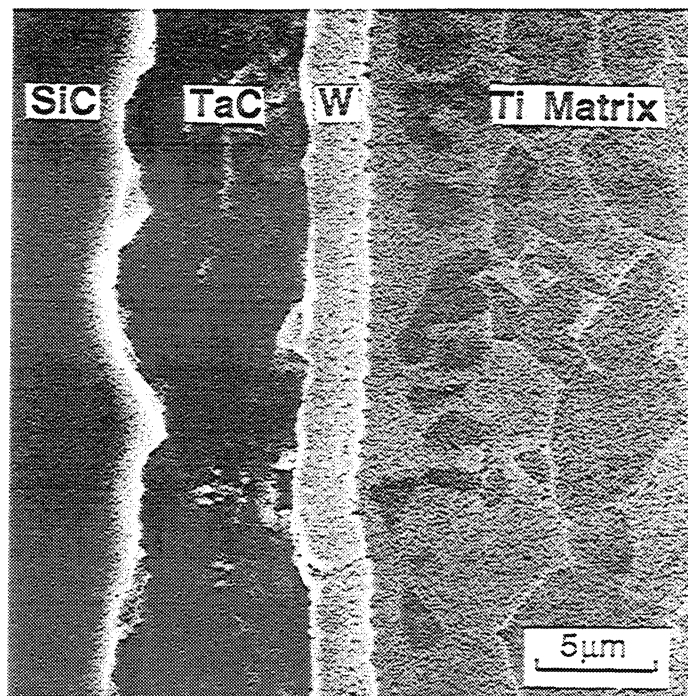


Figure 45. SiC/TaC/W/Ti-22Al-23Nb diffusion couple after bonding at 1000°C / 4 hours. (After Porter et al., Ref. 8)

Although the laboratory studies indicated that the dual refractory metal carbide/refractory metal coating concept would provide the necessary interface bonding and diffusion barrier for SiC in an orthorhombic titanium aluminide matrix, fabrication of coated fibers proved problematic [8]. It was found that the NbC or TaC could be CVD deposited onto SiC fibers at the targeted 2-3 μm , but control of a similar thickness of W was much more difficult [8]. Non-ideal coated fibers were fabricated into small composites for further studies, Figure 46 [8]. EDS traces across the interface indicated that the dual layers had prevented any reaction between the matrix and the SiC fiber.

The coated fibers exhibited reductions in tensile strengths and in Weibull moduli of 50% or more [8]. The conclusion of these researchers was that “the fiber used was from non-optimized production and evaluation was inconclusive” [8]. Thus it appears that additional research is necessary to evaluate the efficacy of the dual layer concept.

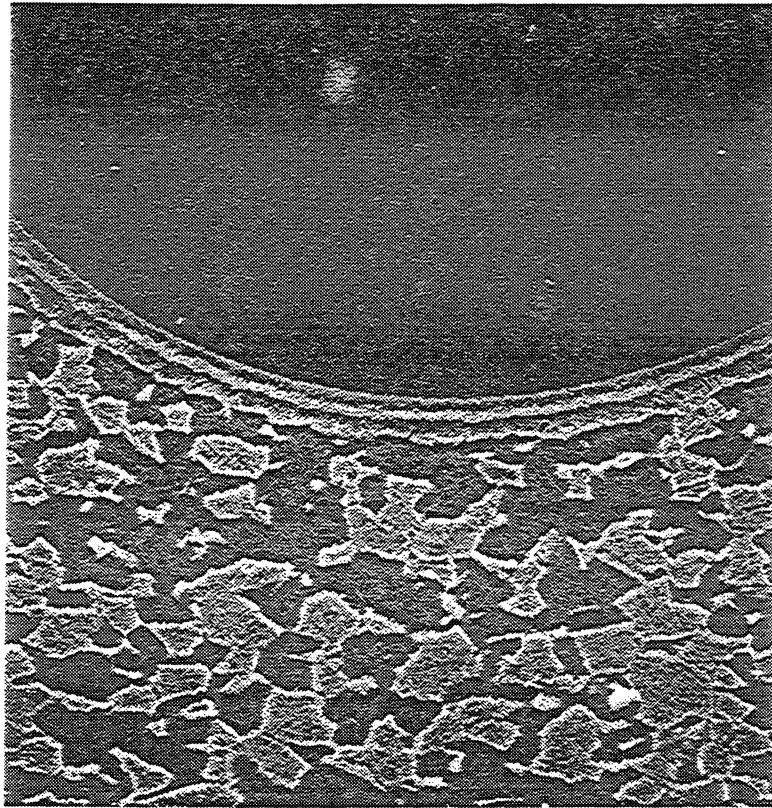


Figure 46. SiC fiber with NbC/W coating in Ti-22Al-23Nb matrix. (After Porter et al., Ref. 8)

Spatially Varied Interface Approach

Maruyama et al. have recently introduced the concept of strong and weak interface regions along each fiber by depositing a controlled pattern of coating onto the fibers, Figure 47 [19]. The researchers deposited banded, helical, and random patterns onto SiC fibers and measured interface strengths after

consolidating in a Ti-6Al-4V matrix [19]. Those results showed interface debond stresses intermediate to those of fully weak and fully strong interfaces, demonstrating successful control of interface strength in transverse tension [19].

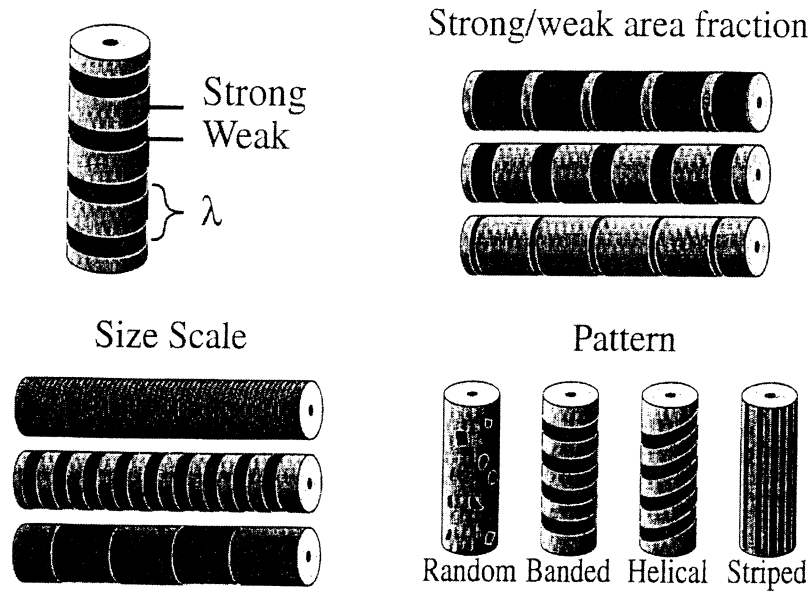


Figure 47. Spatially varied interface design concepts. (After Maruyama et al., Ref. 19)

VI. Composite Processing

Essentially, three processes have been used or are being considered for use in the fabrication of O TMCs. The two processes that have been successfully utilized to date are: 1) foil-fiber-foil and 2) tape casting. Textron, ARC and Allison Engine Company have successfully fabricated O TMCs via the foil-fiber-foil process. Although both Textron and ARC have tape casting facilities, only ARC has successfully fabricated O TMCs using this process. The third process currently under evaluation for O TMC manufacturing is called wire winding. This process has been developed by ARC. Each of the processes is discussed in turn, with emphasis on the positive and negative attributes of each.

Foil-Fiber-Foil

Foil Fabrication

The primary manufacturing method for O TMCs to date has been the foil-fiber-foil process. As the name suggests, this process involves sequential stacking of alternate layers of thin orthorhombic foil and SiC fibers or woven mat into a preform. This preform is subsequently consolidated via hot isostatic pressing (HIP'ing) at combinations of time/temperature/pressure necessary to fully densify the material. For most applications currently under consideration for O TMCs, the fibers are unidirectionally oriented in a multiple ply configuration.

At this point, the primary deterrent to foil-fiber-foil composite fabrication is the production of foil. Early on, the rolling of titanium aluminides, viz. α_2/β alloys like Ti-24Al-11Nb, to 0.13mm (5 mil) foil was a tedious and costly process developed by Texas Instruments (TI) [89], which was done in small batches by highly trained personnel. Unfortunately, TI made a business decision that the near-term markets for titanium aluminide foil were insufficient to continue to be a supplier of these materials.

Prior to Texas Instrument's departure from the foil production business, a consortium study of the effectiveness of several composite fabrication techniques ranked the likelihood of a scale-up success of the currently available approaches for the manufacture of ring inserts for advanced aircraft turbine engines [90]. The study concluded that the two most promising approaches to the fabrication of ring inserts were the "helical" method developed by Allison Engine Company [91], and the "grooved disc" technique developed by Textron [92] Figures 48 and 49.

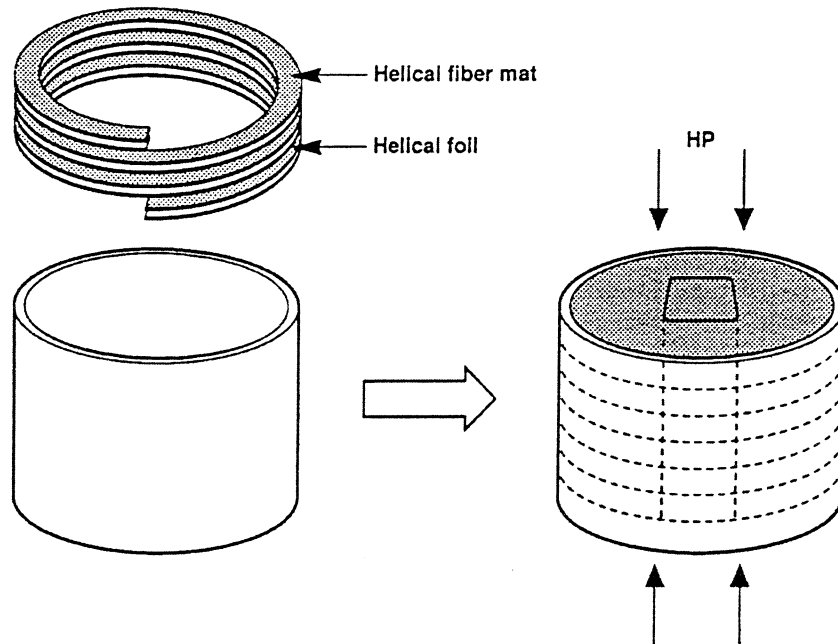


Figure 48. Schematic of Allison's "Helical" Foil-Fiber-Foil Fabrication Process

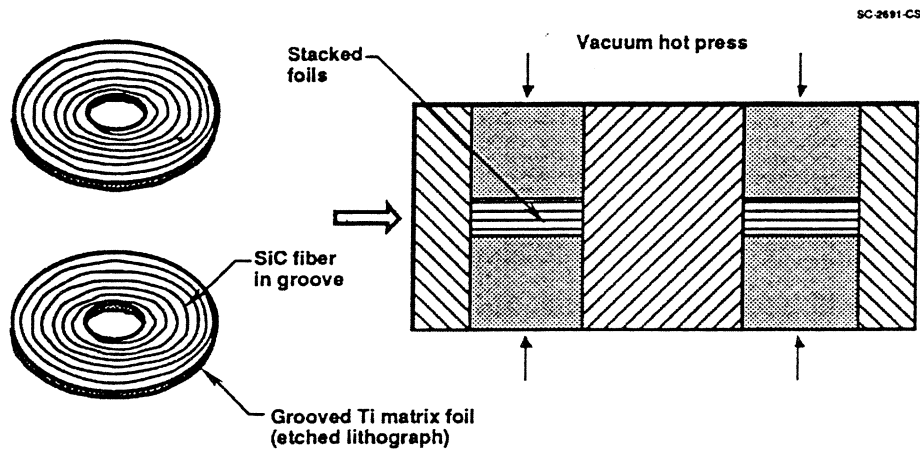


Figure 49. Schematic of Textron's "Grooved Disc" Foil-Fiber-Foil Fabrication Process

Long after the termination of the consortium study, Allison continued to fabricate titanium aluminide ring inserts demonstration within the IHPTET program [93]. The emergence of orthorhombic alloys such as Ti-22Al-23Nb and Ti-22Al-27Nb provided Allison with a potential composite matrix alloy with improved properties (compared to Ti-24Al-11Nb). The departure of TI as a foil supplier, however, necessitated the search for an alternate vendor.

The Wah Chang Company (formerly Teledyne Wah Chang) accepted the challenge to produce foil from orthorhombic alloys. Drawing on their experience with rolling conventional titanium alloys and after a short learning curve, Wah

Chang was successful in supplying Allison with significant quantities of 0.15mm gauge (6 mil) foil of the Ti-22Al-26Nb alloy [93]. Wah Chang's success led to the reduction in cost of foil from the high cost of TI's technique. A back-scattered SEM image of the Ti-22Al-26Nb foil rolled by Wah Chang is shown in Figure 50.

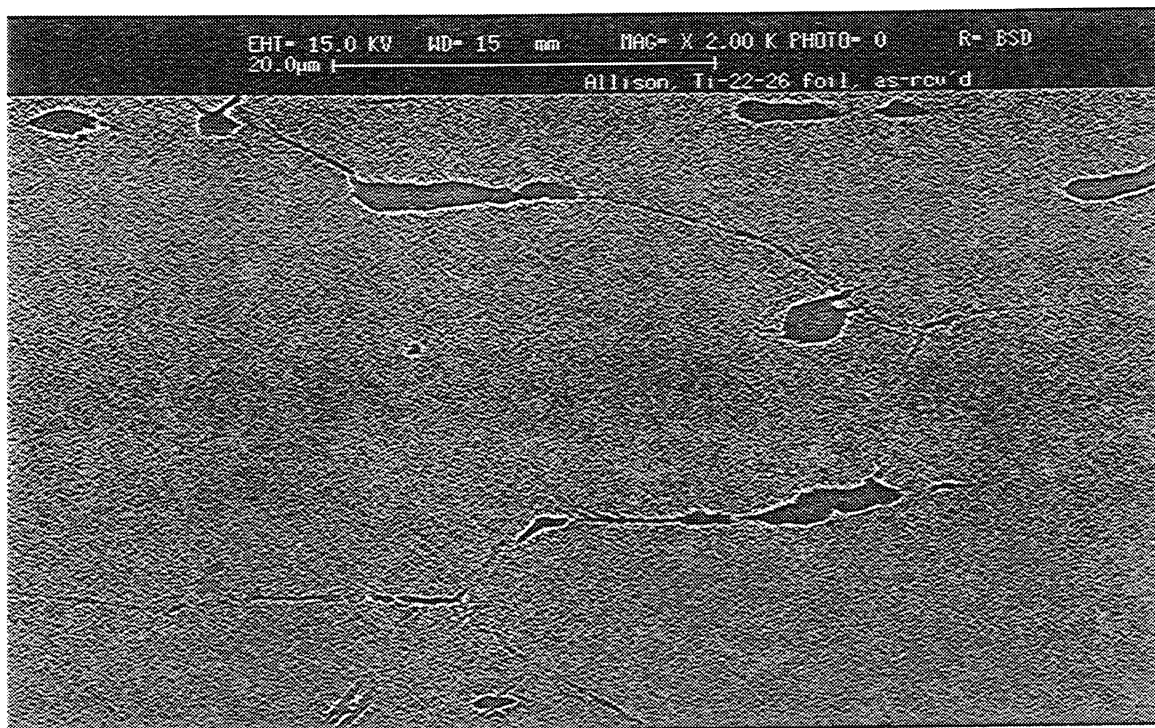


Figure 50. Ti-22Al-26Nb Foil Produced by Wah Chang

More recently, the Allison Engine Company has had difficulty in procuring satisfactory helical woven SiC fibers for their helical ring process. They have thus shifted their fabrication process to the grooved disc technique [92], Figure 49.

Another potential supplier of orthorhombic foil is Sulzer Innotec of Winterthur, Switzerland. This company is currently working to develop production techniques for the fabrication of thin foil of titanium aluminides [94,95].

With the development of second generation alloys (see: IV Matrix Developments), the need to develop reliable processing techniques that would reduce the cost of foil was recognized. An Air Force sponsored program was conducted by a team consisting of General Electric Company, Wah Chang Company, Rockwell Science Center, and Allison Engine Company. This group included a supplier, two end users, and a research laboratory experienced in the metallurgy of orthorhombic alloys [23].

A 2000-pound ingot of a second generation orthorhombic composition, Ti-22Al-24Nb-1.5Mo-0.5Si was forged to 10.2 cm. thick slab that was then hot rolled in several steps to 0.2 cm. sheet, Figure 51. The sheet could be cold-rolled to 0.02 cm. foil in the laboratory, but not in the production mill due to problems with thickness variations and waviness in the hot rolled sheet. It was concluded that a

similar alloy with reduced levels of Mo and Si would be required for processing to foil in the production mill [23].

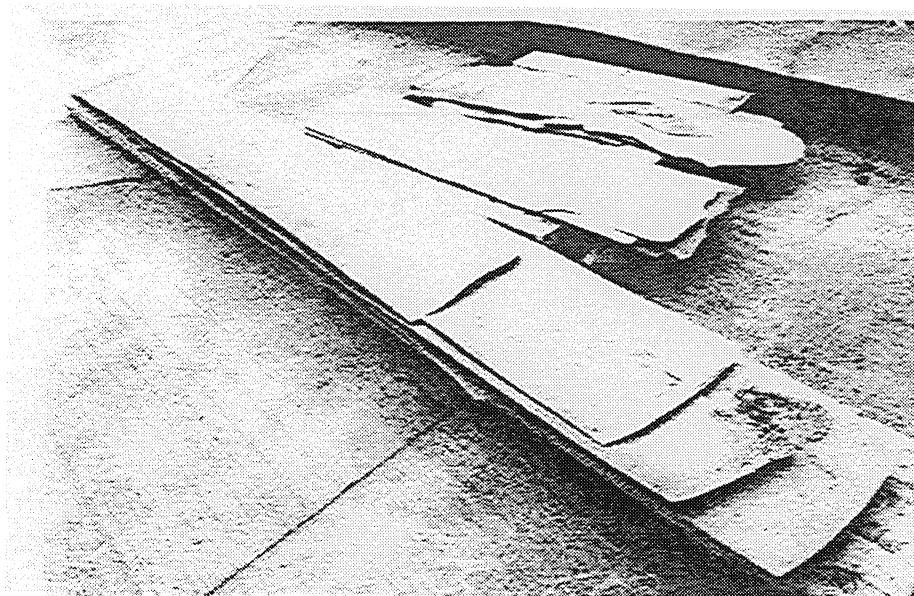


Figure 51. Hot rolled 0.2 cm. sheet of Ti-22Al-24Nb-1.5Mo-0.5Si (Ref 23)

Cost modeling suggested that 0.2 cm. gauge sheet could be fabricated at a cost of ~\$140/lb and that foil (of a cold rollable alloy) could be fabricated at ~\$300/lb [23]. This cost of foil is quite promising, as it starts to become competitive with powder-based MMC fabrication described below. Although the program was terminated before completion, the lessons learned and the cost model offer strong reasons for continued research on foil processing of orthorhombic titanium aluminides.

Foil Texture

Crystallographic texture measurements of cold-rolled orthorhombic foil have generally been limited to the bcc (β or B2) phase primarily because of the weakness of texture of the orthorhombic and alpha-two phases and the coincidence of their x-ray peaks [58,96]. Rollett et al. [96] showed that textures in the orthorhombic and alpha-two phases in cold-rolled Ti-22Al-23Nb were at most 2 times random. The orthorhombic phase showed a concentration of c-axes parallel to the rolling plane normal, whereas the alpha-two phase had c-axes aligned both parallel to the rolling direction and the rolling plane normal.

For the bcc phase, the most dominant component was found in both studies to be $[001]\langle 110 \rangle$, with maximum intensities up to 6 times random [58,96]. Tensile tests conducted on foil extracted at various angles to the rolling direction showed a minimum in yield strength at 45° to the rolling direction as seen in Figure 52 [96]. Simulated tensile test calculations for the individual phases by Rollett et al. demonstrate that yield strengths would be at a minimum at an orientation 45° from the rolling direction for the bcc phase, but no minimum for the orthorhombic phase would be expected [96]. From these calculations, Rollett

et al. concluded that the bcc phase dominated the yield anisotropy. The calculations and the tensile tests indicate a significant reduction in anisotropy of yield strength with post-rolling anneals.

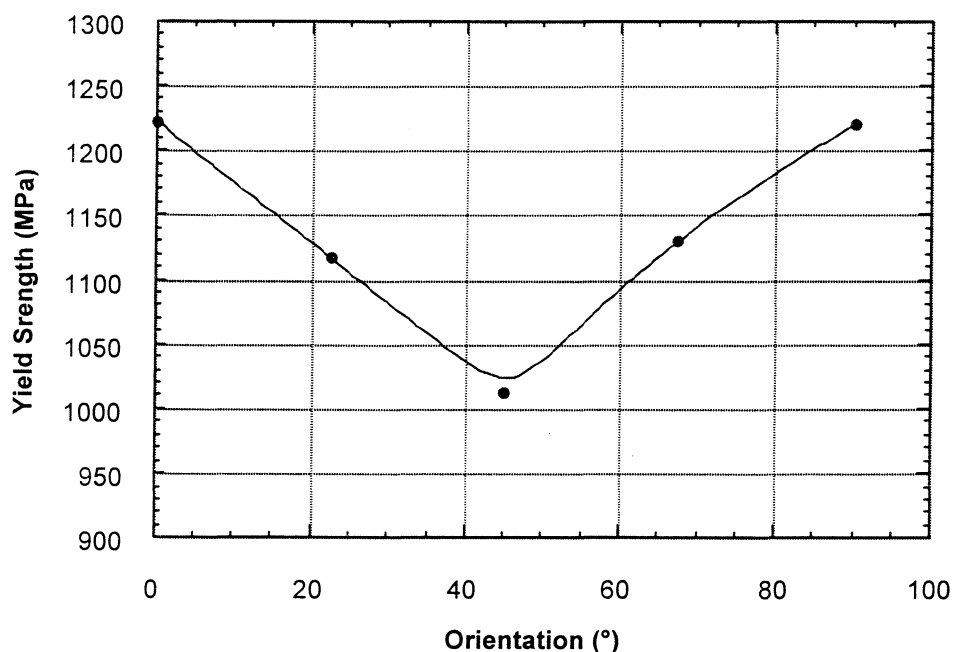


Figure 52. YS vs. Orientation to Rolling Direction for Ti-22Al-23Nb Foil (Ref 96)

Powder Metallurgy (P/M)

Tape Casting

As previously discussed, one of the primary disadvantages of the foil-based composite processing has been the high cost associated with foil production. Although progress has recently been made to suggest foil production costs could be significantly reduced, currently orthorhombic foil (Ti-22Al-26Nb) costs on the order of \$700/lb [22], which precludes the manufacture of affordable O TMCs using a foil-based approach. In addition, as has been seen, anisotropic mechanical behavior due to microstructural and/or crystallographic texturing produced during rolling can also be an issue [96]. Unlike foil, orthorhombic powder input materials can be significantly more affordable currently costing ~ \$70/lb [24]. Furthermore, since powder consolidation is normally accomplished through the use of hot isostatic pressing (HIP'ing), little to no microstructural or crystallographic texturing is expected to occur, and thus, anisotropic behavior is thought to be much less of an issue.

One of the primary means for fabricating O TMCs from powder is via a process called tape casting. Both Textron and Atlantic Research Corporation (ARC) have facilities for tape casting of titanium matrix composites, however, only ARC has successfully fabricated O TMCs via this process. A schematic of the patented [97] ARC tape casting process is shown in Figure 53.

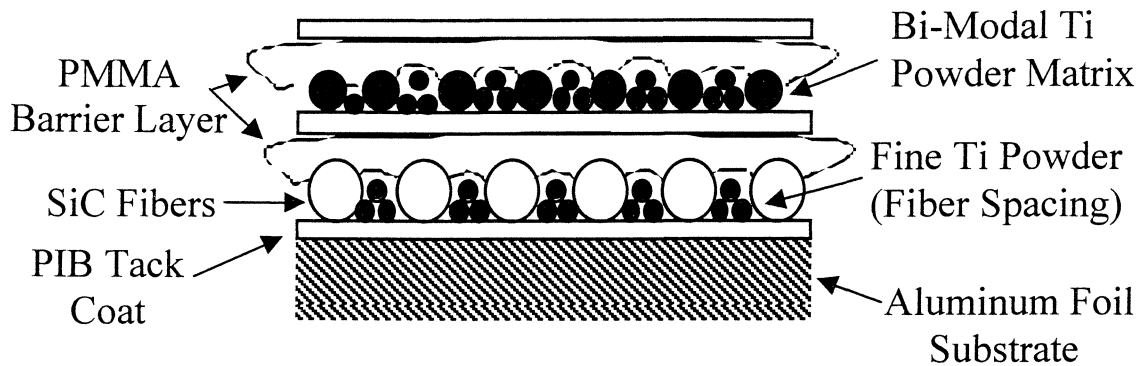


Figure 53. Schematic of ARC's Tape Casting Process

In this process, an aluminum foil substrate (0.75 mm) is typically wrapped around a drum and a thin adhesive layer (tack coat), in this case 1 wt% polyisobutylene (PIB) in a hexane solvent, is applied to its surface via multiple coats. Alternative substrate materials include polyethylene and Teflon. A spool containing the SiC fiber is fed through a tensioning wheel and onto the drum. The fiber is taped to the substrate near one edge of the drum and an aligner is used to space the fiber during feeding. At the completion of the winding process, the remaining fiber end is taped to the substrate. Typically, 1.4 mm (5.6 μm) diameter SiC fiber is used in conjunction with 1.3 mm (5 mil) titanium foil and the fibers spaced at ~ 125 fibers per 254 mm (1 in.). This spacing results in a fiber volume fraction of $\sim 35\text{--}40\%$ depending on the exact foil thickness and cover sheet thickness. Once the fiber is in place, very fine titanium powder ($-200+270$ mesh or $-75\ \mu\text{m}+53\ \mu\text{m}$) of the same composition as the matrix is applied in between the fibers and held in place by the PIB tack coat. These fine powders act to maintain fiber spacing during off-gassing and consolidation. Next a barrier layer of 1 wt% polymethylmethacrylate (PMMA) dissolved in acetone, which is mutually insoluble with the adhesive (tack coat) is applied. The primary purpose of this layer is to prevent successive PIB layers from dissolving in one another. The process is repeated with another PIB tack layer applied to which a bi-modal distribution of titanium powders ($-80+140$ mesh/ $-140+200$ mesh or $-180\ \mu\text{m}+106\ \mu\text{m}/-106\ \mu\text{m}+75\ \mu\text{m}$) is added to form the matrix. Upon completion of the composite preform, the substrate material can be removed and the lay-up is off-gassed at elevated temperature to remove the PIB and PMMA materials. After off-gassing is completed the lay-up is consolidated typically by hot isostatic pressing at temperatures/pressures/times requisite for complete densification. The ARC tape casting process provides for excellent fiber spacing control as demonstrated for the Ultra SCSTM/Ti-22Al-26Nb composite in Figure 54. More information regarding this process can be found in ARC's patent [97].

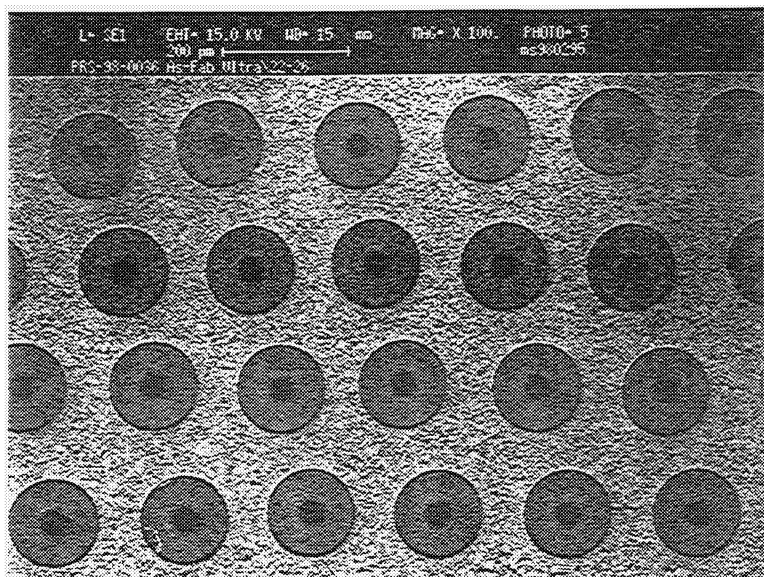


Figure 54. Ultra SCS/Ti-22Al-26Nb Composite Fabricated via Tape Casting

With the aforementioned advantages of powder as compared to foil-based processing, Crucible Research Corporation under Air Force sponsorship has successfully produced numerous orthorhombic compositions in spherical powder form using inert gas atomization (Figure 55) which have exhibited good main alloying elemental and interstitial control. Compositions which have been produced to date include: Ti-22Al-23Nb, Ti-22Al-26Nb, Ti-24.5Al-17Nb-1Mo, Ti-22Al-24.5Nb-1.5Mo and Ti-22Al-24.5Nb-1.5Mo-0.5Si (all at%).

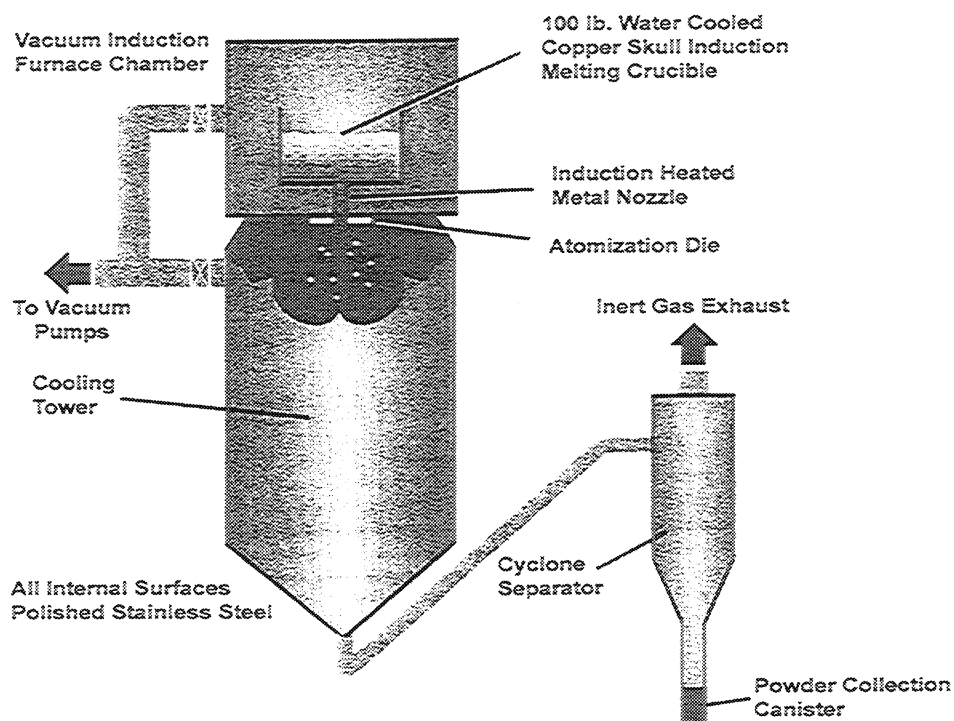


Figure 55. Schematic of the Crucible Research Inert Gas Atomization Unit

Upon atomization orthorhombic alloys form a cellular dendritic network like that shown in Figure 56a for the Ti-22Al-26Nb alloy. Wavelength dispersive spectroscopy (WDS) has shown that the cellular boundaries tend to be high in aluminum, while the cell interiors were niobium rich [25]. This microsegregation is due to constitutional supercooling, such that the last liquid which solidifies at the cell boundaries is high in aluminum. The result of this microsegregation is that a contiguous network of alpha-2 forms at the prior cell boundaries in the as-consolidated neat material which can be seen in Figure 56b. This alpha-2 necklacing in turn results in as-consolidated room temperature ductility for Ti-22Al-26Nb (Table 8), which is inadequate for use as a composite matrix (i.e. ~1.1%). Figure 57 shows how that the contiguous alpha-2 provides a preferential path for fracture during room temperature tensile testing. It should be noted however, that post-consolidation heat treatment has improved room temperature ductility into the usable range for compositing (i.e. ~2.8%), while improving creep performance as well.

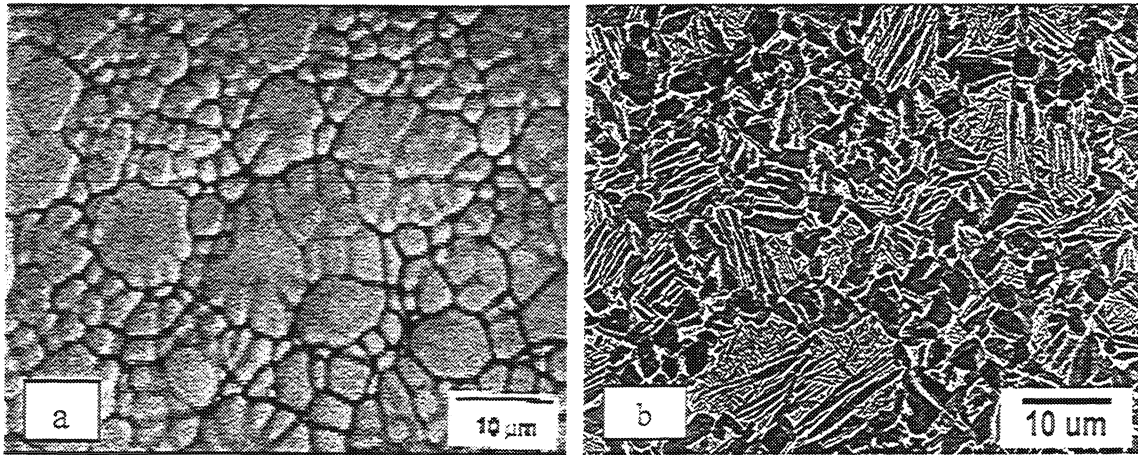


Figure 56. a) Cellular Dendritic Structure Present in As-atomized Ti-22Al-26Nb; and b) Contiguous Alpha-2 Network due to Microsegregation in Neat Ti-22Al-26Nb.

Table 8: Effect of Preliminary Heat Treatment on Room Temperature Tensile Properties of Tape Cast Ti-22Al-26Nb

Condition	UTS (MPa)	YS (MPa)	EI (%)	Modulus (GPa)
As-Consolidated	921	845	1.1	121
Sub-Solvus	881	658	2.8	122
Super-Solvus	858	601	2.3	121

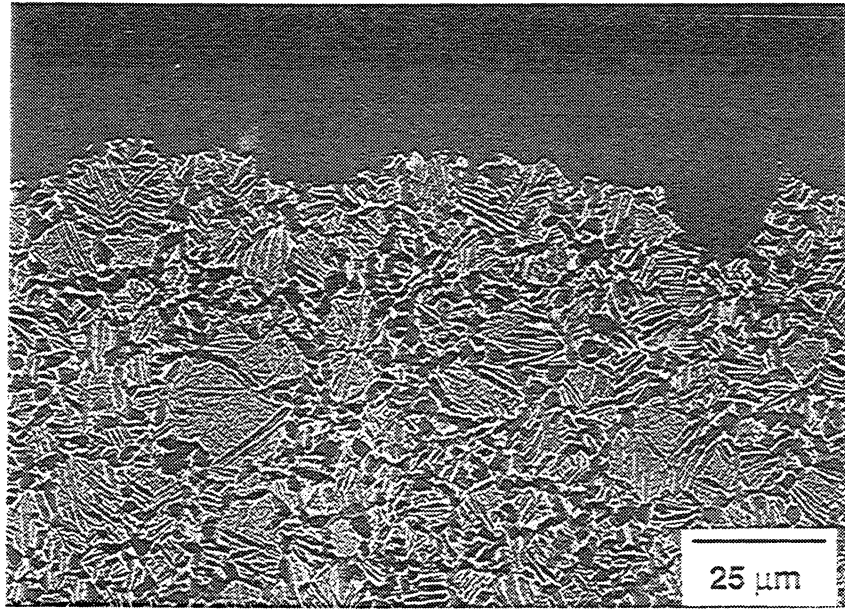


Figure 57. Fracture Along Contiguous Alpha-2 in Tape Cast P/M Ti-22Al-26Nb

As previously noted, a number of orthorhombic compositions have been produced in powder form and evaluated as potential matrix candidates for reinforcement with continuous SiC fibers. Due to the requirement of $\geq 2.5\%$ room temperature ductility for the matrix to effectively load the SiC reinforcement, this is the primary screening factor for P/M-based matrices which tend to exhibit reduced ductility values. Table 9 contains room temperature tensile data for those orthorhombic neat matrices produced via tape casting. It can be noticed that only the Ti-24.5Al-17Nb-1Mo composition exhibited an as-consolidated room temperature ductility which exceeded the minimum matrix ductility requirement. Potential explanations for this have been that the beta phase is disordered in this alloy, and that the lower level of Nb reduces Nb solid solution strengthening of the beta phase [98]. Additional alloying studies based upon the Ti-24.5Al-17Nb base are currently in progress.

Table 9: Room Temperature Tensile Properties for As-Consolidated Tape Cast Orthorhombic Compositions

Alloy	UTS (MPa)	YS (MPa)	EI (%)	Modulus (GPa)
Ti-22Al-23Nb	906	857	2.1	107
Ti-22Al-26Nb	921	845	1.1	121
Ti-24Al-17Nb-1Mo	980	915	4.1	122
Ti-22Al-24.5Nb-1Mo	1071	1060	0.9	119
Ti-22Al-24.5Nb-1Mo-0.5Si	981	927	0.8	136

The primary benefits of the tape cast process versus foil-fiber-foil in the fabrication of O TMCs are: 1) lower cost input material (foil - \$700/lb; powder - \$70/lb); 2) more isotropic properties (little to no texture) and 3) more readily available input materials (powder – single step; foil – multiple steps). However, research studies [98] at the Air Force Materials and Manufacturing Directorate seem to suggest the main issues facing tape casting are the room temperature ductility debit (due to microsegregation in the powder and possibly lack of thermomechanical working), and poor fatigue performance (due to internal defects such as voids associated with incomplete consolidation).

Wire Winding

As previously noted, one of the primary potential applications of O TMCs is that of rotating engine hardware such as compressor rotors. Due to the geometrical constraints of both foil-based and tape cast processing, neither lend themselves particularly well to the fabrication of such hoop wound structures. Therefore, ARC has developed a process for producing rotating components by co-winding wires of matrix material and SiC fibers. A schematic of this patented wire winding process is shown in Figure 58.

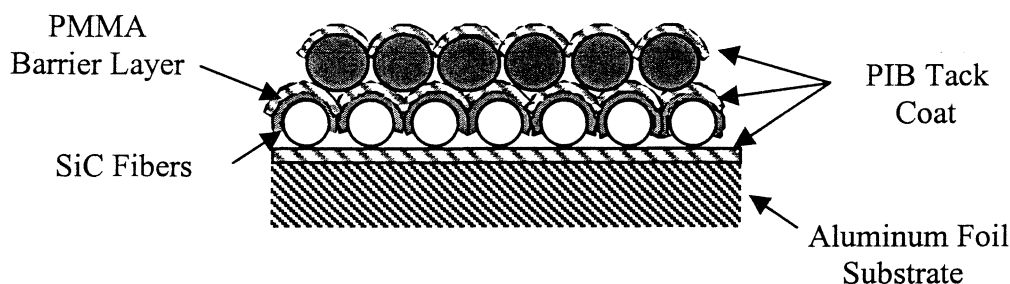


Figure 58. Schematic of ARC's Wire Winding Process

The process that ARC has developed for wire winding [99] is in many ways analogous to that previously described for their tape casting process. An aluminum foil substrate is cleaned on one side, and the other side is then wrapped around a drum. The substrate is used to provide a smooth defect-free surface which will not cause perturbations in the fiber spacing. A thin layer of 1wt% polyisobutylene (PIB) is applied to a substrate of aluminum foil. This tacky layer acts to hold the fibers to the substrate and is chosen such that it exhibits: 1) minimal shrinkage during drying to maintain the wire or fiber spacing, 2) that it is insoluble with any other solvent used in the process, and 3) that it sufficiently adheres to the substrate, but can be removed after outgassing. The fibers are then spooled onto the PIB tack coat using wheel tensioning and fiber alignment mechanisms, the latter which is held near the drum's surface and traverses it, as the fiber is wound onto the drum. The fiber is typically spooled on first, since it has a lower strain than the matrix wire for a given tensioning, and to obtain a preform with no defects, the higher strength material must be on the outside. A barrier layer of polymethylmethacrylate (PMMA) dissolved in acetone is then applied on top of and in between the fibers. Unlike the tape cast process which

uses fine matrix powders to maintain fiber spacing, the wire winding process uses both the PIB tack coat and the PMMA barrier layer to help maintain fiber separation. The characteristics of the PMMA barrier layer are analogous to those described for the PIB tack coat, in that it: 1) must exhibit minimal shrinkage during drying to maintain fiber and wire spacing, 2) be insoluble in any solvent used in the process, and 3) be able to be completely off-gassed. Another tack layer of PIB is added on top of the PMMA barrier, and the matrix wire is spooled onto the drum in a manner completely analogous to the fiber. The wires are wound in the same direction as the fiber, and are set in the fiber grooves to help minimize movement during off-gassing and consolidation. The process is repeated until the preform reaches the requisite number of plies, at which point it is off-gassed at elevated temperature, the substrate backing removed, and consolidated under vacuum via HIP'ing using time/temperature/pressure combinations to ensure complete densification. The fiber used is typically 140 μm (5.6 mil) SiC and the wire is nominally 175 μm (7 mil) and of the desired matrix composition. Composite fiber volume loading can be controlled by varying the diameter of the matrix wire. Typically the wire is circular in cross-section, which provides for a green density of ~80%. However, cross-shaped wire with right angles or radius angles provide for green densities of 90% and 98%, respectively. More details regarding the wire winding process can be found in ARC's patent [99].

The orthorhombic matrix wire used for the wire winding process is made by Dynamet Corporation. Current practice uses HIP'ing to consolidate orthorhombic powder to ~38 mm (1.5 in) bar. This is followed by a series of two hot extrusions at 7:1 to 12.7 mm (0.5 in.) and 5.1 mm (0.2 in.) rods. The rod material is then cold drawn 40-50% to 175 μm (7 mil) wire. Intermediate anneals are used to enable additional working at each step of the process, and currently all elevated temperature processing is undertaken at a constant maximum (non-optimized) temperature of 1032°C. Dynamet under sponsorship from ARC has successfully produced Ti-22Al-26Nb wire from Crucible gas atomized powder. The microstructure of the as-drawn and vacuum annealed wire for this composition is shown in Figure 59. Much like the structure for the Ti-22Al-23Nb foil shown previously, the primary α -2 grains have been extremely microstructurally textured in the direction of the hot extrusion and cold drawing. The volume fraction of α -2 is on the order of 25% which is considerably higher than that found in the foil product. The scale of the orthorhombic + beta microstructure is extremely fine.

Table 10 contains room temperature tensile results for Ti-22Al-26Nb in wire, tape cast neat, and foil neat forms. The tensile strength and total elongation of the wire exceed those values for both the as-consolidated neat foil and tape cast materials. It should be noted that consolidated wire neat data was not available at the time of this publication. However, it would appear that the additional thermomechanical processing the material receives during hot extrusion and cold working may be producing texturing (microstructural and/or crystallographic) which helps improve mechanical performance. However, it is very possible that this same texturing could produce anisotropic mechanical

behavior in a consolidated component. The degree of this anisotropy and its effect on mechanical performance will need to be assessed.

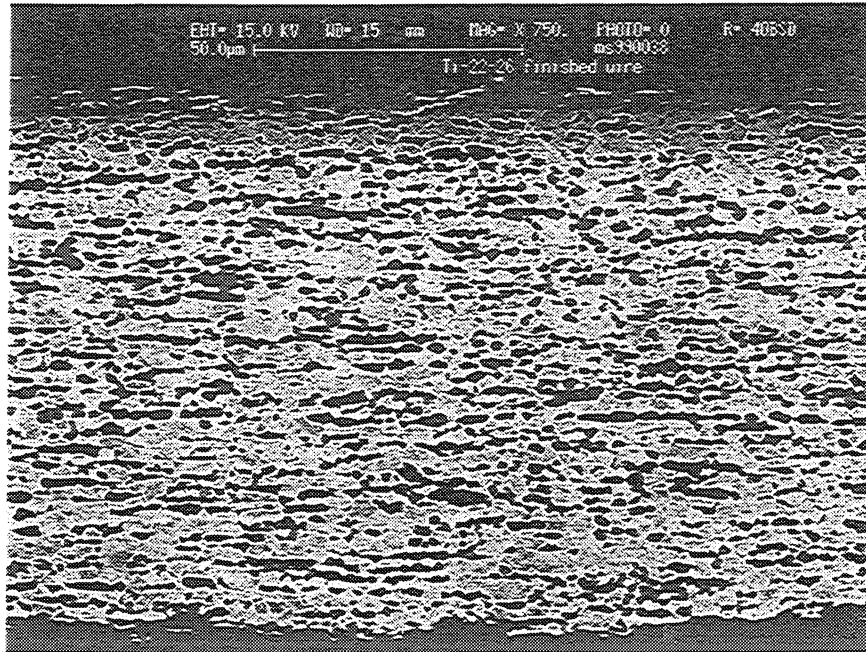


Figure 59. Ti-22Al-26Nb Wire Produced by Dynamet

The primary benefits of the wire winding process in the fabrication of O TMCs versus foil-fiber-foil and tape casting is that the wire process is better suited for making hoop wound components from a geometrical standpoint, and its potentially superior tensile properties. The downside to the wire winding process is the cost in making batches of wire versus production quantities of coiled wire. The Air Force Materials and Manufacturing Directorate in conjunction with the Propulsion Directorate is sponsoring at the time of this publication, the fabrication and testing of two SiC/Ti-22Al-26Nb rings made via wire winding by ARC.

Table 10: Room Temperature Tensile Properties of Ti-22Al-26Nb in Wire, Tape Cast Neat and Consolidated Neat Foil Forms (from Smith ref 100).

Material Form	UTS (MPa)	Elongation (%)
Consolidated Neat Foil	1050	5.0
Consolidated Tape Cast	921	1.1
Wire	1215	8.8

VII. Mechanical Behavior of Composites

The goal behind the development of metal matrix composites based on orthorhombic alloys was to alleviate some of the shortfalls associated with earlier composites based on α_2 matrices and the inherent temperature limitations of TMCs based on conventional titanium alloys. Some of these deficiencies are pointed out by Larsen, et al. [101, 102]. One point of that comparison is the general inability of cross-ply $[0/90]_s$ and quasi-isotropic $[0/\pm 45/90]_s$ composites to meet or surpass the mechanical properties available in the monolithic materials. This is true for all SiC/Ti composites due to the weak fiber/matrix interface. Therefore, components manufactured from O TMC materials must be chosen based on the improved longitudinal mechanical properties of a unidirectional composite and take into account the limited off-axis properties. This section will focus, therefore, solely on unidirectional composites with the primary emphasis on loading in the fiber direction. The off-axis behavior will be discussed mainly in light of the inherent limitations of this loading orientation and the improvements offered by matrix modification.

Performance Requirements

One of the most attractive applications for O TMC materials is the hoop-reinforcement of axial compressor rotors, with maximum use temperatures in the interval of 590°- 760°C, taking advantage of the high temperature capability of orthorhombic matrices. The combination of high axial strength and lower density offered by such composite materials would reduce centrifugal forces on high speed, rotating structures. Also, such an application could take full advantage of the composite's longitudinal strength without requiring significant off-axis reinforcement.

Preliminary mechanical property requirements for such structural components were extracted from Porter, et al. [8] and Russ, et al. [15]. These property requirements are a simplification of the structural needs of an advanced turbine engine, but nonetheless, they serve as a useful metric in the development of new material systems. The requirements shown in Table 11 represent the tensile, creep and fatigue properties for three components. The components are: blisk/bling (integrally bladed disk / integrally bladed ring); impeller; and an alternate blisk/bling design (blisk/bling 2). The impeller and blisk/bling2 designs are the same as the "impeller" and "blisk/bling" shown for the matrix material in Table 2. The composite requirements are presented in terms of absolute values, rather than on a density or fiber volume fraction corrected basis.

Table 11. Composite Property Requirements for Blisk/Bling and Impeller Applications (after Ref. 8)

Property	Blisk/Bling 1	Impeller	Blisk/Bling 2
Tension (longitudinal)	540-760°C 1172 MPa	20°C / 1655 MPa 482°C / 1241 MPa	650°C / 1380 MPa
Tension (transverse)	540-760°C 103 MPa	705°C / 276 MPa	705°C / 145 MPa
Creep (longitudinal)	705°C / 483 MPa 540°C / 634 MPa $t_r \geq 300$ hours	705°C / 414 MPa 600 hours / $\epsilon \leq 0.5\%$	650°C / 1035 MPa 10 hours / $\epsilon \leq 0.24\%$ 510°C / 1035 MPa 900 hours / $\epsilon \leq 0.24\%$
Creep (transverse)	705°C / 55 MPa 540°C / 97 MPa $t_r \geq 300$ hours	650°C / 138 MPa 600 hours / $\epsilon \leq 0.5\%$	705°C / 110 MPa 10 hours / $\epsilon \leq 0.24\%$ 565°C / 110 MPa 900 hours / $\epsilon \leq 0.24\%$
Fatigue	650-760°C 0-634 MPa 10,000 cycles	485°C 900-1034 MPa 15,000 cycles	650-760°C -24-1035 MPa 24,000 cycles
Thermal Fatigue	Ambient to 815°C	Ambient to 705°C	Ambient to 815°C
TMF	none reported	none reported	none reported

t_r = rupture time

ϵ = creep strain

The composite mechanical performance is strongly dependent on the properties of the fiber reinforcements, the fiber volume fraction and the processing history of the composite. The largest volume of mechanical property data for O TMCs is for the SCS-6TM/Ti-22Al-23Nb composite. The studies include tensile, creep, fatigue, fatigue crack growth, thermomechanical fatigue and the influence of high temperature environment. These results are used as the baseline mechanical properties for this report. Additional results are introduced in order to understand the influences of fiber, processing, and matrix alloy composition.

SCS-6TM/Ti-22Al-23Nb

The goal behind the development of O TMCs was to alleviate the deficiencies in α_2 TMCs, namely poor room temperature ductility and strength, relatively high reaction rates with the SiC reinforcements, inadequate high temperature creep resistance, and low resistance to interstitial attack at elevated temperatures [13,15]. One of the first comparisons of orthorhombic and α_2

composites is the study by Smith, et al., [13]. Here the first generation orthorhombic composite, SCS-6TM/Ti-21Al-22Nb, showed improved mechanical properties over the SCS-6/Ti-24Al-11Nb composite. The promise shown by this new composite system spawned the manufacture of a large quantity of SCS-6TM/Ti-22Al-23Nb composite that represents the most studied of the orthorhombic titanium matrix composites. Russ, et al. [15] conducted a review of the properties of this system relative to the mechanical behavior of α_2 (SCS-6TM/Ti-24Al-11Nb) and β (SCS-6TM/Timetal@21S) TMCs. These two data sets indicate that orthorhombic TMCs reinforced with SCS-6TM fibers offer mechanical performance that meets nearly all aspects of the IHPTET hardware requirements in Table 11. A more complete comparison of the pertinent mechanical behavior of these two early SCS-6TM reinforced orthorhombic composites with the α_2 and metastable β composites is presented here, incorporating additional SCS-6TM/Timetal@21S data [103, 104] and SCS-6TM/Ti-24Al-11Nb data from Gambone [105]. Generally the results from the α_2 and metastable β composites are shown as best fit trend lines with the data for the orthorhombic composites presented along with trend lines.

Tensile

The comparison of the longitudinal and transverse tensile strength is shown in Figures 60 and 61, respectively. In both orientations, the Timetal@21S composite exhibits the best room temperature strength, while the orthorhombic alloys exhibit the best high temperature strength. This result is likely due to the high strength of Timetal@21S at room temperature that is substantially degraded at temperatures above 400°C. The orthorhombic composites exhibit a substantial improvement over the α_2 material at all temperatures, which is due to the higher strength [13] of the orthorhombic alloys. The greatest strength difference between the orthorhombic composites is in the room temperature transverse strength. This could be due to the limited transverse ductility in the Ti-21Al-22Nb foil [13] that was unidirectionally rolled as compared to the Ti-22Al-23Nb foil which was cross rolled and exhibited higher transverse ductility [106] and less anisotropy. Since the strength is similar at elevated temperatures, it is unlikely that the slight difference in fiber volume fraction played much of a role. This clearly indicates that the mechanical behavior of the matrix is important to the transverse tensile properties of the composite. However, a comparison of the α_2 and orthorhombic composites indicates that the longitudinal strength is not dominated solely by the reinforcing fiber but also by the strength and ductility of the matrix as well. The fiber/ matrix reaction layer, as impacted by the matrix composition and the processing parameters, will also have an effect on the composite strength. The shear and normal transfer of load between fiber and matrix will influence both the longitudinal and transverse strength, respectively.

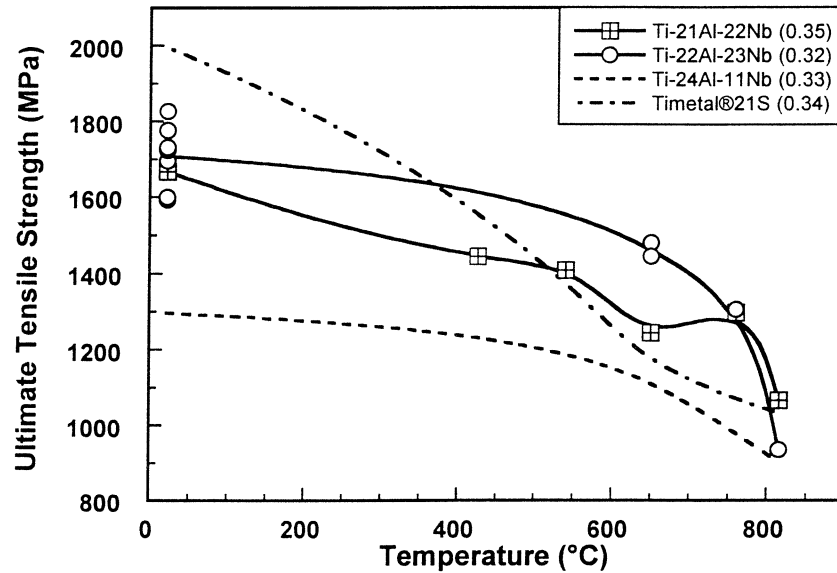


Figure 60. Comparison of ultimate tensile strength of longitudinal composites.

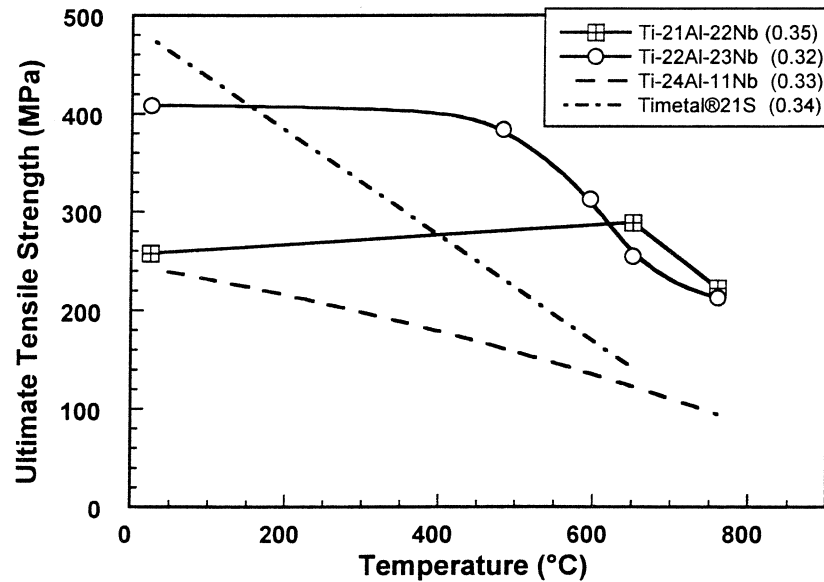


Figure 61. Comparison of ultimate tensile strength of transverse composites.

Thermal Cycling

Thermal fatigue of TMCs is problematic due to the mismatch of the coefficient of thermal expansion between the titanium base matrix and SiC fiber. This mismatch results in a large axial tensile stress in the matrix and large compressive stress in the fiber at room temperature [107]. Cycling between room and elevated temperatures can result in a severe degradation in composite strength [104, 108]. The primary driver behind the strength loss has been shown to be an environmental embrittlement of the matrix [104, 109]. A comparison of the residual ambient temperature strength of the three classes of materials is shown in Figure 62. All were subject to 500 cycles in laboratory air with a maximum temperature of 815°C and different minimum temperatures – resulting

in the temperature range shown on the abscissa. The thermal cycle in all cases had a period of 4 minutes consisting of 30-second hold times at T_{\max} and T_{\min} with 1.5 minutes used to heat and cool the specimens. As can be seen, the orthorhombic composite retained over 90 percent of its strength after the most severe temperature cycling as compared to 80 and 10 percent for the β and α_2 composites, respectively. After the most severe thermal cycling, the orthorhombic composite contained no surface cracks [13] while the both the Timetal®21S [104] and α_2 [108] composite did. This indicates that the orthorhombic composite has the best time/ temperature resistance of the three composite systems. However, the minimal damage observed in the orthorhombic composite does not indicate that it is completely impervious to damage due to thermal cycling. Indeed, subsequent studies at higher numbers of cycles resulted in environmental damage in the orthorhombic composite. The Timetal®21S composite showed an even more severe degradation in strength with increased cycle period or long isothermal exposure at elevated temperatures [104].

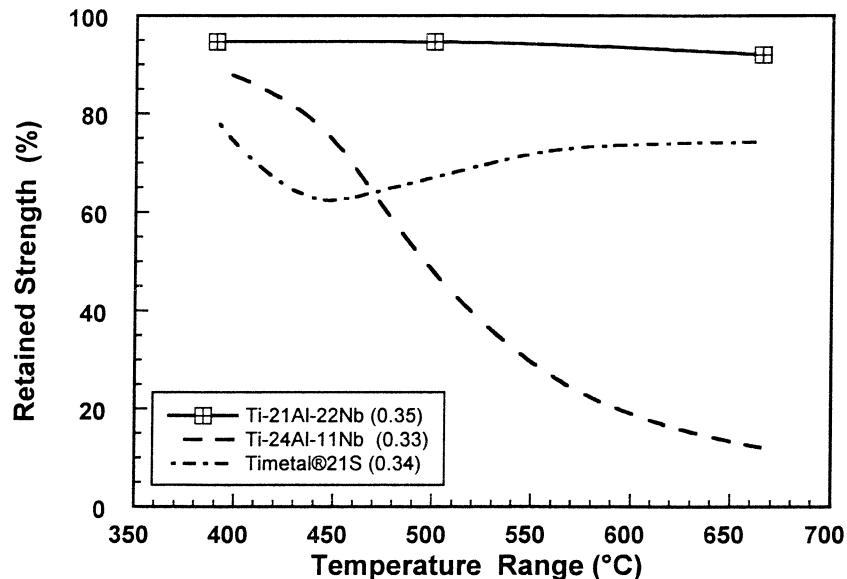


Figure 62. Residual RT tensile strength as a function of thermal cycling temperature range for 500 cycles at 815°C maximum temperature (after [13]).

Creep

The creep behavior of the orthorhombic composites is compared to the β and α_2 composites in Figures 63 and 64. Stress as a function of the Larson-Miller Parameter (in terms of time to rupture) for longitudinal composites is shown in Figure 63. The general applicability of LMP to the creep of composites is not well understood, however, it does provide means of comparison for the different composite materials. It is apparent that the O TMC has the best creep resistance that is only slightly better than the Timetal®21S composite. Both of these composites offer substantially better creep resistance than the α_2 composite.

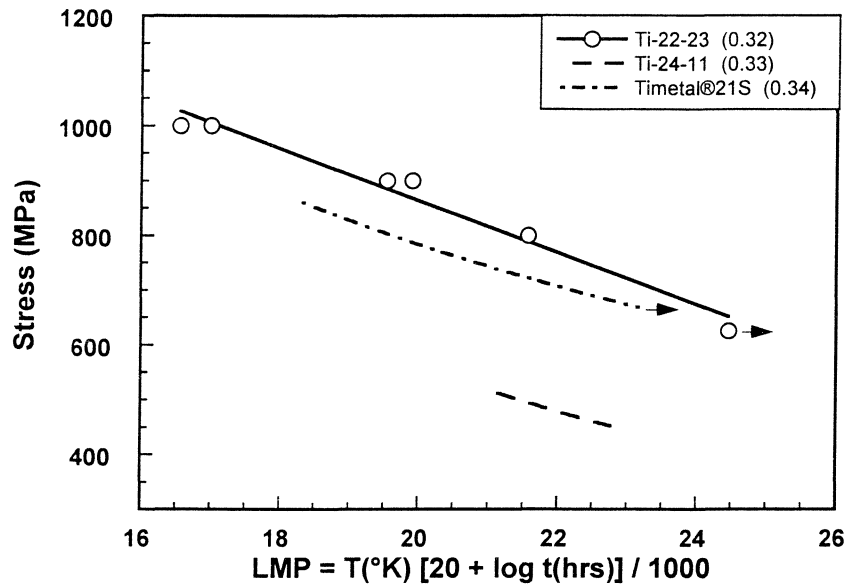


Figure 63. Creep-rupture comparison of longitudinal composites using the Larson-Miller Parameter.

Stress as a function of the Larson-Miller Parameter (in terms of time to 0.5% creep strain) for transverse composites is shown in Figure 64. Here, it is important to compare the composites in terms of LMP to a particular strain level since the overall composite strain is not held in check by the reinforcing fibers. Based on limited data, the two orthorhombic composites have higher creep resistance than the Timetal®21S and apha-2 composites – especially at low values of LMP (which correspond to lower temperatures and/or times).

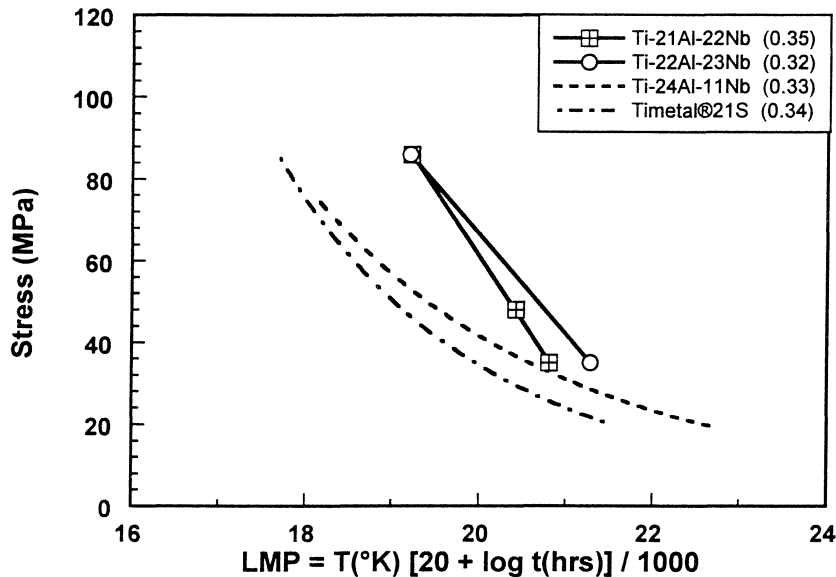


Figure 64. Comparison of creep behavior of transverse composites using the Larson-Miller Parameter to 0.5% creep strain.

Based on the general creep resistance of the matrix materials, as shown previously in Figure 37 [65] (also having similar microstructures to the composites in Figure 64), the ranking of the transverse composite creep roughly follows that of the monolithic creep behavior. However, in the longitudinal composites, Figure 63, the Timetal®21S creep resistance is nearly as good as the Ti-22Al-23Nb composite – even though the monolithic matrix creep resistance is vastly different. Also, the creep resistance of monolithic α_2 is only slightly lower than Ti-22Al-23Nb, yet the longitudinal composite creep resistance is substantially lower – than even the Timetal®21S composite! This clearly indicates that while transverse composite creep resistance is controlled by the matrix creep response, the longitudinal composite creep behavior is not. Most likely, matrix ductility and strength, environmental attack, and composite manufacturing processes affect the longitudinal composite creep behavior - of course, the reinforcing fiber also plays a very strong role.

Isothermal Fatigue

A comparison of the isothermal fatigue behavior of the three composite systems at 650°C is shown in Figure 65. Though the Ti-22Al-23Nb and Timetal®21S composites were tested at 1 Hz and the α_2 composite at 3 Hz, this relatively small difference in cyclic frequency should have no influence on the fatigue life. At high stresses and short lives, the three composite systems have a similar fatigue resistance, while at lower stresses and longer lives, the orthorhombic composite offers a 100 MPa improvement in fatigue strength. This is likely due to the stronger matrix and lower susceptibility to environmental attack than the other composite systems.

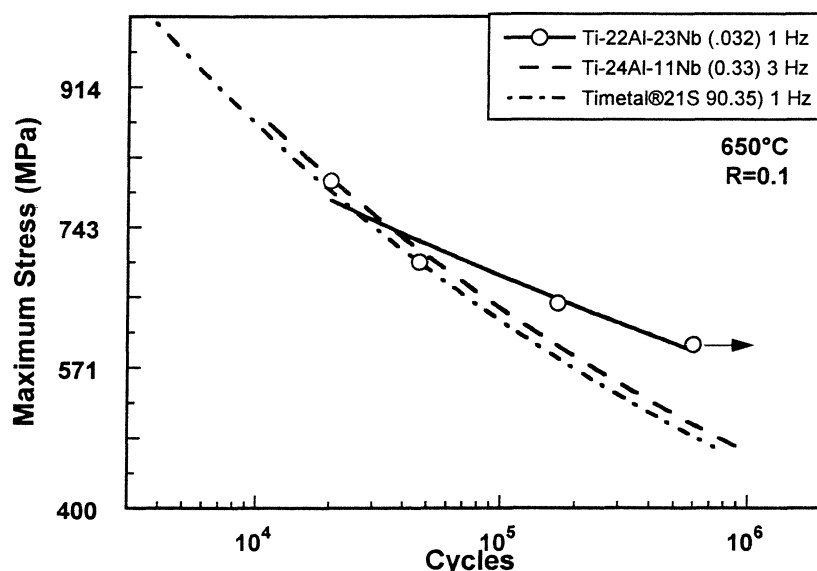


Figure 65. Comparison of the isothermal fatigue behavior of longitudinal composites at 650°C.

Thermomechanical Fatigue

A comparison of the out-of-phase (OP-TMF) and in-phase the thermomechanical fatigue (IP-TMF) behavior of the three composite systems is shown in Figures 66a and 66b, respectively. Though there is not a specific TMF requirement for hoop-wound structures, Table 11, the difference in coefficient of thermal expansion can lead to serious damage accumulation in titanium-base composites [110-112]. OP-TMF results in a large matrix stress range and damage quickly accumulates in the matrix. The orthorhombic and Timetal®21S composites have higher OP-TMF resistance than the α_2 composite, which is likely due to the better environmental resistance of the orthorhombic composite and the high ductility of the Timetal®21S composite systems. Note that both composites performed the best in terms of retained strength following thermal cycling, Figure 62, which has similarities to OP-TMF [108]. The majority of TMF tests on the orthorhombic and Timetal®21S were conducted with a 3 minute cycle (~ 0.006 Hz) as compared to the 6 minute (~ 0.003 Hz) cycle for the α_2 composite. One test of the Ti-21Al-22Nb composite was conducted at the lower cyclic frequency and showed only a small reduction in OP-TMF life. Therefore, the reduced OP-TMF resistance of the α_2 composite is not solely due to the slower frequency.

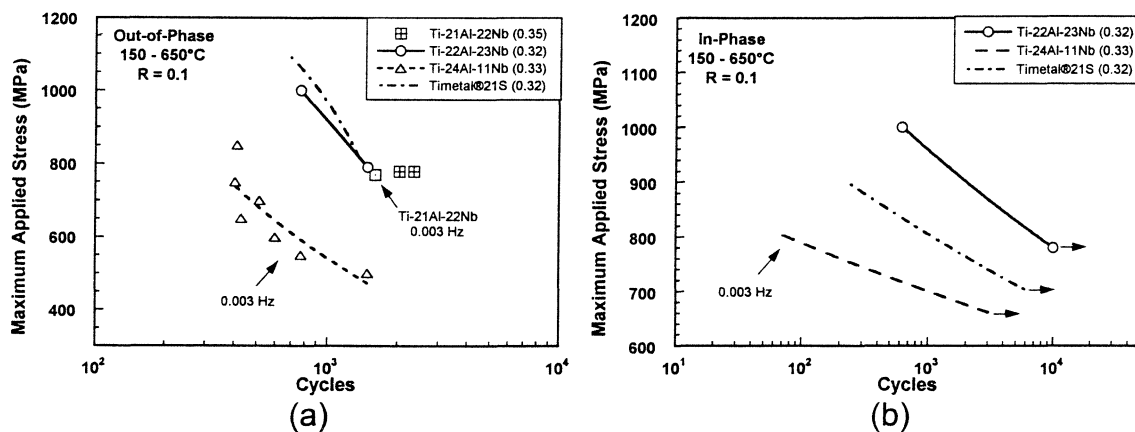


Figure 66. Comparison of the out-of-phase (a) and in-phase (b) thermo-mechanical fatigue behavior of longitudinal composites.

IP-TMF results in a low matrix stress range, but higher maximum and alternate stresses in the fiber. Hence, this failure is typically fiber dominated [112]. The comparison of the three composite systems, Figure 66b, however, shows a significant deviation in IP-TMF behavior for composites having the same reinforcing fiber. Nicholas and Johnson [113] have discussed the similarities between IP-TMF and creep failure in TMCs. Their experimental and analytical work points out similarities in failure mechanism and time dependent relaxation of stress in the matrix and subsequent overload of the fibers. In light of this, considering the differences in creep response of the three matrix materials indicates that the orthorhombic composite should have the best performance with the Timetal®21S composite having the worst. However, the poorest performance

shown by the α_2 composite may be in some part due to the slower fatigue frequency - 0.003 Hz versus 0.006 Hz for the others.

Again, these results show that the matrix mechanical behavior and/or composite processing do have an influence on the fiber dominated properties of a TMC. The matrix creep behaviors in Figure 37 show that the creep resistance of Timetal®21S is substantially lower than that of either Ti-24Al-11Nb or Ti-22Al-23Nb. Based on a “time to failure” concept, the Ti-24Al-11Nb composite should fail at only slightly less than half the number of cycles than the orthorhombic composite. Since this is clearly not the case, Figure 66b, the composite processing or environmental degradation of the α_2 composite must also be playing a role in the IP- TMF performance.

Fatigue Crack Growth

The fatigue crack growth resistance of the Ti-22Al-23Nb composite was examined and compared to the α_2 and Timetal®21S composites by Jira and Larsen [114]. These results are shown in Figure 67a & b for room temperature and 650°C respectively along with closure corrected (da/dN vs. ΔK_{eff}) trend lines for the fiberless matrix. All tests were conducted using middle hole tension specimens with crack initiation from circular holes in the center of the specimen having a nominal 0.25W diameter. At room temperature, Figure 67a, the crack growth rates for all composites decrease with increasing length and applied ΔK . Here the retardation of crack growth was clearly due to unbroken fibers bridging the cracks. At 650°C, fiber bridging was less effective at reducing the crack growth rates - all composites exhibited increasing crack growth rates with the increase in crack length and applied ΔK .

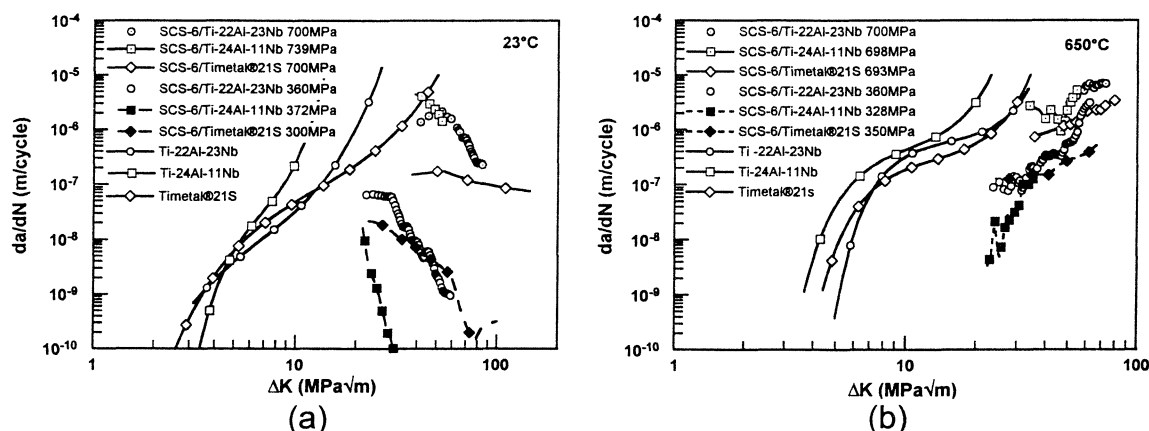


Figure 67. Comparison of the fatigue crack propagation behavior of the three composite systems at; (a) room temperature and (b) 650°C (after Ref. 114).

The monolithic crack growth curves show little difference in the threshold regime at either temperature; however, at room temperature, the apparent fracture toughness ranks in the order: Timetal®21S > Ti-22Al-23Nb > Ti-24Al-11Nb. Based on the modeling of Jira and Larsen [114], the bridged fatigue crack growth resistance should vary in a similar manner. However, the Ti-24Al-11Nb composite has the lowest crack growth rates at both of the nominal stress levels

examined. This likely indicates the myriad of factors that contribute to the crack growth resistance in composites, such as residual stresses, crack bridging and the interface strength or character – all of which are affected by both matrix material and processing conditions.

VIII. Damage Mechanisms

The ultimate goal driving the development of O TMCs is to insert these materials into fracture critical components of gas turbine engines. To reduce the failure risk of these components, a better understanding of failure mechanisms is paramount to incorporating them into component design methodologies. To this end, much of the research on the mechanical performance of O TMCs is aimed at gaining this understanding. This section examines three general areas of damage mechanisms and the extent to which they play a role in the mechanical behavior of O TMCs.

Environmental Attack

One form of high temperature damage that is of primary concern for all structural applications is the deleterious effect of an air environment. Both titanium and aluminum are very reactive metals in a high temperature, oxidizing environment, which leads to damage as a function of time at temperature. The general phenomenon of oxidation of orthorhombic alloys has been covered in Section IV, Matrix Development. This section will deal with the influence of oxidation on the mechanical performance of the composite system. The basic problem of embrittlement in Ti-22Al-23Nb neat materials was described by Rosenberger [115] where a reduction in tensile ductility, from 5.4% to 1.2%, was found after a 760°C / 100 hour exposure to laboratory air. The fracture surfaces of the exposed specimens showed a brittle annulus of 30 μm at the specimen surface - indicating the depth of oxygen penetration. This depth is similar to that found in the oxidation study by Brindley, et al. [69] who found that the formation of an alpha case is not necessary for embrittlement to occur. An additional (and curious) finding of the study by Rosenberger is that a 760°C / 100 hour exposure in a dynamic vacuum (2×10^{-6} torr) also resulted in a decrease in ductility (to 1.7%) and the formation of a brittle annulus 10 μm deep at the surface of the specimen. This indicates severe sensitivity to even minute levels of oxygen at this temperature.

Longitudinal orthorhombic composites are more tolerant of high temperature exposure as the overall composite strain is predominately limited by the strain capability of the SiC fibers. One instance, however, where environment was found to have a strong influence on the composite mechanical behavior is during fatigue. Russ, et al. [116] studied the damage progression during isothermal fatigue loading of SCS-6™/Ti-22Al-23Nb composites in laboratory air and high vacuum (2×10^{-6} torr). A pronounced environmental effect was observed at temperatures greater than 430°C with the fatigue life being an order of magnitude longer in vacuum as compared to air, Fig, 68. Also a change in fatigue cracking and accumulation of damage was observed that is covered in more detail in the next section. It appears, however, that crack propagation in the matrix is greatly reduced in the high vacuum environment.

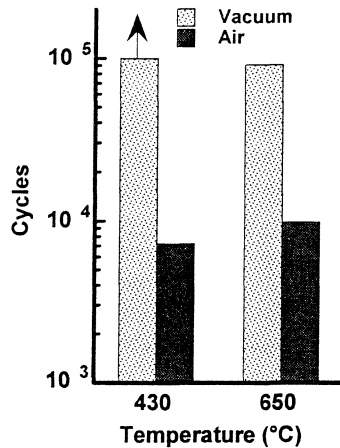


Figure 68. Comparison of the fatigue life at 430° and 650°C for specimens tested at 900MPa, 0.1 Hz, R=0.1. Arrow indicates runout at 10⁵ cycles. [116]

Another instance where environment plays a strong role in the mechanical performance of longitudinal composites is OP-TMF [119] or stress-free thermal fatigue (a form of OP-TMF) [104]. Brindley, et al. [119] examined the surfaces and crack faces in non-isothermal fatigue specimens (essentially OP-TMF) and found similar penetration of oxygen in several different composites all reinforced with the SCS-6™ fiber, though the orthorhombic composite SCS-6™/Ti-20Al-24Nb and an $\alpha_2+\beta$ composite showed lesser depths of embrittlement than the $\alpha+\beta$ and $\beta+\alpha$ composites. This study also found that the depth of environmental attack in the cracks that form during OP-TMF cycling is similar to the depth that forms on the surface of the composite – indicating a possible increase in penetration rate at the tips of the cracks.

Environment can have a pronounced effect on transverse composites – especially when the ends of the fibers are exposed to the environment. Woodard, et al. examined the creep behavior of transverse Sigma 1140+/Ti-22Al-23Nb [117] and SCS-6™/Ti-22Al-23Nb [118] composites. Generally the transverse creep strength of the composite in high vacuum (10⁻⁷ torr) was similar to that monolithic material [117]. An analysis of the published results for the two composite systems is shown in Fig. 69 and compared to the creep results shown in Fig. 64. The Sigma 1140+/Ti-22Al-23Nb composite has a substantially higher creep resistance in vacuum and the SCS-6™/Ti-2Al-23Nb composite also shows a modest increase in creep resistance. Here, the environment attacks the carbon coating of the SiC fiber and reduces the bond strength between the fiber and matrix. Pushout tests were utilized to measure remaining bond strength in crept specimens and it was found that the pushout strength was very low for specimens tested in an air environment. Some of the difference in transverse creep response of the two composite systems could be due to variations in uniformity of the fiber spacing that was documented to have a pronounced effect on the steady state creep rate [118]. One additional assumption is that the environmental influence would be less at higher applied stresses where the initial loading would surpass the bond strength.

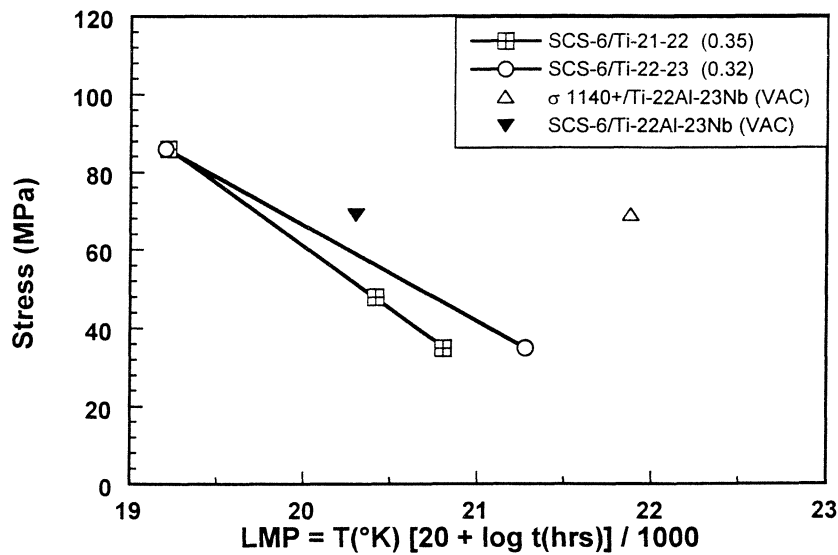


Figure 69. Comparison of creep behavior of transverse composites in air (from Fig. 64) and vacuum [117-118] using the Larson-Miller Parameter to 0.5% creep strain.

As mentioned earlier, it is necessary to protect orthorhombic materials from environmental attack for use temperatures greater than 600°-700°C. To this end, several attempts have been made to develop coating techniques to provide environmental protection under fatigue loading conditions where the environmental attack has a documented deleterious effect on life. Brindley, et al. [33] documented that embrittlement occurs a factor of 100 times faster than oxidation for orthorhombic alloys. They conducted limited testing on monolithic Ti-19Al-23Nb coupons coated with Ti-Si+Ge and Ti-Si+B codeposited via cementation methods. Isothermal fatigue tests conducted at 700°C with a strain range of 0.26% resulted in a reduction in fatigue life from 11,000 cycles to 2500 and 1500 for the Ti-Si+Ge and Ti-Si+B coatings, respectively. Rosenberger, et al. [34] examined the effect of a TiAl₃+two-phase glass (TPG) coating on the fatigue behavior of a SCS-6™/Ti-22Al-23Nb composite, under 650°C isothermal fatigue conditions and 150° - 650°C OP-TMF conditions. This coating system was designed to provide a reaction barrier (EB-PVD aluminum to form TiAl₃) and an oxygen diffusion barrier (TPG applied by the sol-gel process). The lower melting phase of the TPG was meant to heal cracks or damage in the coating. There was no improvement in the OP-TMF ($R=0.1$ / $\sigma_{\max} = 780$ MPa / $\nu = 0.06$ Hz) resistance with the coating. Both lives were ~1500 cycles. However, under the isothermal fatigue conditions, ($R=0.1$ / $\sigma_{\max} = 900$ MPa / $\nu = 0.1$ Hz) the fatigue life decreased from about 7500 to 1900 cycles. Though the OP-TMF results show some promise, there is clearly much additional work that needs to be done on environmentally protective coatings for O TMCs that work under fatigue loading.

Fatigue cracking

The evolution of fatigue damage in O TMCs has been studied by a number of researchers [18,116,120]. Understanding this evolution is important as it guides the damage-tolerant life prediction methodology that is needed for components manufactured from this material [116]. Russ, et al. [116] examined the influences of temperature, stress range and environment on the isothermal fatigue resistance of SCS-6™/Ti-22Al-23Nb (at%) [0]₄ composites over the temperature range from 20°C to 650°C. The fatigue results of this study are shown in Fig. 70.

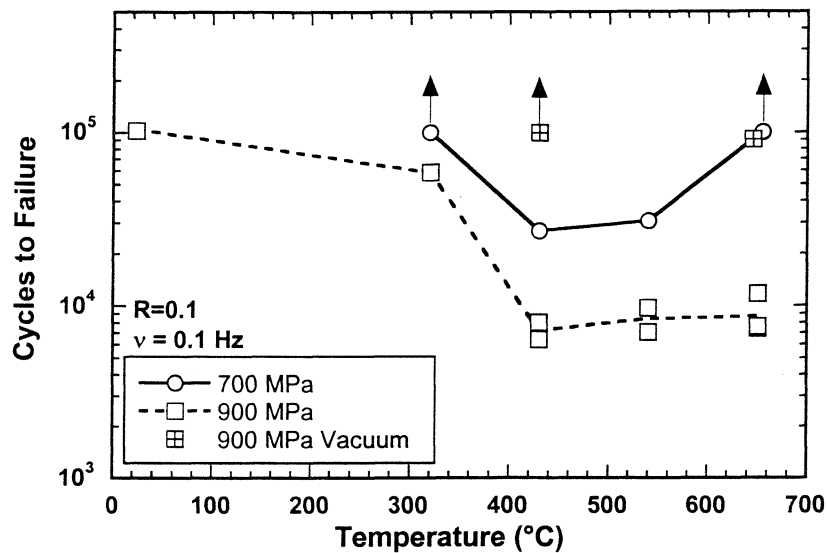


Figure 70. Influence of temperature, maximum stress and environment on fatigue life for SCS-6™/Ti-22Al-23Nb [0]₄ composites, arrows indicate runout (after [116]).

At 900 MPa fatigue lives decreased with increasing temperature until 430°C, at which point a gradual increase with temperature was noted. At 700 MPa, fatigue lives were longer and a more prominent increase in life at the highest temperature, 650°C, was achieved. This increase in fatigue life at 650°C was attributed to a reduction in the matrix stress range as the matrix relaxed shedding load to the fibers. As previously noted, there is a pronounced effect of environment on the high temperature fatigue life. With the increase in temperature, there was a pronounced change in the damage accumulation as detected with ultrasonic surface-wave C-wave scans and verified with SEM, Fig. 71.

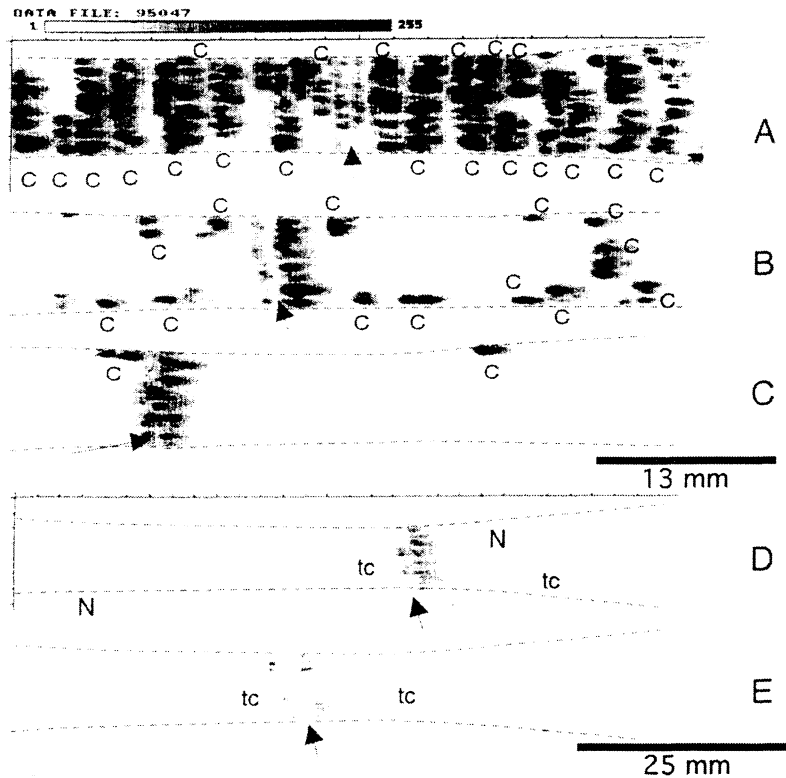


Figure 71. Ultrasonic surface-wave C-scans of 900 MPa tests at (a) 20°C, (b) 320°C, (c) 430°C, (d) 540°C, and (e) 650°C. C, tc, and N indicate cracks, thermocouple weld marks, and no damage optically identified, respectively [116].

At 20°C, the specimen has a large number of cracks (distributed cracking) that traverse the entire cross section of the specimen. With an increase in temperature, the number of cracks decreased such that at 540°C and above, only a single crack was found that led to failure of the specimen. Specimens tested with a maximum stress of 700 MPa exhibited distributed damage up to 540°C, though it appears that the number of cracks decreased with the decrease in maximum stress [120]. In the vacuum environment, cracks initiated at numerous sites even at 650°C, indicating the strong influence of environment on the matrix crack growth process at elevated temperatures.

The change in damage accumulation, distributed cracking versus the growth of a single crack, indicates a change in the effectiveness of fiber bridging [116, 120]. The clearest example of this is the fact that cracks grow to cover the entire cross section of the specimen before failure. Therefore at lower temperatures and lower stresses, the crack growth law used for damage tolerant design should include the beneficial effects of fiber bridging while at higher temperatures, in an air environment, bridging plays a lesser role. Wang, et al. [120] developed a model that is calibrated at room temperature to predict the residual tensile strength of the composite after damage has accumulated during fatigue loading. A key aspect of the model is the incorporation of a shear-lag model to take into account the bridging strength of the fibers. Concomitant with this is the fact that the stiffness reduction in the composite during the

accumulation of fatigue damage is correlated with the length of the cracks and not the crack density [18,120].

Effect of service representative loading

Another aspect of mechanical performance of O TMCs is their performance under actual service loading conditions – which is more complex than the simple isothermal and thermomechanical loading discussed previously. In both military and commercial applications, engines will encounter minor throttle movements as well as periods of steady cruise when the engine will see relatively steady loading. These two aspects of loading have not been addressed in the baseline mechanical property data. Chatterjee, et al. [121] and Gabb, et al. [122], have explored the behavior of an SCS-6™/Ti-22Al-23Nb composite under a representative mission loading profile. Both studies incorporated a simple mission profile that is meant to simulate the operating conditions of a gas turbine engine compressor. This mission, shown in Fig. 72, attempts to capture aspects of a complex cycle, i.e., thermomechanical loading, lags in temperature, hold times at max load and a mix of major and minor cycles.

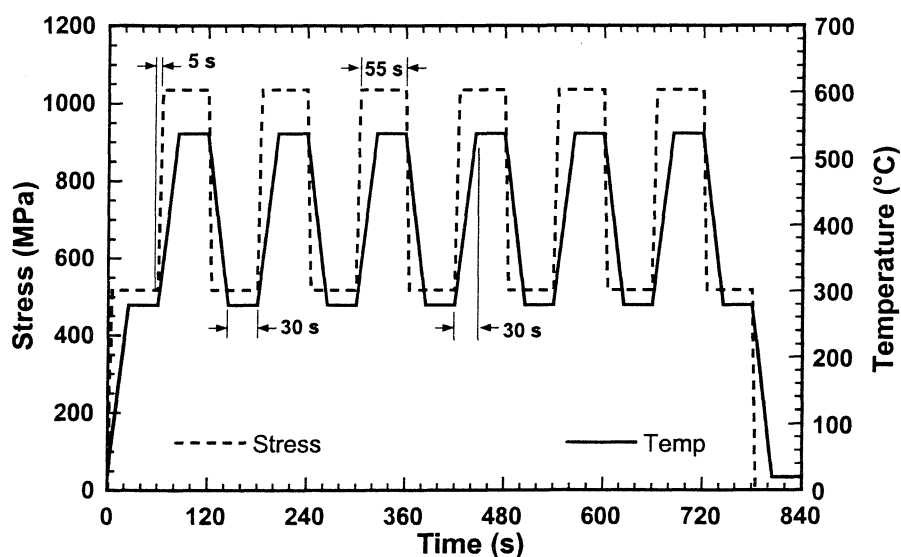


Figure 72. Simplified compressor mission incorporating thermomechanical loading, lags in temperature, hold times at max load and a mix of major and minor cycles [121].

This simplified mission cycle consists of one “Type I” cycle (min-max-min) and six “Type III” subcycles (mean-max-mean). The Type I cycle is meant to represent starting the engine, accelerating the engine, stabilizing at max power, and shutting down the engine. The Type III cycle is meant to represent the throttle excursion from idle to max power and back to idle which is represented as the subcycles with a stress ratio of $R=0.5$. The conditions of $\sigma_{\max} = 1035$ MPa and $T_{\max} = 538^{\circ}$ were chosen as baseline conditions for the O TMC evaluation.

The triplicate tests of the baseline mission has a average life of 1235 cycles which is nearly an order of magnitude lower than comparable isothermal, IP-TMF, OP-TMF or OP non-isothermal cycling as shown in Figure 73. The reduction in fatigue life of the mission cycle was accompanied by an increase in maximum strain during loading. This ratcheting was attributed to the hold times at maximum load and the accompanying relaxation of stress in the matrix that would tend to overload the fibers – causing the reduction in life.

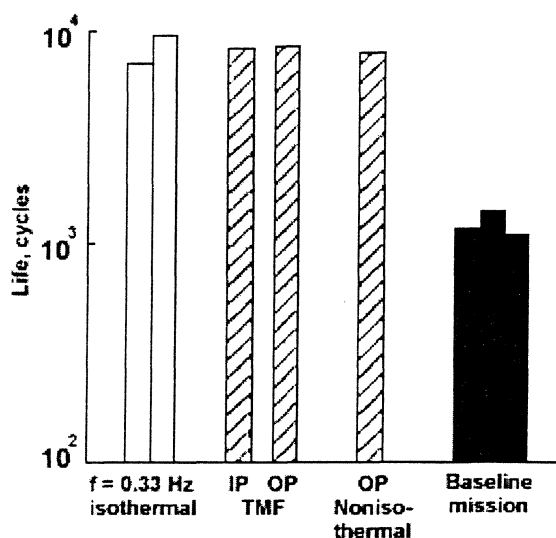


Figure 73. Comparison of baseline mission spectrum fatigue to isothermal, IP-TMF, OP-TMF, and OP non-isothermal fatigue data. [121].

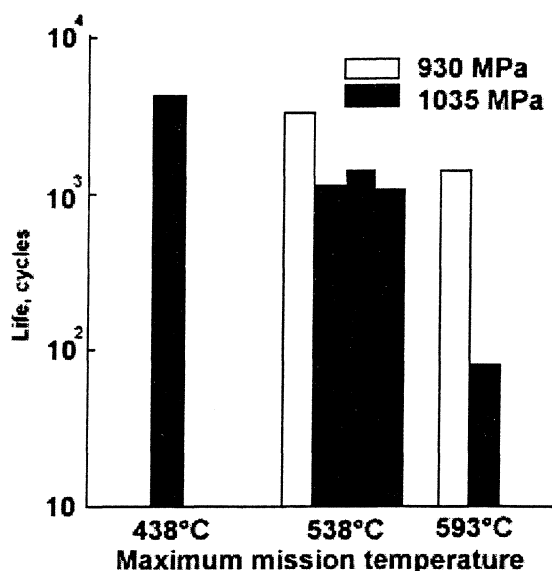


Figure 74. Effect of spectrum maximum stress and maximum temperature on the mission life. [121].

The cyclic mission goals of 3000 cycles could be met by either decreasing the stress on the composite or reducing the maximum stress of the cycle. The effect of both of these is shown in Figure 74. The mission response of the

composite clearly drops off steeply at temperatures above 538°C where even a reduction in the maximum cyclic stress, to 930 MPa, was unable to meet the required 3000 mission cycles.

The primary driver for the difference in performance between simple thermomechanical cycling and the mission loading is the dwell time at maximum temperature [122]. Figure 75 shows a comparison of continuous cycling isothermal fatigue life with a generic mission cycle incorporating various hold periods and the baseline mission profile. The generic mission cycle has the same thermal phasing and thermal lag characteristics without the sub cycling (Type III cycles). The baseline mission cycle, however, incorporates a combined dwell period of 180 seconds at maximum stress and temperature, yet has a longer life than the generic mission cycle with a dwell period of 150 seconds. It was found that the subcycling has a beneficial effect on fatigue performance, likely through an interruption of the matrix stress relaxation [122].

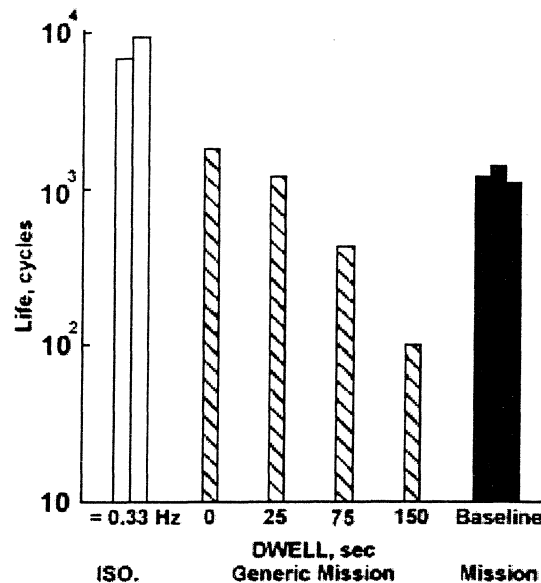


Figure 75. Comparison of the baseline mission cycle fatigue life with isothermal fatigue and a generic mission cycle incorporating various hold periods at maximum load. [122].

From this work, it is clear that the behavior of O TMCs under mission representative loading is not well predicted by simple isothermal or thermomechanical loading. To incorporate O TMCs in full-life gas turbine engine components, additional analytic and experimental efforts must be placed on this aspect of composite performance.

IX Constituent Effects on Composite Properties

It was demonstrated that the O TMC offered the best combination of mechanical properties when compared to TMCs based on Timetal[®]21S, a conventional metastable β titanium alloy, or Ti-24Al-11Nb, an α_2 based titanium aluminide matrix [15, 114]. However, deficiencies in longitudinal creep and fatigue, as well as transverse strength and creep, remained. The best near-term means to improve the longitudinal properties of the composite, without significant debits in other properties, is through the incorporation of a fiber with higher strength. Transverse property improvements could then be met through improvements in the matrix creep or strength properties, fiber/matrix interface strengthening, and/or a reduction in the fiber volume fraction due to substantial improvements in longitudinal properties. The Ultra SCSTM fiber appears to offer such benefits based on the preliminary mechanical property data that exists on O TMCs reinforced with this fiber [29, 123].

Effect of fiber

Rosenberger, et al. [29], have compared mechanical properties of Ultra SCSTM/Ti-22Al-23Nb composites to SCS-6TM/Ti-22Al-23Nb and Trimarc 1[®]/Ti-22Al-23Nb composite systems. (Henceforth these composites are called Ultra SCSTM composites, SCS-6TM composites, and Trimarc 1[®] composites, respectively). Generally, improvements in all longitudinal properties were offered by the Ultra SCSTM composites with no adverse effect on the transverse mechanical properties.

Figure 76 shows a comparison of the longitudinal ultimate tensile strength as a function of temperature for the three composite systems. Clearly, the Ultra SCSTM composite exhibits the highest strength over the entire temperature range – offering an increase in strength of more than 100 MPa and 400 MPa over the SCS-6TM and Trimarc 1[®] composites, respectively. The strength increase was accompanied by an increase in the strain-to-failure, which is consistent with the apparent strengthening mechanism in the fiber, believed to be due to a significant refinement of the β SiC microstructure resulting in higher intrinsic notch toughness.

A slight increase in transverse tensile strength was observed in the Ultra SCSTM composite compared to the SCS-6TM composite. This is likely due to the slightly lower fiber volume fraction of the Ultra SCSTM (0.30 vs 0.33). Notable is the finding that the transverse tensile strength of the Trimarc 1[®] composite, having a fiber volume fraction of 0.35, is less than half of the other two at room temperature. This is likely a result of the slightly higher fiber volume fraction and the weaker fiber/ matrix bond with this fiber.

The longitudinal creep-rupture behavior of the three composite systems is compared in Fig. 77. Here, the sustained load level (stress) is compared to the LMP calculated as, $LMP = T[20 + \log(t_r)]/1000$ (K log hrs $\times 10^{-3}$), using time to rupture (t_r) in hours. The results are reasonably represented using a linear fit which lends validity to the comparison. The Ultra SCSTM reinforced composite shows approximately a 200 MPa improvement in performance over the SCS-6TM composite and better than a 400 MPa improvement over the Trimarc 1[®]

composite. The slope of the fits for the SCS-6TM and Ultra SCSTM are similar (which may indicate similar damage mechanisms), while the Trimarc 1[®] composite has a steeper negative slope. This difference in slope may be due to the reaction between the tungsten and SiC within the fiber, as mentioned in an earlier section, in the case of the Trimarc 1[®]. The reaction would be more severe at higher temperatures or longer times associated with the higher values of LMP.

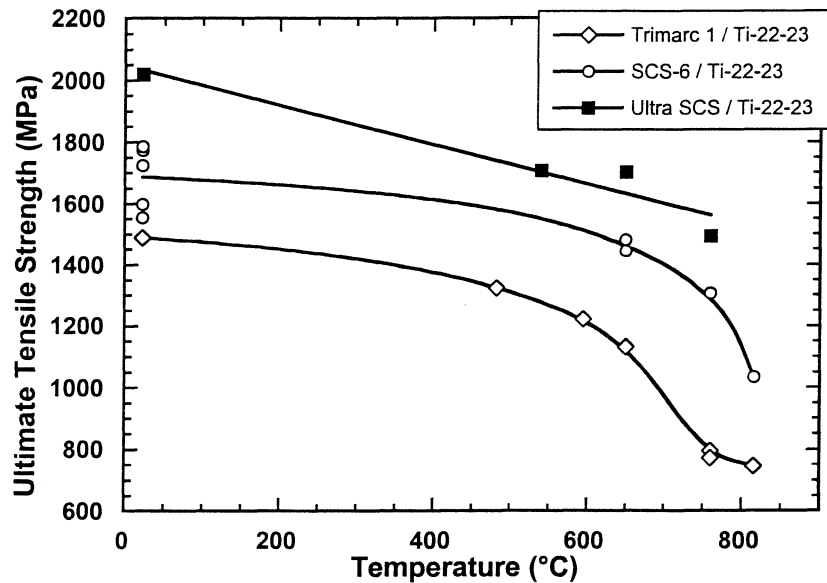


Figure 76. Comparison of the ultimate tensile strength of the three composite systems [29].

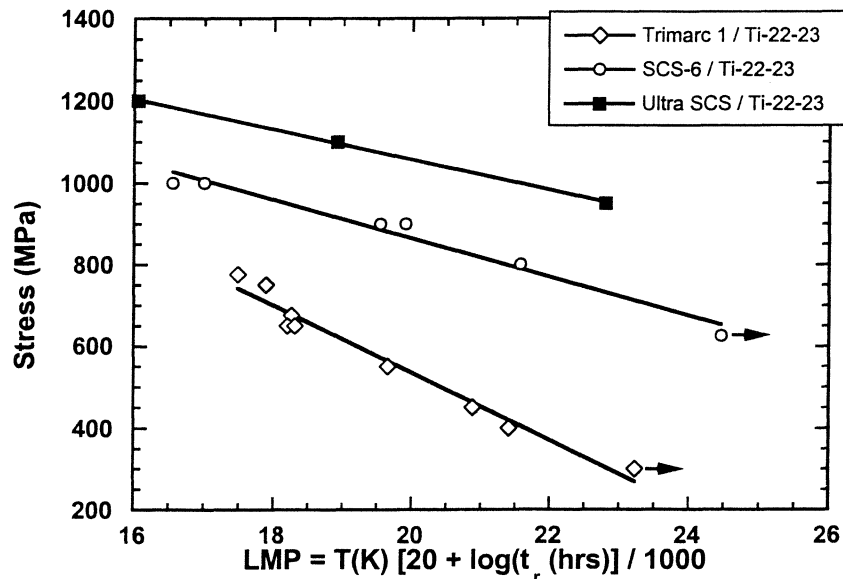


Figure 77. Comparison of the longitudinal creep behavior of the three composite systems [29].

The transverse creep behavior is nearly identical for the three composite systems [29]. This indicates that the weaker fiber/ matrix bond in the Trimarc 1[®] composite at room temperature is not adversely affecting the high temperature transverse creep resistance. Clearly there is little beneficial contribution of fiber / matrix bonding at higher temperatures in these composites.

Figure 78 shows a comparison of the isothermal fatigue lives for the three composite systems tested at 650°C. The Ultra SCS[™] composite exhibits an increase in fatigue life by a factor of approximately five over the other composite systems at high stresses while there is only a slight improvement at lower stresses. This observation suggests that at higher stresses the fatigue behavior is dictated by the strength of the fibers, while at lower stresses, crack initiation and growth in the matrix material may dominate the fatigue life.

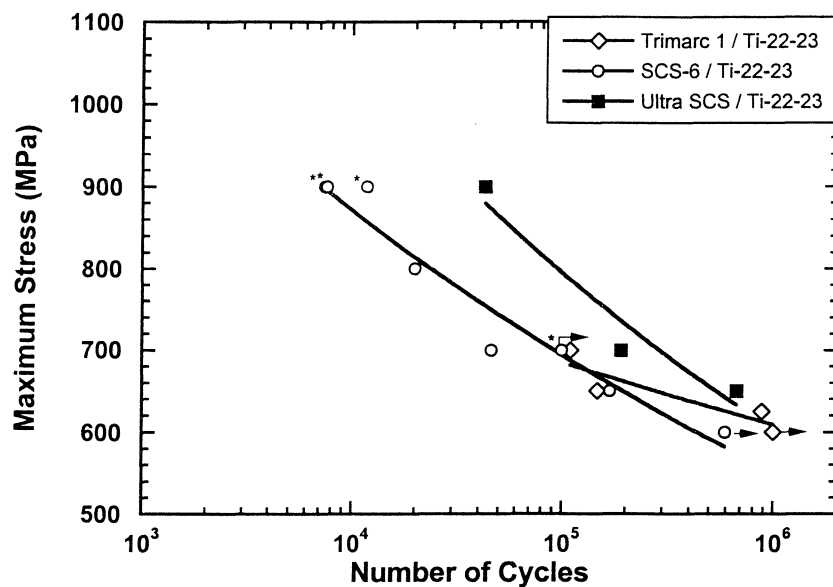


Figure 78. Fatigue behavior of SCS-6[™], Trimarc 1[®], and Ultra SCS[™] composites at 650°C, R = 0.1, frequency = 1.0 Hz (* indicates 0.1 Hz) [29].

The effect of temperature on isothermal fatigue is shown in Fig. 79 for the SCS-6[™] and Ultra SCS[™] composites at a constant maximum stress of 900 MPa and R = 0.1. The Ultra SCS[™] tests were conducted at a frequency of 1 Hz, while the SCS-6[™] composite data were generated at a frequency of 0.1 Hz however it is believed that this has no effect on the results [29]. The Ultra SCS[™] composite shows an improvement in life by nearly an order of magnitude compared to the SCS-6[™] composite system over the entire temperature range examined. The lives at the higher temperatures are approximately an order of magnitude lower than that observed at lower temperatures. This decrease in fatigue life at high temperatures has been shown, in SCS-6[™] composites [116], to be due to a change in damage mechanisms. The higher cyclic life observed at low temperatures was found to correspond to a distributed form of damage that was consistent with fiber bridging mechanisms. The higher cyclic life of the Ultra SCS[™] versus SCS-6[™] composites is consistent with this presumption.

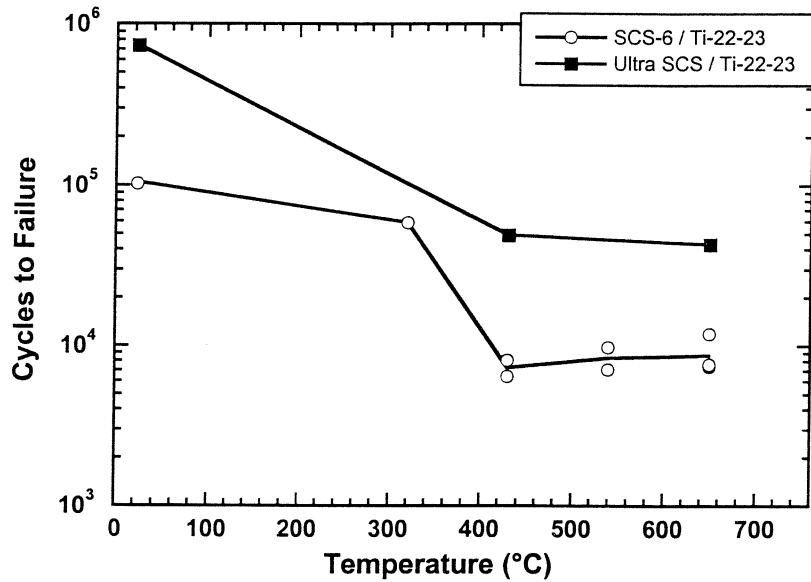


Figure 79. Temperature effects on the fatigue behavior of O TMCs with SCS-6™ and Ultra SCS™ fiber reinforcements ($\sigma_{\max} = 900$ MPa, $R=0.1$; frequency = 1.0Hz for Ultra SCS™/Ti-22Al-23Nb, 0.1 Hz for SCS-6™/Ti-22Al-23Nb) [29].

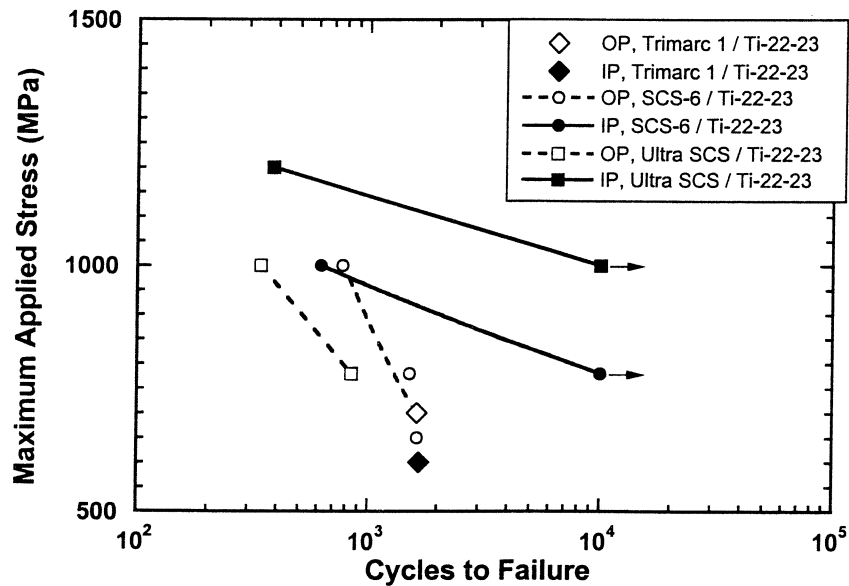


Figure 80. Thermomechanical fatigue comparison of the three orthorhombic composites (150-650°C, $R=0.1$, Frequency = 0.006 Hz) [29].

A comparison of the TMF behavior of the three composite systems is shown in Figure 80. Under IP testing the Ultra SCS™ composites exhibit a 200 and 500 MPa increase in fatigue resistance over the SCS-6™ and Trimarc 1® composites, respectively. While under OP testing, the Ultra SCS™ composite performed slightly worse than the other two composites. The improved IP TMF performance of the Ultra SCS™ composite is expected based on the increase in the fiber strength. The slight decrease in OP TMF life, however, is surprising and

may represent the fatigue limiting property of any TMC, having constituents with a high mismatch in coefficient of thermal expansion and modulus.

Effect of Matrix Modification

As mentioned at the beginning of this section, the majority of the composite mechanical property data has been generated for orthorhombic alloys having the Ti-22Al-23Nb matrix. There has been a considerable effort devoted to the development of heat treatments that improve the creep and tensile behavior of the monolithic orthorhombic materials, but only a little effort has gone into the addressing the influence of matrix properties on the composite mechanical response. Clearly there was an improvement in composite performance in the initial switch to an orthorhombic matrix as documented by Russ, et al. [15], however, the attempts, to date, have only indicated modest further improvements in *composite* properties though alloy refinement. The Ti-22Al-26Nb foil produced by Wah Chang [66] has been used to produce Ultra SCSTM / Ti-22Al-26Nb composites by Allison [123]. The higher niobium matrix has shown some improvements in tensile and creep properties compared to Ti-22Al-23Nb and was thought to offer improved composite performance. A comparison of the tensile strength of the two composite systems having Ultra SCSTM fibers with a nominal fiber volume fraction of 0.3 is shown in Fig. 81. Though the data for the Ultra SCSTM / Ti-22Al-26Nb composite [123] represent the average of several data points, it is apparent that the improved tensile properties of the higher niobium matrix are not improving the composite tensile strength.

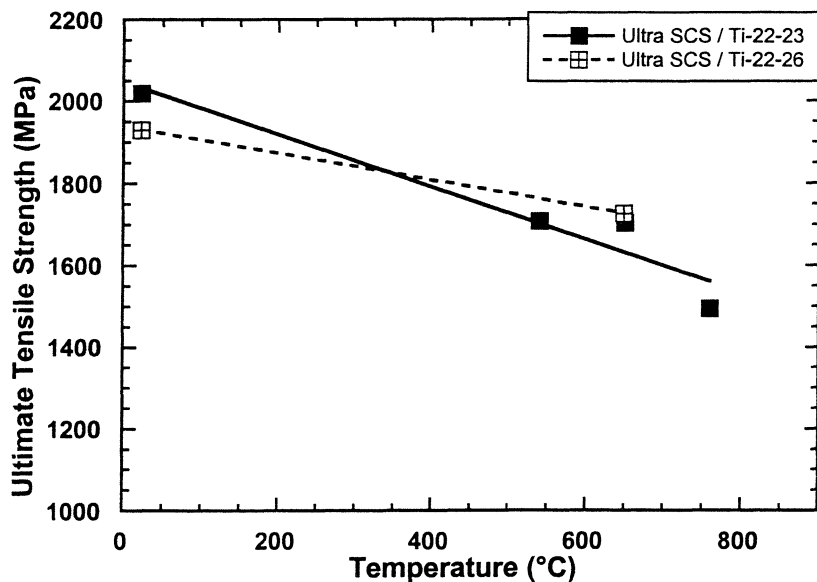


Figure 81. Comparison of the tensile strength of Ultra SCSTM reinforced O TMCs having Ti-22Al-23Nb [29] and Ti-22Al-26Nb [123] matrices ($v_f = 0.3$).

The isothermal fatigue behavior of the Ultra SCSTM / Ti-22Al-26Nb composite is compared to Ultra SCSTM / Ti-22Al-23Nb in Fig. 82. Though only a single data point exists for the Ti-22Al-23Nb composite at room temperature, it appears that the higher niobium composite offers decreased fatigue resistance.

It was reported that little fiber bridging was occurring in the Ultra SCSTM / Ti-22Al-26Nb composite [123] which may be the reason for the decreased performance. This could be due to differences in the processing as well as intrinsic differences of the fatigue behavior of the higher niobium matrix.

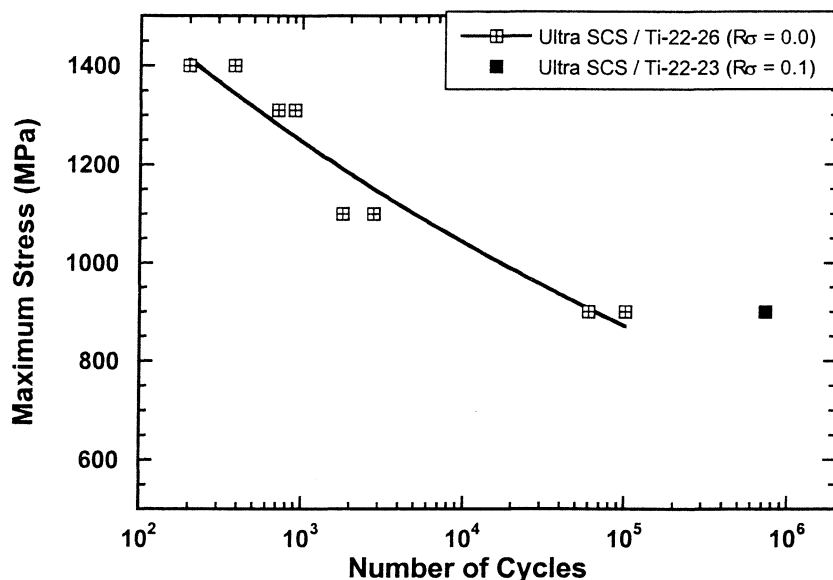


Figure 82. Comparison of the isothermal fatigue of Ultra SCSTM reinforced O TMCs having Ti-22Al-23Nb [29] and Ti-22Al-26Nb [123] matrices ($\nu_f = 0.3$).

Transverse creep resistance is one area where matrix modification has improved composite performance. Krishnamurthy, et al. [124] have shown that the sub- or supra-transus heat treatment of a SCS-6TM / Ti-22Al-23Nb composite in vacuum (10^{-6} torr) improves the transverse creep resistance, as shown in Fig 83. The heat treatments, shown in Table 12, represent two variations (Type I & II) of sub- and supra-transus heat treatments that are shown in Fig. 83. The two data points for the supra-transus, heat-treated condition represent the two different heat treatments (Type I showing the best transverse creep resistance). The sub-transus heat-treatment was largely unaffected by the Type I & II differences. One possible side effect of the heat treatment was also examined – that being the decrease in tensile ductility of the matrix following heat treatment. At room temperature, there was no reduction in ductility or strength of the longitudinal composites as a result of any heat treatment schemes. This indicates that the fiber strength is not adversely affected by the heat treatment. Studies of the effect of heat treatment on the fatigue and fatigue crack growth remain to verify the overall beneficial effect of such heat treatment schemes for composites.

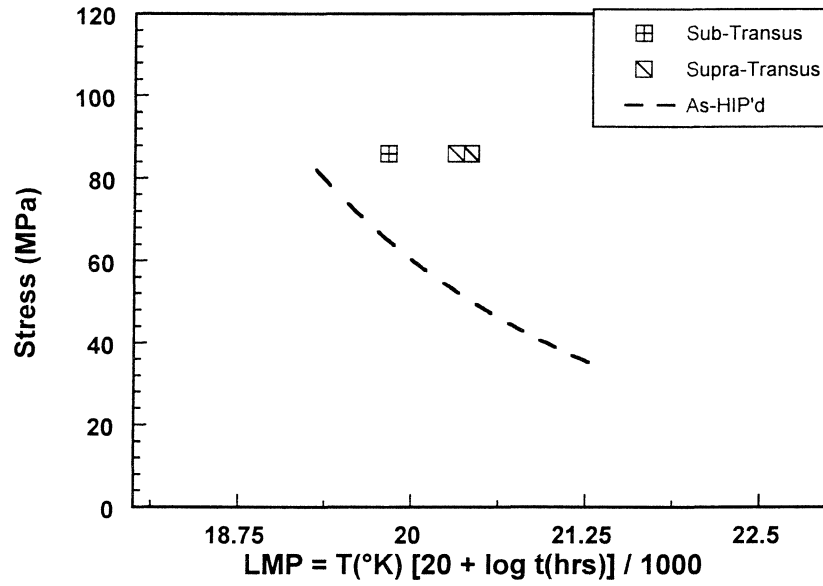


Figure 83. Comparison of the transverse creep resistance of As-HIP'd and heat treated SCS-6TM/Ti-22Al-23Nb composites (from [124]).

Table 12. Heat treatment of SCS-6TM/Ti-22Al-23Nb Composite [124]

Designation	Solution treatment for 2 hr (°C)	Cooling rate (°C min ⁻¹)	Aging treatment (°C/h)
Supra-transus HT (Type I)	1125	28	815/8 +FC
Sub-transus HT (Type I)	1050	28	815/8+FC
Supra-transus HT (Type II)	1160	2.8	815/8+FC
Sub-transus HT (Type II)	1085	2.8	815/8+FC

X. Summary

The Materials and Manufacturing Directorate of the Air Force Research Laboratory at Wright-Patterson AFB, OH has led the development of a new class of titanium aluminide composites based upon the Ti_2AlNb , orthorhombic "O" phase. Due to their high specific strength, these composites reinforced with continuous SiC monofilaments and referred to as O TMCs are being considered for applications at temperatures up to 700°C in hoop wound rotating engine components such as blisks, blings, impellers and remote rings.

Four SiC monofilaments have been evaluated as reinforcements for orthorhombic matrices: Trimarc 1[®], Trimarc 2[®], SCS-6[™] and Ultra SCS[™]. In addition a large diameter version of the Ultra SCS[™] fiber has also been manufactured in very modest quantities and preliminary evaluations made as a candidate reinforcement for O TMCs. The Trimarc 1[®] fiber which utilizes a tungsten (W) core has been shown to be inadequate as a potential reinforcement for O TMCs due to chemical reaction between the W and SiC during primary and secondary processing at elevated temperatures, resulting in a debit in fiber tensile strength. The Trimarc 2[®] and SCS-6[™] fibers made by Atlantic Research Corp. and Textron Systems are both deposited on a carbon monofilament (CMF) and do not exhibit chemical reactions between the CMF and SiC during elevated temperature primary or secondary processing. The tensile strengths of these two fibers are very similar, and they can be thought of as essentially interchangeable as reinforcements for O TMCs. The Ultra SCS[™] fiber made by Textron Systems utilizes a very fine SiC grain size to produce tensile strengths $\geq 30\%$ higher than for the Trimarc 2[®] and SCS-6[™] fibers. In addition, it too is deposited on a CMF substrate and is chemically stable during elevated temperature processing. As such, the Ultra SCS[™] fiber is the leading candidate fiber for those applications which are fiber strength critical. The experimental large diameter Ultra SCS fiber provided for the highest as-produced fiber strengths of all the monofilaments evaluated, but degraded during elevated exposure in a Ti-22Al-23Nb matrix, most likely the result of non-optimized fiber coating thickness and possibly coating composition.

In terms of matrix development, two ternary compositions, Ti-22Al-23Nb and Ti-22Al-27Nb (at. %) have received the most attention as first generation matrices. Although both compositions have been shown to contain up to three phases: α_2 , Ti_3Al (α_2); beta ($\beta/\text{B2}$); and orthorhombic, Ti_2AlNb (O); the $\alpha_2 + \text{B2}$ and $\alpha_2 + \text{B2} + \text{O}$ phase fields are much broader for an alloy such as Ti-22Al-23Nb than for an alloy such as Ti-22Al-27Nb. Consequently from a phase equilibria standpoint, the volume fraction of α_2 is typically higher in Ti-22Al-23Nb than in Ti-22Al-27Nb. The beta phase can be either ordered (B2) or disordered (β), depending on alloy composition and temperature. In addition to main alloying compositional effects, interstitial elements such as oxygen can play a key role in phase stability. Oxygen has been shown to be a potent α_2 stabilizer in Ti-22Al-23Nb with a 7°C increase in the B2/B2+ α_2 solvus temperature with a 100wppm increase in oxygen, such that for oxygen levels ≥ 980 wppm, the Ti-22Al-23Nb alloy falls in the three-phase, B2+O+ α_2 , field at 900°C, but in the B2+O phase at oxygen levels ≤ 980 wppm. Such phase constituency effects not

only affect primary and secondary processing, but the resulting mechanical performance as well. For example, the best combination of tensile strength and ductility for the Ti-22Al-23Nb matrix was obtained after solution treating high in the O+B2+ α_2 region followed by slow cooling and intermediate temperature aging, which produced low volume fractions of equiaxed primary α_2 , and increased volume fractions of lenticular O in a B2 matrix. In general, these first generation matrices exhibited improved tensile, creep and fracture resistance compared to their Ti₃Al predecessors, along with decreased reactivity with SiC reinforcements. However, for some of the more demanding applications such as impellers, which exhibit high tangential loads, increased matrix creep performance was required. In addition, these alloys suffered from environmental degradation due to breakaway oxidation ($\geq 700^\circ\text{C}$) and interstitial embrittlement ($\geq 500^\circ\text{C}$).

Second generation alloys were developed incorporating alloying additions such as Mo and Si for improved creep resistance, and Ta for oxidation improvement. Alloys which were evaluated included: Ti-22Al-24Nb-1.4Mo-0.5Si (foil), Ti-24.5Al-17Nb-1Mo (powder), Ti-22Al-24.5Nb-1.5Mo-1Ta (powder), Ti-22Al-24.5Nb-1.5Mo-1Ta-0.5 Si (powder). The Mo additions were found to be particularly beneficial in terms of improved creep resistance, however this was at the expense of ductility and rollability to foil. The Si seemed to provide no benefit to creep improvement. The Ta addition did provide some improvement to bulk oxidation resistance, but these improvements were small, and there was no improvement in interstitial embrittlement. The Ti-24.5Al-17Nb-1Mo alloy provided for increases in creep resistance, while exhibiting usable levels of ductility in as-consolidated powder form. Although both heat treatment and Mo additions resulted in increased matrix creep resistance, demanding applications such as impellers with high centrifugal loads will require additional creep performance. It may be possible to obtain these increases from the fiber.

In the fiber direction, normal and shear stresses can effectively transfer load from the matrix to the fiber. However, in off-axis orientations, the fiber/matrix interface is inherently weak. All SiC/Ti composites including O TMCs exhibit a chemical reaction during primary and secondary processing. The resulting reaction zone has been shown to consist of a complex combination of low strength and low ductility intermetallic compounds of complex titanium carbides and silicides. This reaction zone in combination with a weak carbon/carbon interface present in coating of the SiC reinforcement result in a weak fiber/matrix interface. However, this weak fiber/matrix interface is both positive and negative. The weak interface promotes crack deflection and resulting in crack bridging which acts to improve fatigue crack growth resistance of the composite. However, being weak, load-carrying capability of the interface in off-axis orientations is very poor as verified by fiber push-out, fiber pull-out and cruciform transverse tensile tests. Modeling studies have indicated that increases in fiber/matrix interface strength can be made without adversely affecting crack bridging characteristics. Indeed recent studies with spatially varied interfaces in SiC/Ti-6Al-4V(wt %) have shown increased transverse load carrying capability can be achieved without sacrificing fatigue crack growth

resistance. In addition, dual interface coatings (e.g. NbC/W and TaC/W) have been used to limit to amount of chemical reaction between the fiber and matrix. However, application of these coatings resulted in degradation of the fiber's tensile strength.

Fabrication of O TMCs has been accomplished by both foil-based and powder-based processing. Foil-based processing involves producing foil (~0.13mm thick), stacking up alternating layers of fiber and foil, and consolidating by hot isostatic pressing (HIP'ing). The two foil-based processing methods are: included helical foil (i.e. slinky) and grooved foil (i.e. phonograph). Although both techniques have successfully produced O TMCs, the latter has been favored due to the difficulty in procuring helical woven SiC fiber for the former. The sole producer of orthorhombic foil is currently the Wah Chang company and costs are on the order of \$700/lb due to multiple processing steps: ingot melting, forging, hot rolling and cold rolling (the latter two steps requiring intermediate elevated temperature annealing). However, recent Air Force sponsored research has demonstrated a reduction in foil costs to around \$300/lb may to possible with process improvements such as coil-to-coil rolling. However, the issue with foil-based processing is the cost and long lead times associated with the foil's production.

Powder-based processing methods include tape casting and wire winding. Both processes currently use gas atomized orthorhombic powders produced by Crucible Research Center for approximately \$70/lb. The tape cast process involves the production of a green "tapes" using a mixture of powder and organic binders, which are layered with woven SiC fiber mats. After outgassing to remove the organic binder, the lay-up is consolidated by HIP'ing. The wire winding process starts by HIP'ing of the powder to a cylindrical shape, which is then hot extruded to a thin rod form. This rod is subsequently cold extruded to ~0.19mm wire. The wire is co-wound on a drum with SiC fiber and HIP'd to a composite. The issue with the powder-based processing is found in chemical microsegregation within the powder during atomization. This microsegregation of Al to the cell boundaries promotes the formation of a contiguous network of low fracture resistant α_2 phase in the consolidated matrix providing for a preferential path for crack progression resulting in low ductility (typically $\leq 2.5\%$). This issue can be mitigated to a large extent by hot working the consolidated powder material, as is done in the production of wire for the wire winding process. In this manner, the material becomes microstructurally and/or crystallographically textured, with very usable resulting ductilities (i.e. $\geq 7\%$). Thus, the wire winding process is the preferred powder-based technique for fabricating O TMCs, particularly for hoop wound components for which wire winding is very well suited.

Of the candidate TMCs, those manufactured with an orthorhombic matrix appear to offer the best mechanical performance and balance of properties. Both α_2 (SCS-6/Ti-24Al-11Nb) and metastable titanium (SCS-6/Timetal®21S) composites were found to offer lower levels of tensile and creep strength, fatigue and thermomechanical fatigue resistance than similar orthorhombic TMCs. The O TMCs offer increased performance in both the

longitudinal and transverse directions. Further improvements in longitudinal properties have been realized by the incorporation of the higher strength fiber, Ultra SCSTM. Here the longitudinal (monotonic and cyclic) properties were observed to be ~200 MPa for nominally similar fiber volume fractions (~0.3 vf). This aids the composites in meeting the component structural requirements and enlarges the design window. The primary area of mechanical behavior that requires further experimental and analytic examination is that of dwell during fatigue loading. The studies, to date, of the influence of mission loading on the fatigue resistance of O TMCs have clearly highlighted this as a life limiting area.

Though considerable effort has been spent in the development of better orthorhombic compositions and microstructures, data regarding their influence on composite properties remains spotty. Demonstrated improvements in composite transverse creep resistance show that gains can be met through these avenues, though improvements will be evolutionary rather than revolutionary. The revolutionary gain in composite mechanical performance has already been met through the incorporation of orthorhombic alloys for the matrix and the high strength fiber, Ultra SCSTM.

XI. References

1. D. Banerjee, A.K. Gogia, T.K. Nandi, and V.A. Joshi, "A New Ordered Orthorhombic Phase in Ti₃Al-Nb Alloy", *Acta Metall.*, Vol. 36, 1988, pp. 871-882.
2. B. Mozer, L.A. Bendersky, W.J. Boettinger and R.G. Rowe, "Neutron Powder Diffraction Study of the Orthorhombic Ti₂AlNb Phase," *Scripta Metallurgica*, 24, 1990, 2363-8.
3. L.A. Bendersky, W.J. Boettinger and A. Roytburd, "Coherent Precipitates in the B.C.C./Orthorhombic Two-Phase Field of the Ti-Al-Nb System," *Acta Metall.Mater*, 39, 1991, 1059-69.
4. D.A. Koss, D. Banerjee, D.A. Lukasak, and A.K. Gogia, "A Review of the Deformation and Fracture of Ti₃Al-Based Alloys", in *High Temperature Aluminides and Intermetallics*, eds. Whang, S.H. et. al., The Minerals, Metals, and Materials Society, 1990, 175-196.
5. R.G. Rowe, "The Mechanical Properties of Ternary and Quaternary Ti₂NbAl-Based Titanium Aluminide Alloys", *Titanium '92 Science and Technology*, ed. F. H. Froes and I. Caplan, The Minerals, Metals, and Materials Society, vol 1, 1993, 343-50.
6. A.P. Woodfield, S.K. Srivatsa, S.F. Gruber, and V.K. Vasudaven, "Processing Development for Orthorhombic Titanium Alloys", N68335-93-C-0221, May 1996.
7. P.R. Smith and J.A.,Graves, "Monotonic Behavior of Neat High Temperature Titanium Alloys for Use as Composite Matrices", *Scripta Metallurgica et. Materialia*, Vol. 32, Issue 5, 1 March 1995, 695-700.
8. Porter, J.R., Chesnutt, J.C., Rhodes, C.G. and Hall, J.A., "Advanced Ti-Based MMC Development", AFRL-ML-WP-TR-1998-4075, May 1998.
9. P.R. Smith, M.L. Gambone, D.S Williams,. and D.L., Garner, "Heat Treatment Effects on SiC Fiber", *J. Material Science*, Vol. 33, 1998, 1-18.
10. M.L. Gambone and D.B. Gundel, "The Effect of W-Core/SiC Reaction on the Strength of SiC fibers in SiC/Ti-Alloy Composites," *Proceedings of CMMC'96*, San Sebastian, Spain, September, 1996.
11. M.L. Gambone, "SiC Fiber Strength After Consolidation and Heat Treatment in Ti-22Al-23Nb Matrix Composite", *Scripta Materialia*, Vol. 34, No. 3, 1996, pp. 507-512.

12. R.B. Daidone, Atlantic Research Corporation, Wilmington, MA., Private Communication, Feb 1999.
13. P.R. Smith, J.A. Graves and C.G. Rhodes, "Comparison of Orthorhombic and Alpha-Two Titanium Aluminides as Matrices for Continuous SiC-Reinforced Composites," Metallurgical Transactions, 25A, 1994, 1267-83.
14. C.G. Rhodes, "Characterization of Fiber/Matrix Interfaces by Transmission Electron Microscopy in Titanium Aluminide/SiC Composites", in Intermetallic Matrix Composites II, eds. Miracle, D.B., Anton, D.L. and Graves, J.A., Materials Research Society, Vol. 273, 1992, 17-29.
15. S.M. Russ, J.M. Larsen, and P.R. Smith, "Mechanical Property Assessment of SCS-6/Ti-22Al-23Nb", WL-TR-95-4068, Orthorhombic Titanium Matrix Composites, ed. Smith, P.R., July 1995, 162-179.
16. P.K. Brindley, "Tensile and Creep Properties of Powder Processed Ti-22Al-23Nb and SiC/Ti-22Al-23Nb Composites", WL-TR-95-4068, Orthorhombic Titanium Matrix Composites, ed. Smith, P.R., July 1995, 210-225.
17. R. John, and J.R. Jira, "Fatigue Crack Growth Behavior of Ultra SCS/Ti-22Al-26Nb", presented at AeroMat '98, Tysons Corner, VA., June 1998.
18. Y.C. Her, P.C. Wang, and J.-M. Yang. "Interface-Controlled Fatigue Cracking of SCS-6/Ti-22Al-23Nb Orthorhombic Titanium Aluminide Composite", Metallurgical Transactions A, Vol. 29A, Nov. 1998, 2737-2746.
19. B. Maruyama, and D.B. Gundel, "Spatially Varied Interfaces", Scripta Materialia, Vol. 35, No. 3, 1996, 391-395.
20. S. Krishnamurthy and D.B. Miracle, "On the Role of Carbon Diffusion during Fiber/Matrix Reaction in SiC Fiber Reinforced Ti-Based MMCs," in the Proceedings of ICCM-11, Volume III: Metal Matrix Composites and Physical Properties, Technomic Publishing Co., Inc., 1997, pp. 399-408.
21. J.A. Graves, P.R. Smith, and C.G. Rhodes, "Evaluation of a Ti-22Al-23Nb Orthorhombic Alloy for Use as the Matrix in a High Temperature Ti-Based Composite", in Intermetallic Matrix Composites II, eds. Miracle, D.B., Anton, D.L. and Graves, J.A., Materials Research Society, Vol. 273, 1992, 31-42.
22. C.C. Wojcik, Teledyne Wah Chang, Albany, OR, Private Communication, Dec 98.
23. R.G. Rowe, et. al., "Orthorhombic Titanium Aluminide Composite Matrix Processing Optimization", AFRL-ML-WP-TR-1998-4189, Sept 1998.

24. C.F. Yolton, Crucible Research Center, Pittsburgh, PA., Private Communication, April 1998.
25. P.R. Smith, A.H. Rosenberger, and M.J. Shepard, "Tape Cast Second Generation Orthorhombic-Based Titanium Aluminide Alloys for MMC Applications", *Scripta Materialia*, Vol. 41, No. 2, 1999, 221-228.
26. P.R. Smith, Materials and Manufacturing Directorate, Wright-Patterson AFB, OH, Unpublished Research, 1998.
27. W. Koop, "IHPTET – Air Dominance Through Propulsion Superiority", AFRL/PRT Brochure, 1998.
28. P.R. Smith, J.A. Graves, and C.G. Rhodes, "Evaluation of an SCS-6/Ti-22Al-23Nb Composite", in *Intermetallic Matrix Composites II*, eds. Miracle, D.B., Anton, D.L. and Graves, J.A., Materials Research Society, Vol. 273, 1992, 43-52.
29. A.H. Rosenberger, P.R. Smith, and S.M. Russ, "Preliminary Mechanical Property Assessment of an Ultra SCS/Ti-22Al-23Nb Composite", Accepted by *J. Composites Technology and Research*, Dec 98.
30. P. Sorensen, "Intermetallic MMC Compressor Rotor II", AF Contract# F33615-94-C-2410.
31. P.R. Smith, A.H. Rosenberger, M.J. Shepard, and R. Wheeler, Air Force Materials and Manufacturing Directorate, unpublished research 1999.
32. R.R. Cerchiara, G.H. Meier, and F.S. Pettit, "Mechanisms for Oxidation of Ti-22Al-23Nb SiC Reinforced Composites at Temperatures Between 500°C to 900°C in Oxygen, Air and Water Vapor", in *Orthorhombic Titanium Matrix Composites II*, ed. Smith, P.R., WL-TR-97-4082, July 1997, 326-341.
33. W.J. Brindley, P.A. Bartolotta, and J.W. Smith, "Coating Issues for Orthorhombic-Titanium Alloys", in *Orthorhombic Titanium Matrix Composites II*, ed. Smith, P.R., WL-TR-97-4082, July 1997, 342-367.
34. A.H. Rosenberger, S. Sankaran, P.R. Smith, D. Glass, and D. Rice, "Multilayer Coating for the Oxidation Protection of Orthorhombic Titanium Aluminides During Fatigue", in *Orthorhombic Titanium Matrix Composites II*, ed. Smith, P.R., WL-TR-97-4082, July 1997, 368-378.
35. G. Das, "Microstructural Characteristics of Ceramic Reinforcements for Composites", in AF Report No. WL-TR-91-4020, *Titanium Aluminide Composites*, eds. Smith, P.R., et al., Feb 1991, 20-58.

36. J.D. Casey and J. Geller, "Elemental Composition Profile of SCS-6 SiC Fiber as Determined by Auger Electron Spectroscopy", in Proc. Titanium Aluminide Composite Workshop, edited by P.R. Smith, S.J. Balsone, and T. Nicholas, Report No. WL-TR-91-4020, Materials Directorate, Wright Laboratory, WPAFB, OH, Feb. 1991, 59-72.
37. X.J. Ning, P. Pirouz, and P.D. Lagerlof, J. Mater. Res. 5 (12) (1990) 2865-2876.
38. M.R. Favaloro, Textron Systems Division, Private Communication, May 1999.
39. M.L. Gambone, D.I. Garner, and D.S. Williams, "The Effect of Composite Fabrication Processes on the Strength of Ultra SCS® Fiber", in AF Report WL-TR-97-4082, Orthorhombic Titanium Matrix Composites II, ed. Smith, P.R., July 1997, 29-46.
40. V. Fry, "Advanced Chemical Vapor Deposition (CVD) Fibers for Metal Matrix Composites", AF Report No. WL-TR-93-4050, Materials Directorate, Wright Laboratory, WPAFB, OH, April 1993.
41. C.R. Rowe, Atlantic Research Corp., Private Communication, May 1999.
42. P.R. Smith and W.J. Porter, "The Effect of Heat Treatment on the Tensile and Creep Behavior of Neat Matrix Ti-22Al-23Nb", Journal Material Science, 32, 1997, 6215-6220.
43. R.G. Rowe, "Recent Developments in Ti-Al-Nb Titanium Aluminide Alloys," High Temperature Aluminides & Intermetallics, S.H. Whang et al., eds., TMS-AIME, Warrendale, PA, 1990, pp. 375-401.
44. R.G. Rowe, "The Mechanical Properties of Titanium Aluminides Near Ti-25Al-25Nb," Microstructure/Property Relationships in Titanium Aluminides and Alloys, Y.W. Kim and R. R. Boyer, eds., TMS, Warrendale, PA, 1991, pp. 387-398.
45. S. Das, T.J. Jewett, and J. H. Perepezko, "High Temperature Phase Equilibria of Some Ternary Titanium Aluminides," Structural Intermetallics, R. Darolia et al., eds., TMS, Warrendale, PA, 1993, pp.35-43.
46. K. Muraleedharan, A.K. Gogia, T.K. Nandy, D. Banerjee, and S. Lele, "Transformations in a Ti-24Al-15Nb Alloy: Part I. Phase Equilibria and Microstructure," Met. Trans., vol. 23A, 1992, pp. 401-415.
47. R.G. Rowe, D. Banerjee, K. Muraleedharan, M. Larsen, E.L. Hall, D.G. Konitzer, and A.P. Woodfield, "Phase Equilibria in Ti-Al-Nb Alloys Near Ti₂AlNb,"

Titanium '92 Science and Technology, F.H. Froes et al., eds, TMS, Warrendale, PA, 1993, pp. 1259-1266.

48. H.T. Kestner-Weykamp, C.H. Ward, T.F. Broderick, and M.J. Kaufman, "Microstructures and Phase Relationships in the $Ti_3Al + Nb$ System," *Scripta Met.*, vol. 23, 1989, pp. 1697-1702.

49. D. Banerjee, A.K. Gogia, T.K. Nandy, R. Muraleedharan, and R.S. Mishra, "The Physical Metallurgy of Ti_3Al Based Alloys," Structural Intermetallics, R. Darolia et al., eds., TMS, Warrendale, PA, 1993, pp.19-33.

50. D.B. Miracle, C.G. Rhodes, and M.A. Foster, "Phase Equilibria in Ti-Al-Nb Orthorhombic Alloys," Titanium '95, P. Blenkinsop et al., eds., University Press, Cambridge, UK, 1996, pp. 372-379.

51. C.G. Rhodes, "Order/Disorder Temperature of the BCC Phase in Ti-21Al-26Nb," *Scripta Mater.*, vol. 38, 1998, pp. 681-685.

52. R.A. Amato, and D.R. Pank, "Advanced Titanium Matrix Alloy Development", WL-TR-92- 4035, Titanium Matrix Composites, eds. Smith, P.R. and Revelos, W.C., April 1992, 80-97.

53. C.G. Rhodes and S. Leutjering, "Microstructure Evolution at Use Temperatures in Ti-22Al-23Nb," presented at AeroMat '98, Tysons Corner, VA, June 1998.

54. C. J. Boehlert, B.S. Majumdar, and V. Seetharaman, "Processing and Heat Treatment Effects on the Phase Evolution, Tensile, and Creep Behavior of an Orthorhombic Ti-25Al-25Nb Alloy," Deformation and Fracture of Ordered Intermetallic Materials, W.O. Soboyejo et al., eds., TMS, Warrendale, PA, 1997, pp. 565-582.

55. R.G. Rowe and M.F.X. Gigliotti, "Creep and Discontinuous Precipitation in a Ti_3Al-Nb Alloy at 923K," *Scr. Metall. Mater.*, vol. 24, 1990, pp. 1209-1214.

56. Y. Yamabe, N. Honjo, and M. Kikuchi, Proc. of Int. Symp. On Intermetallic Compounds, Structure and Mechanical Properties (JIMIS-6), O. Izumi, ed., The Japan Institute of Metals, 1991, pp. 809-817.

57. H-G. Yi and J.K. Park, "Effect of Prior Continuous Precipitation on the Discontinuous Precipitation of Al-Zn Alloys," *Scripta Metall. & Mater.*, vol. 25, 1991, pp. 1799-1804.

58. C.G. Rhodes, J.A. Graves, P.R. Smith, and M.R. James, "Characterization of Orthorhombic Titanium Aluminide Alloys," Structural Intermetallics, R. Darolia et al., eds., TMS, Warrendale, PA, 1993, pp. 45-52.

59. S.L. Semiatin and P.R. Smith, "Microstructural Evolution During Rolling of Ti-22Al-23Nb Sheet," *Mat. Sci. & Engr.*, vol. A202, 1995, pp. 26-35.
60. C.C. Wojcik, R. Roessler, and R. Zordan, "Titanium Aluminide Foil Processing," Advances in the Science and Technology of Titanium Alloy Processing, I. Weiss et al., eds., TMS, Warrendale, PA, 1996, pp. 293-300.
61. R.G. Rowe, D.G. Konitzer, A.P. Woodfield, and J.C. Chesnutt, "Tensile and Creep Behavior of Ordered Orthorhombic Ti₂AlNb-Based Alloys," *Mat. Res. Soc. Conf. Proc.*, Vol.213, High Temperature Ordered Intermetallic Alloys IV, L.A. Johnson et al., eds., MRS, Pittsburgh, PA, 1991, pp.703-708.
62. P.R. Smith, W.J. Porter, W.J. Kralik, and J.A. Graves, "The Effect of a Post-Consolidation Heat Treatment on the Tensile and Creep Behavior of Neat Ti-22Al-23Nb," Metal Matrix Composites, Vol. 2, Proc. 10th International Conf. on Composite Materials, A. Poursartip et al., eds., 1995, pp. 731-738.
63. F.C. Dary and T.M. Pollock, "Effects of High-Temperature Air and Vacuum Exposures on the Room-Temperature Tensile Behavior of the (O+B2) Titanium Aluminide, Ti-22Al-23Nb," *Mater. Sci. and Engr*, vol. A208, 1996, pp. 188-202.
64. A.K. Gogia, T.K. Nandy, K. Muraleedharan, and D. Banerjee, "The Effect of Heat Treatment and Niobium Content of the Room Temperature Tensile Properties and Microstructure of Ti₃Al-Nb Alloys," *Mater. Sci. & Engr.*, vol. A150, 1992, pp. 73-86.
65. P.R. Smith and J.A. Graves, "Tensile And Creep Properties of High Temperature Titanium Alloys in "Neat" Matrix Form," WL-TR-95-4068, 1995, pp. 139-149.
66. R.W. Hayes, "Minimum Strain Rate and Primary Transient Creep Analysis of a Fine Structure Orthorhombic Titanium Aluminide," *Scripta Mater.*, vol. 34, 1996, pp. 1005-1012.
67. R.W. Hayes and C.G. Rhodes, "Microstructure Evolution in an Orthorhombic Titanium Aluminide as a Function of Temperature-Strain-Time," in Advances in the Science and Technology of Titanium Alloy Processing, I. Weiss et al., eds., TMS, Warrendale, PA, 1996, pp. 507-515.
68. R.R. Cerchiara, G.H. Meier, and F.S. Petit, "Oxidation Studies on Ti-Al-Nb Neat and Composite Materials at Temperatures Between 500° and 900°C," WL-TR-95-4068, 1995, pp. 15-40.
69. W.J. Brindley, J.L. Smialek, J.W. Smith, and M.P. Brady, "Environmental Effects on Orthorhombic-Ti Matrix Materials," WL-TR-95-4068, 1995, pp. 1 – 14.

70. F.S. Petit, unpublished research. See also, "Composite Development," in Orthorhombic Titanium Matrix Composites, P.R. Smith, ed., WL-TR-95-4068, July 1995, pp. 412 - 413.
71. C.G. Rhodes and R.A. Spurling, "Fiber-Matrix Reaction Zone Growth Kinetics in SiC-Reinforced Ti-6Al-4V as Studied by Transmission Electron Microscopy," Recent Advances in Composites in the United States and Japan, J.R. Vinson and M. Taya, eds., ASTM STP 864, ASTM, Philadelphia, PA, 1985, pp. 585-599.
72. C.G. Rhodes, A.K. Ghosh, and R.A. Spurling, "Ti-6Al-4V-2Ni as a Matrix Material for a SiC-Reinforced Composite," *Met. Trans.*, vol. 18A, 1987, pp. 2151-2156.
73. D.M. Bowden, S.M.L. Sastry, and P.R. Smith, "Reactions Between Ti3Al-Nb and Mixed Second Phases," *Scripta Met.*, vol. 23, 1989, pp. 407-410.
74. S.F. Baumann, P.K. Brindley, and S.D. Smith, "Reaction Zone Microstructure in a Ti3Al + Nb / SiC Composite," *Met. Trans.*, vol. 21A, 1990, pp. 1559-1569.
75. D.R. Baker, P.J. Doorbar, and M.H. Loretto, "Fibre-Matrix Reaction Zones in Model Silicon Carbide-Titanium Aluminide Metal-Matrix Composites," *Mat. Res. Soc. Symp. Proc. Vol 170 Tailored Interfaces in Composite Materials*, Mat. Res. Soc., Pittsburgh, PA, 1990, pp. 85-90.
76. D.B. Gundel and F.E. Wawner, "Interfacial Reaction Kinetics of Coated SiC Fibers with Various Titanium Alloys," *Scripta Met. & Mater.*, vol. 25, 1991, pp. 437-441.
77. C.G. Rhodes and R.A. Spurling, "Fiber/Matrix Interface Reactions in SiC Reinforced Titanium Alloys," Developments in Ceramic and Metal-Matrix Composites, K. Upadhyaya, ed., TMS, Warrendale, PA, 1992, pp. 99-113.
78. D.R. Schuyler, M.M. Sohi, R.L. Hollars, and J.D. Pugnale, "Feasibility of Aluminide Metal Matrix Composites for 1400°F Applications," Final report No. 21-7798, U.S. Navy, NADC, Contract No. N62269-86-C-0248, 1991.
79. D.B. Marshall, M.C. Shaw, and W.L. Morris, "Measurement of Interfacial Debonding and Sliding Resistance in Fiber Reinforced Intermetallics," *Acta Metall. Mater.*, vol 40, 1992, pp. 443-454.
80. D.B. Marshall, "An Indentation Method for Measuring Matrix-Fiber Frictional Stresses in Ceramic Composites," *J. Am. Cer. Soc.*, vol. 67, 1984, pp. 259-260.

81. B.S. Majumdar and G.M. Newaz, "Inelastic Deformation of Metal matrix Composites: Plasticity and Damage Mechanisms," *Phil. Mag. A*, vol. 66, 1992, pp. 187-212
82. D.B. Gundel, B.S. Majumdar, and D.B. Miracle, "Evaluation of the Transverse Response of Fiber-Reinforced Composites using a Cross-Shaped Sample Geometry," *Scripta Metal. & Mater.*, vol. 33, 1995, pp. 2057-2065.
83. D.B. Marshall, W.L. Morris, B.N. Cox, J. Graves, J.R. Porter, D. Kouris, and R.K. Everett, "Transverse Strengths and Failure Mechanisms in Ti_3Al Matrix Composites," *Acta Metall.*, vol. 42, 1994, pp. 2657-2673.
84. S.G. Warrier, D.B. Gundel, B.S. Majumdar, and D.B. Miracle, "Stress Distribution in a Transversely Loaded Cross-Shaped Single Fiber SCS-6/ $Ti-6Al-4V$ Composite," *Scripta Mater.*, vol. 34, 1996, pp. 293-299.
85. M-J. Pindera and A.D. Freed, "The Effect of Matrix Microstructure on Thermally Induced Residual Stresses in SiC /Titanium Aluminide Composites," *J. Engr. Mater. & Techn.*, vol. 116, 1994, pp. 215-221.
86. A.K. Misra and S.M. Arnold, "Compliant Layer for the $Ti_3Al+Nb/SCS-6$ Composite System," NASA Technical Memo. 105344, 1991.
87. R.R. Kieschke and T.W. Clyne, "Control over Interfacial Bond Strength in Ti/SiC Fibrous Composites," in Fundamental Relationships Between Microstructures and Mechanical Properties of Metal Matrix Composites, TMS, Warrendale, PA, 1990, pp. 325-340.
88. K.L. Choy, "Functionally Graded Coatings on SiC Fibers for Protection in Ti -Based Metal Matrix Composites," *Scripta Mater.*, vol. 34, 1996, pp. 1753-1758.
89. S.C. Jha, J.A. Forster, A.K. Pandey, and R.G. Delagi, "MMC's Via titanium Aluminide Foils," *Adv. Mater. & Proc.*, April, 1991, pp. 87-90.
90. J.A. Graves, A.H. Muir, and C.G. Rhodes, "Manufacturing Science for Titanium Aluminide Composite Engine Structures," Wright Laboratory, Wright-Patterson AFB, HO, WL-TR-92-4100, Dec. 1992.
91. J.R. Roessler, A. Chatterjee, L.E. Brown, and G.E. Richardson, "Materials Processing and Fabrication of Advanced MMC Compressor Rotors," in Orthorhombic Titanium Matrix Composites II, P.R. Smith, ed., WL-TR-97 4082, July 1997, pp. 115 – 124.
92. R.C. Lewis and P. Nagy, "MMC Ring Fabrication with Grooved Foil Preforms," Titanium Metal Matrix Composites II, P.R. Smith and W.C. Revelos, eds., WL-TR-93-4105, November 1993, pp. 131-157.

93. A. Chatterjee, Allison Engine Company, personal communication.
94. C. Bassi, J.A. Peters, and J. Wittnauer, "Processing Titanium Aluminide Foils," *J. Metals*, Sept. 1989, pp. 18-20.
95. J.A. Peters and C. Bassi, "Isothermal Transformations in a β -stabilized Ti_3Al Intermetallic," *Scripta Met. & Mater.*, vol. 24, 1990, pp. 915-920.
96. A.D. Rollett, P.R. Smith, and M.R. James, "Texture and Anisotropy of Ti-22Al-23Nb Foil," in Orthorhombic Titanium Matrix Composites II, P.R. Smith, ed., Wright Laboratory, WL-TR-97-4082, July 1997, pp. 143-157.
97. W.H. Hanusiak, L.B. Hanusiak, J.M. Panell, S.R. Spear and C.R. Rowe, "Methods of Making Preforms for Composite Material Manufacture", U.S. Patent No 5,624,516, April, 1997.
98. P.R. Smith, M.J. Shepard, A.H. Rosenberger, and R. Wheeler, Materials and Manufacturing Directorate, Air Force Research Laboratory, Wright-Patterson AFB, OH., 1999, Unpublished Research
99. W.H. Hanusiak, L.B. Hanusiak, J.M. Parnell, S.R. Spear and C.R. Rowe, "Wire Preforms for Composite Material Manufacturing and Methods of Making," U.S. Patent No. 5,763,079, June 1998.
100. P.R. Smith, Materials and Manufacturing Directorate, Air Force Research Laboratory, Wright-Patterson AFB, OH., 1999, Unpublished Research.
101. J.M. Larsen, S.M. Russ, and J.W. Jones, "Possibilities and Pitfalls in Aerospace Applications of Titanium Matrix Composites," Report AGARD-R-7966, NATO Advisory Group for Aerospace Research and Development (AGARD), Specialized Printing Services Ltd., Loughton, Essex, 1994, pp. 1.1-1.21
102. J.M. Larsen, S.M. Russ, and J.W. Jones, "An Evaluation of Fiber-Reinforced Titanium Matrix Composites for Advanced High Temperature Aerospace Applications," *Metallurgical Transactions A*, 26A, 1995, pp. 3211-3223.
103. M. Khobaib, R. John, and N.E. Ashbaugh, "Sustained Load Behavior of SCS-6/Timetal 21S Composite," *Life Prediction Methodology for Titanium Matrix Composites*, ASTM STP 1253, W.S. Johnson, et al., eds., American Society for Testing and Materials, 1996, pp. 185-207.
104. W.C. Revelos, J.W. Jones, and E.J. Dolley, "Thermal Fatigue of a SiC/Ti-15Mo-2.7Nb-3Al-0.2Si Composite," *Metallurgical and Materials Transactions*, 26A, 1995, pp. 1167-1181.

105. M.L. Gambone, *Fatigue and Fracture of Titanium Aluminides*, WRDC-TR-89-4145, Wright Research and Development Center, Materials Laboratory, WPAFB, OH, 1990.
106. M.A. Foster P.R. Smith and D.B. Miracle, "The Effect of Heat Treatment on Tensile and Creep Properties of "Neat" Ti-22Al-23Nb in the Transverse Orientation, *Scripta Metallurgica*, 33(6), 1995, pp. 975-981.
107. T. Nicholas and J.L. Kroupa, "Micromechanical Analysis and Life Prediction of Titanium Matrix Composites," *Journal of Composites Technology & Research*, 20(2), 1998, pp. 79-88.
108. S.M. Russ, "Thermal Fatigue of Ti-24Al-11Nb/SCS-6," *Metallurgical Transactions*, 21A, 1990, pp. 1595-1602.
109. W.C. Revelos and P.R. Smith, "Effect of Environment on the Thermal Fatigue Response of an SCS-6/Ti-24Al-11Nb Composite," *Metallurgical Transactions*, 23A, 1992, pp. 587-595.
110. T.P. Gabb, J. Gayda, and R.A. MacKay, "Isothermal and Nonisothermal Fatigue Behavior of a Metal Matrix Composite," *Journal of Composite Materials*., Vol. 24, 1990, pp. 667-686.
111. S.M. Russ, T. Nicholas, M. Bates, and S. Mall, "Thermomechanical fatigue of SCS-6/Ti-24Al-11Nb Metal Matrix Composite," *Failure Mechanisms in High Temperature Composite Materials*, AD-Vol. 22 / AMD-Vol. 122, G. K. Haritos, G. Newaz, and S. Mall, Eds., American Society of Mechanical Engineers, New York, 1991, pp. 37-43.
112. R.W. Neu and T. Nicholas, "Methodologies for Predicting the Thermomechanical Fatigue Life of Unidirectional Metal Matrix Composites," *Advances in Fatigue Lifetime Predictive Techniques: 3rd Volume*, ASTM STP 1292, M. R. Mitchell and R. W. Landgraf, Eds., American Society for Testing and Materials, Philadelphia, 1996, pp. 1-23.
113. T. Nicholas and D.A. Johnson, "Time- and Cycle-Dependent Aspects of Thermal and Mechanical Fatigue in a Titanium Matrix Composite," *Thermomechanical Fatigue Behavior of Materials ASTM STP 1263*, M.J. Verilli and M.G. Castelli, Eds, American Society for Testing and Materials, Philadelphia, 1994, pp. 331-351.
114. J.R. Jira and J.M. Larsen, "The Contribution of Matrix Alloy to the Fatigue Crack Growth Resistance of Three Classes of Titanium Matrix Composites," in *Fatigue '96 Proceedings of the Sixth International Fatigue Congress*, G. Lütjering and H. Nowack, Eds., Elsevier Science Ltd., Oxford, U.K., 1996, pp. 1785-1790.

115. A.H. Rosenberger, "Preliminary Assessment of the Environmental Sensitivity of Ti-22Al-23Nb (a/o) Neat Laminates," WL-TR-95-4068, 1995, pp. 41-51.
116. S. M. Russ, A.H. Rosenberger, and D.A. Stubbs, "Isothermal Fatigue of a SCS-6/Ti-22Al-23Nb Composite in Air and Vacuum," *Recent Advances in Composite Materials*, S. R. White, H. T. Hahn, and W. F. Jones, Eds. American Society of Mechanical Engineers, New York, 1995, pp. 13-22.
117. S. Woodard, T. Pollock, and F.-C. Dary, "Creep Deformation of Composite and Monolithic Ti-22Al-23Nb Material," *Orthorhombic Titanium Matrix Composites*, WL-TR-95-4068, Wright Laboratory Materials Directorate, WPAFB, OH 1995, pp. 120-138.
118. S. Woodard and T. Pollock, "Transverse Creep in Ti-22Al-23Nb SiC-reinforced Composites," *Orthorhombic Titanium Matrix Composites II*, WL-TR-97-4082, Wright Laboratory Materials Directorate, WPAFB, OH 1997, pp. 265-276.
119. W.J. Brindley, T.P. Gabb, and J.W. Smith, "Embrittlement of the Surfaces and Crack Faces of TMCs During Fatigue," *Orthorhombic Titanium Matrix Composites*, WL-TR-95-4068, Wright Laboratory Materials Directorate, WPAFB, OH 1995, pp. 52-63.
120. P.C. Wang, S.M. Jeng, J.-M. Yang, and S.M. Russ, "Fatigue Damage Evolution and Property Degradation of a SCS-6/Ti-22Al-23Nb 'Orthorhombic' Titanium Matrix Composite," *Acta Mater.*, 44(8) 1996, pp. 3141-3156.
121. A. Chatterjee, R. Ress, T.P. Gabb, and J. Gayda, "Simplified Mission Profile Testing of Orthorhombic TMCs," *Orthorhombic Titanium Matrix Composites II*, WL-TR-97-4082, Wright Laboratory Materials Directorate, WPAFB, OH 1997, pp. 277-288.
122. T.P. Gabb, J. Gayda, A. Chatterjee, and R. Ress, "Mission Cycle Behavior of Orthorhombic Titanium Matrix Composite," *Structural Intermetallics 1997*, M. V. Nathal, et al., eds., The Minerals, Metals, and Materials Society, Warrendale, PA, 1997, pp. 913-922.
124. A. Chatterjee, J.R. Roessler, L.E. Brown, P.W. Heitman, and G.E. Richardson, "Microstructure and Mechanical Properties of Ultra SCSTM Fiber Reinforced Orthorhombic Ti-22Al-26Nb Composites," *Structural Intermetallics 1997*, M. V. Nathal, et al., eds., The Minerals, Metals, and Materials Society, Warrendale, PA, 1997, pp. 905-911.
125. S. Krishnamurthy, P.R. Smith, and D.B. Miracle, "Modification of the Transverse Creep Behavior of an Orthorhombic Titanium Aluminide Based Ti-

22Al-23Nb/SiC_f Composite Using Heat Treatment," Materials Science and Engineering, A243, 1998, pp. 285-289.

